UNIVERSITAT POLITÈCNICA DE VALÈNCIA

DEPARTAMENTO DE QUÍMICA

INSTITUTO UNIVERSITARIO MIXTO DE TECNOLOGÍA QUÍMICA (UPV – CSIC)

Doctoral Thesis

# *Photoredox catalysis for environmental and chemical applications. A mechanistically-based approach.*

**Rebeca Martínez Haya**

Directors:

**Prof. Miguel A. Miranda Alonso**

**Dra. Mª Luisa Marín García**

Valencia, November 2018

# CERTIFICATION

Miguel Ángel Miranda Alonso and Maria Luisa Marín García, Professors of the Universitat Politècnica de València:

Certify that the Doctoral Thesis entitled “Photoredox catalysis for environmental and chemical applications. A mechanistically-based approach” has been developed by Rebeca Martínez Haya under their supervision in the Instituto Universitario Mixto de Tecnología Química (UPV-CSIC).

Prof. Miguel A. Miranda Alonso  Prof. Mª Luisa Marín García

La tesis. La tesis doctoral. Un trabajo que no es un trabajo, es formación, es curiosidad, son ganas de aprender y de superarse, es creatividad, es responsabilidad y nervios… Pero sobre todo, es una etapa en la que te sumerges en la ciencia y así, casi sin darte cuenta, conoces a fondo esta bonita profesión. Se requiere cierta vocación, así como mucha dedicación y sobre todo, paciencia. Para mí, ha supuesto una etapa de mi vida de la que estoy muy orgullosa, en la que no solo he aprendido química o ciencia, sino que también me ha ayudado a evolucionar como persona y como profesional.

Por todo esto, me gustaría mucho dar las gracias a quienes me dieron la oportunidad de vivir esta aventura, mis directores de tesis. A Miguel Ángel, por ser la *luz* que nos dirige a todos y todas cuando más lo necesitamos. Y a Marisa, para la que no tengo palabras, por ser la mejor profesora de química que he tenido, por su paciencia, su comprensión y su entusiasmo a la hora de enseñar, pero también por toda la ayuda y consejos de puertas afuera del laboratorio, he tenido mucha suerte. Y hablando de suerte y laboratorio, no puedo dejar de recordar a todos los compañeros y compañeras que hemos convivido en el 1A1 y en el 1A2, a Paula, Faber, Gemma y Vicky, Ofelia y Cris, Mauri, Paloma, a las nuevas incorporaciones Óscar y Alice, a las *otras* jefas Virginie, Chelo e Inma,… gracias por la ayuda y por todos los buenos momentos. ¡Ha sido un placer fotoquímic@s!

Por otro lado, todo esto no habría sido posible sin financiación. Por lo que quiero agradecer, tanto al Severo Ochoa como a la Asociación Apadrina la Ciencia, por financiar mis contratos de investigación. También al DAAD, cuya financiación me permitió realizar mi estancia, donde conocí a una gran compañera, Leyre, a la cual también le estoy muy agradecida por esos seis meses en Regensburg.

Ya por último, y a quienes más debo, muchísimas gracias a mi familia, a mis padres Felipe y Chelo, y a mi hermana Sara, por haberme apoyado durante toda mi vida en las decisiones más importantes, dándome ánimo y aliento. Gracias. Y para finalizar, gracias de todo corazón a quien ha sido mi pilar más fuerte durante esta etapa, Jorge. Contigo los retos son más fáciles, los sueños más bonitos y la vida más divertida. Por que sigamos construyendo pilares y aprendiendo juntos en el camino.

# ABREVIATURES AND SYMBOLS

| | |
|---|---|
| A | Acceptor |
| ACF | Acetaminophen |
| ACN | Acetonitrile |
| ACP | Acetamiprid |
| AO/RP | Advanced Oxidation and Reduction Processes |
| AOP | Advanced Oxidation Processes |
| ARP | Advanced Reduction Processes |
| BaOH | Barium hydroxide |
| CAF | Caffeine |
| CECs | Contaminants of Emerging Concern |
| CBZ | Carbamazepine |
| CLOF | Clofibric acid |
| D | Donor |
| DABCO | 1,4-Diazabicyclo[2.2.2]octane |
| DCF | Diclofenac |
| DIPA | Diisopropylamine |
| DMA | *N,N'*-Dimethylaniline |
| DMF | *N,N'*-Dimethylformamide |
| DMSO | Dimethyl sulfoxide |
| Eps | Emerging Pollutants |
| $E^*$ | Energy of the excited state |
| $E^0_{red}$ | Reduction potential |
| $E_S$ | Energy of the singlet excited state |
| $E_T$ | Energy of the triplet excited state |
| EDF | Exponential Decay Fitting |
| GA | Gallic acid |
| I | Intensity |
| ic | Internal conversion |
| isc | Intersystem crossing |
| *i*-PrOH | Isopropanol |
| K | Complex formation constant |
| $k_q$ | Kinetic constant |
| Ksv | Stationary Stern Volmer constant |
| $NMQ^+$ | *N*-Methylquinolinium |
| $O_2^{\cdot-}$ | Superoxide radical anion |
| PC | Photocatalyst |
| PN | Perinaphthenone |
| RB | Rose Bengal |
| RF | Riboflavin |
| ROS | Reactive Oxygen Species |
| SCE | Saturated calomel electrode |
| $S_0$ | Ground state |

| | |
|---|---|
| $S_1$ | Singlet excited state |
| TCA | 2,4,6-Trichloroanisole |
| TCP | 2,4,6-Trichlorophenol |
| TCS | Triclosan |
| TEA | Triethylamine |
| THF | Tetrahydrofurane |
| $TPP^+$ | 2,4,6-Triphenylpyrylium |
| $TPTP^+$ | 2,4,6-Triphenylthiapyrylium |
| $T_1$ | Triplet excited state |
| UV | Ultraviolet |
| UV-vis | Ultraviolet - Visible |
| $\Delta G^0$ | Gibbs Free energy |
| $^1O_2$ | Singlet oxygen |
| $\Phi_F$ | Fluorescence quantum yield |
| $\Phi_{ISC}$ | Intersystem crossing quantum yield |
| $\tau$ | Lifetime |

# OUTLINE

# 1. Introduction

## 1.1. Photochemistry

Life on Earth would not have been possible without Sun irradiation. This source of energy provides both heat and light, which are needed for the majority of the biological and chemical functions of living beings. In fact, the probably most important process on Earth, photosynthesis, could not take place without sunlight. Due to its impact on our planet, photosynthesis has tried to be mimicked by scientists for years. More specifically, it was Giacomo Ciamician who around one century ago encouraged scientific community to copy Nature with the objective of synthesizing chemicals using sunlight as a "green" energy source. Actually, he is considered as a founder of the field currently known as photochemistry.[1]

The conceptual framework of photochemistry is now firmly established. As a first approach, photochemistry is the branch of chemistry responsible for studying and explaining the chemical and physical effects of light, from UV to the near infra-red (200 – 780 nm), in molecules. However, to be able to absorb that light, molecules need chromophore moieties in their structure. According to the IUPAC, a chromophore is *the part of a molecular entity consisting of a single atom or a group of them in which the electronic transition responsible for a specific spectral band is approximately localized.*[2] Among the typical atoms or group of atoms that form a chromophore are organic functional groups such as olefins, aromatic rings, ketones or enones. Then, the first stage in a photochemical process is the absorption of light by the chromophore, to reach an excited state of the molecule: $M + h\nu \rightarrow M^*$. The energy of the incident photon must be adequate to be photochemically active. It means that the energetic gap between both states of the molecule should correspond to the energy of the photon. This statement is the Grotthus-Draper law and is known as the first principle of photochemistry: "only that light which is absorbed by a system can induce a photochemical change". The processes that a molecule may suffer upon absorption of light can be analysed with the Jablonski diagram, Figure 1.

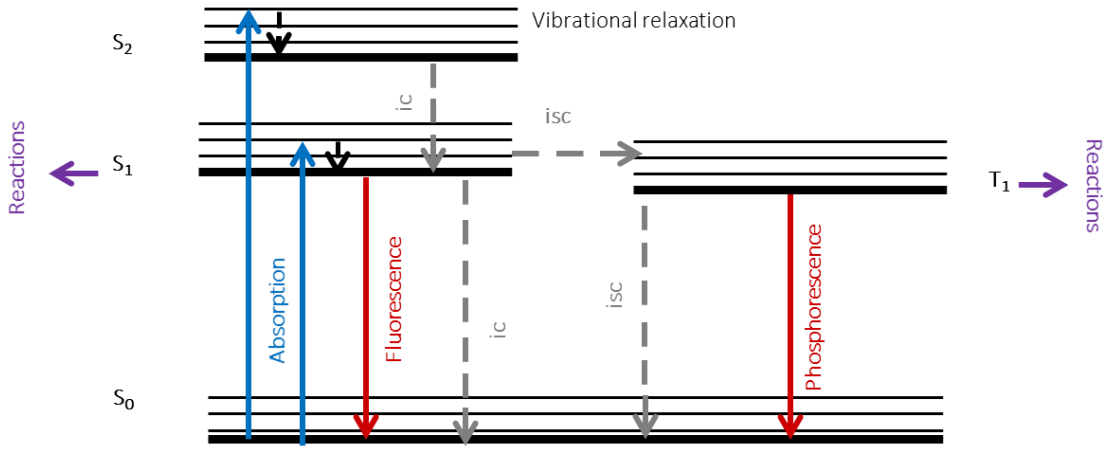


**Figure 1**: Jablonski diagram

The diagram starts from a molecule in the ground state ($S_0$), see Figure 2. Through the photon **absorption** process, an electron is promoted to a more energetic electronic level, known as first, second, etc., singlet excited states ($S_1$, $S_2$, etc.). Usually, the electron reaches the first singlet excited state ($S_1$), see Figure 2, since in case it would have reached any further level ($S_2$, etc.) it rapidly (in few picoseconds or even less) relaxes through **internal conversion** to the $S_1$. The electron can reach any of the vibrational levels within the $S_1$, but typically it relaxes to the lowest vibrational one through a rapid process called **vibrational relaxation** that normally takes few picoseconds.

The lifetime of the molecule at the $S_1$ is usually in the range of nanoseconds and there are several processes that can take place from here. For instance, it can return to the ground state by a radiative process (**fluorescence emission**) or by thermal conversion (**internal conversion**). Moreover, the molecule can suffer spin conversion to the first triplet excited state through **intersystem crossing**. In case of reaching the triplet excited state ($T_1$), see Figure 2, several processes may also happen; a non-emissive deactivation by **intersystem crossing** back to the ground state or a radiative deactivation by **phosphorescence emission**. In addition, singlet or triplet excited states (or even both) can react with a suitable molecule present in the media through **electron** or **energy transfer processes**; [3] these processes will be deeply explained in section 1.2. The spin conversion associated to the intersystem crossing makes lifetimes of triplets longer, in the order of microseconds, compared to those of the singlets.

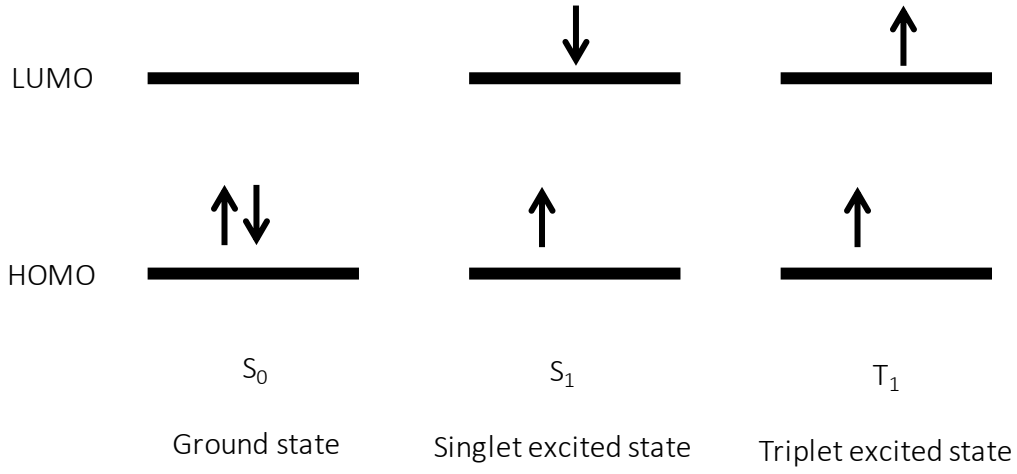


Figure 2: Spin electron configuration in the HOMO and LUMO.

In addition, it is worth mentioning that the pathways that a molecule can pursue after the absorption of light are not exclusive, but competitive among them. Therefore, the mechanistic understanding of a system is crucial for its optimization.

At this point, a comparison between classical chemistry and photochemistry can be made regarding the energy needed to activate a reaction. In classical chemistry, this energy is known as Thermal Activation Energy, while the energy employed in a photochemical process is given by the absorbed photons: for every quantum of light that is absorbed, only one molecule of substrate can react (in addition, other non-reactive photophysical processes such as internal conversion or luminescence emission may also occur), this is the Stark-Einsten law postulated at the beginning of the 20$^{th}$ century and known as the second law of photochemistry. The main difference between them arises in the range of energy that they manage: with the Thermal Activation, the translational, rotational and vibrational degrees of freedom are involved, but not the electronic ones, which can only be photochemically excited. For instance, the photons absorbed in the UV-vis range, comprise energies from 41 kcal mol$^{-1}$, at 700 nm, to energies as high as 143 kcal mol$^{-1}$, at 200 nm, being able to break a wide range of covalent bonds in organic chemistry, *ie.* from O-O bonds (35 kcal mol$^{-1}$) to O-H bonds (110 kcal mol$^{-1}$).[4] Therefore, the energy obtained by the excited molecule minimizes the energetic barrier to afford a subsequent chemical reaction, see Figure 3 . Moreover, photochemical reactions may be,

in principle, more selective than thermal ones, as modulation of light allows exciting an only one molecule in a mixture, while in a thermal reaction the entire pot should be heated to run the reaction.

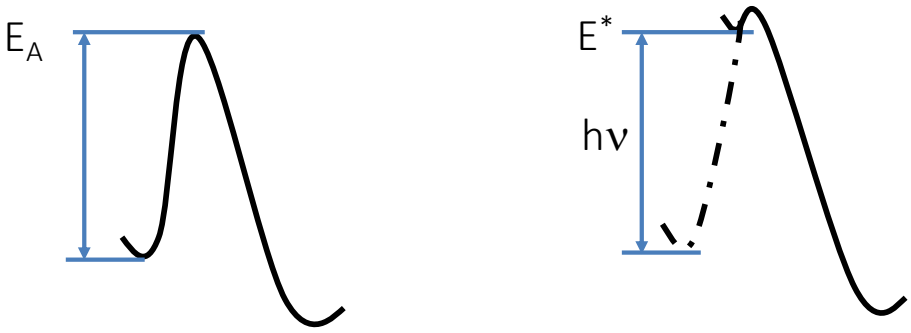


**Figure 3**: Simplified reaction coordinate system to compare the energetic barrier of a thermal (left) to a photoinduced (right) reaction, where $E_A$ represents the activation energy and hν the energy absorbed by the molecule to reach an excited state ($E^*$).

## 1.2. Energy transfer and electron transfer processes

When a molecule at any excited state (singlet or triplet) interacts with a second molecule in its ground state, several processes can follow that interaction: they include electron transfer and energy transfer, as anticipated in section 1.1. To explain these phenomena, the possible overlap between the molecular orbitals of the donor (D) and the acceptor (A) should be considered for both processes, and in addition, in the specific case of energy transfer, the interaction of an oscillating dipole electric field should also be taken into account.

Electron transfer requires orbital overlap between one molecule that is the donor (D), and the other one that is the acceptor (A). When the acceptor is at any excited state ($A^*$) the electron transfer will take place from the HOMO of D to the HOMO of $A^*$, resulting in the corresponding radical ions $A^{\cdot-}$ and $D^{\cdot+}$, see Figure 4A. On the contrary, when the donor is the excited species ($D^*$), electron transfer will take place from the LUMO of $D^*$ to the LUMO of A, resulting again in the corresponding radical anions $D^{\cdot+}$, and $A^{\cdot-}$, see Figure 4B. The capability of the excited molecules to act as electron donors and acceptors is a key factor for the photoredox catalysis and will be discussed in section 1.3.

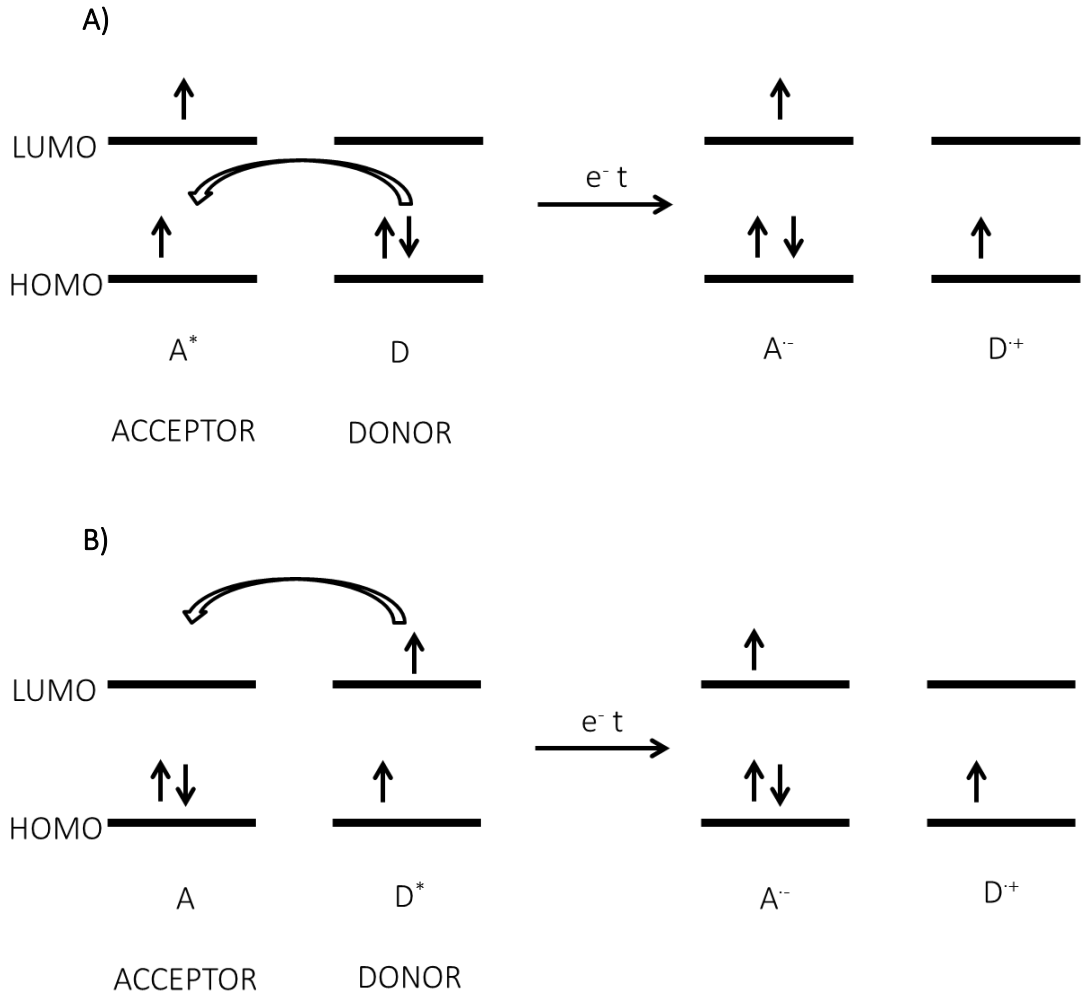


**Figure 4**: Representation of the electronic configurations involved in an electron transfer process, when the excited species is the acceptor (**A**) or the donor (**B**).

Energy transfer processes could take place through two mechanisms: the Dexter mechanism, which involves electron exchange and requires orbital overlap, or the Förster mechanism which involves a through space interaction dipole-dipole. In the case of energy transfer through electron exchange or Dexter mechanism, see Figure 5, an electron from the LUMO of the excited species ($D^*$) travels to the LUMO of the accepting species (A), and an electron from the HOMO of the accepting species (A) travels to the HOMO of the donor species ($D^*$). As a result, the donating species returns to the ground state and the accepting species reaches an excited state. Since Dexter mechanism requires molecular orbital overlap between D and A, the process is highly distance-dependent. In addition, the energy transfer will be possible regardless the singlet or triplet nature of $D^*$, see Figure 5A and B.

A)

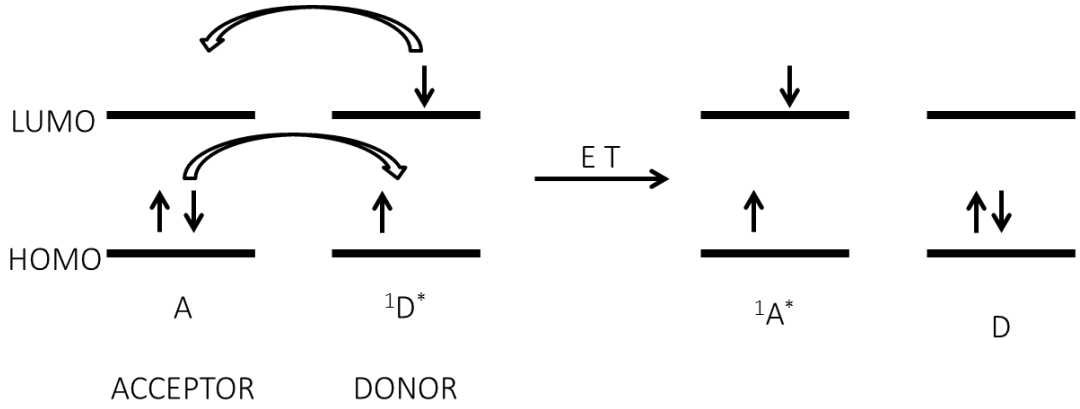


B)

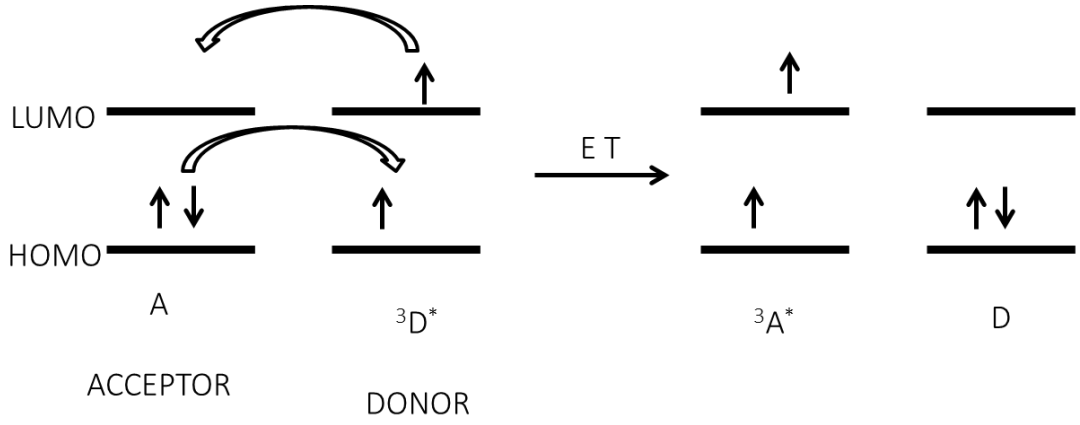


Figure 5: Representation of the electron exchange involved in an energy transfer process through a Dexter mechanism. The excited species is at the singlet excited state (A) or at the triplet excited state (B).

In the dipole – dipole interactions or Förster mechanism, an oscillating electric field induces the movement of one electron from the LUMO to the HOMO of the excited molecule ($D^*$) and the movement of a second electron from the HOMO to the LUMO of the second molecule (A), as a result, the excited molecule returns to its ground state (D) and the acceptor molecule reaches the excited state ($A^*$), see Figure 6. Since no electron is exchanged, there is no need for orbital overlap and that is why distances between both species can be longer than in the Dexter mechanism. However, due to the spin conservation, the Förster mechanism will only be possible when the donor is a singlet. The reason is simple, in the simultaneous electron movement from the LUMO to the

HOMO of the excited donor and from the HOMO to the LUMO of the acceptor, each species conserves its electrons. Therefore, when the excited species is a singlet, multiplicity is conserved, see Figure 6A, but when it is a triplet the spin inversion will not allow carrying out the process, see Figure 6B. [3, 5]

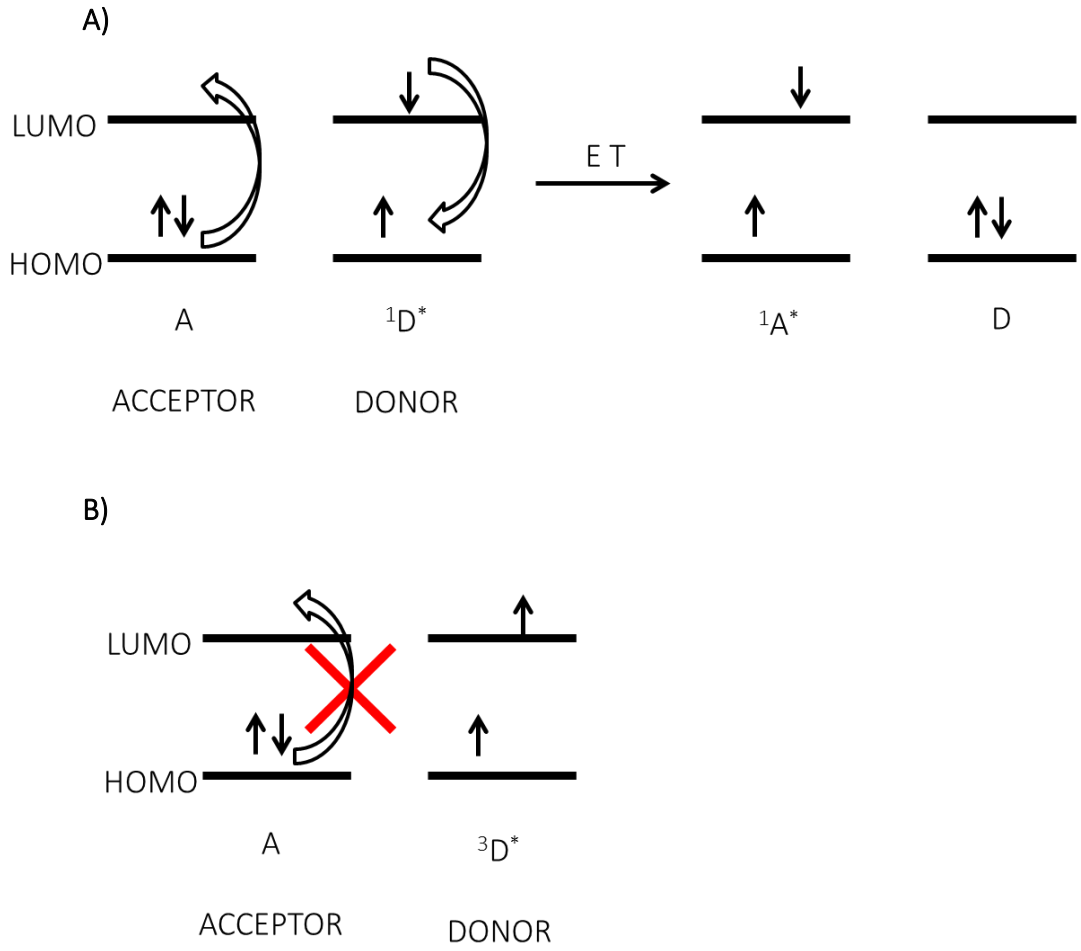


**Figure 6**: Representation of the electron exchanges involved in an energy transfer process through a Förster mechanism, when the donor is at the singlet excited state (**A**) or at the triplet excited state (**B**).

In the present dissertation electron transfer will be studied in detail for several photoredox systems. However, energy transfer is out of the scope and will just be applied in future sections as the process to obtain the singlet oxygen species ($^1O_2$) from oxygen.

## 1.3. Photoredox processes. Thermodynamic and kinetic analysis of photoredox processes

Photoredox processes are being exploited as catalytic cycles and are becoming a hot field considered as Green Chemistry. Photocatalysis has found applications in the degradation of recalcitrant pollutants from industrial wastewaters and more recently, in synthetic routes for new industrial procedures, among other applications. Its wide use is mainly due to the selective and mild conditions that it offers. The selectivity comes from the presence of specific chromophores in the molecular structure of the photocatalyst; therefore, depending on the selected photocatalyst, the wavelength of the irradiation source is modulated. On the other hand, the mild conditions come from the properties of the excited states, that offer the capability of acting as better electron donors and acceptors. This phenomenon can be explained by comparison of the electron affinity (EA) and the ionization potential (IP) from the ground and the excited states of a diamagnetic molecule, see Figure 7. The IP for the excited molecule is lower than that of the molecule at the ground state; while the EA is higher. Then, the addition of an electron to the half-filled HOMO of the excited molecule is more exothermic than its addition to the LUMO of the ground state molecule; therefore, the reduction process is thermodynamically more favored for an excited molecule. Regarding to the oxidation, removing an electron from the half-filled LUMO of the excited molecule is less endothermic than when it is taken from the HOMO of the ground state molecule (IP from the LUMO *vs* IP from the HOMO).[6]

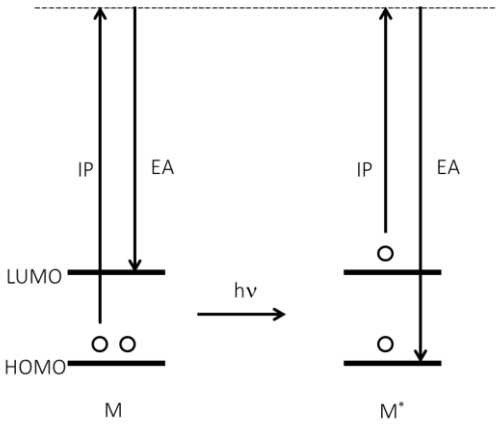


**Figure 7**: Reduction and oxidation of a molecule in its ground (left) or excited (right) state.

This behavior can be mathematically explained with the Gibbs free energy expression, for the case of the ground state molecule (Eq. 1), or with its adaptation to the photoredox reaction, with the photoinduced free Gibbs energy equation, for the case of the excited molecule (Eq. 2).[7]

A typical redox process between two molecules at the ground state can be described as:

$$D + A \rightarrow D^{\cdot+} + A^{\cdot-}$$

Therefore, the thermodynamic feasibility of the process will be calculated according to the Gibbs free energy:

$$\textbf{Eq. 1.} \quad \Delta G^0 = -[E^0_{red}(A/A^{\cdot-}) - E^0_{red}(D^{\cdot+}/D)] + \Delta E_{Coulombic}$$

Where $E^0_{red}(A/A^{\cdot-})$ is the reduction potential of the accepting species, $E^0_{red}(D^{\cdot+}/D)$ is the reduction potential of the donating species and $\Delta E_{Coulombic}$ measures the interactions between the ions in the dielectric constant of the employed solvent. The latter term could be discarded when polar solvents, with high dielectric constants that reduce the Coulombic attraction between ions, are used.[6]

In the case of a photoredox system in which, for example, the acceptor species is the excited molecule, the process can be described as:

$$A + h\nu \rightarrow A^*$$

$$A^* + D \rightarrow A^{\cdot-} + D^{\cdot+}$$

In this case, the thermodynamics needs to take into account the energy of the excited species, and it will be given by the photoinduced Gibbs free energy equation:

$$\textbf{Eq. 2.} \quad \Delta G^0_{et} = -[E^o_{red}(A/A^{\cdot-}) - E^o_{red}(D^{\cdot+}/D)] - E^*(\mathrm{A}) + \Delta E_{Coulombic}$$

Where $E^*(\mathrm{A})$ is the energy of the excited state of the molecule (singlet or triplet). Attending now to Eq. 2, it is easy to observe how the subtraction of the energy of the excited state results in a more thermodynamically favored process. Under this concept relies one of the most energetic advantages of photochemistry. In some cases, it is used

the redox potential of the excited state, that, rearranging from Eq. 2, can be defined as in Eq. 3.

$$\textbf{Eq. 3}\ (E^0_{red}(A/A^{\cdot -}))^* = E^o_{red}(A/A^{\cdot -}) + E^*(\mathrm{A})$$

Eq. 2 will be very useful in further experimental sections to assess whether a photochemical reaction will be thermodynamically favorable. However, this analysis is not enough to confirm whether a photoredox process will take place. Since the participating species exhibit short lifetimes, kinetics of the excited state molecules will be crucial to understand if a process will take place or not. More specifically, the lifetime of the excited species will act as a "timer", then the reaction must take place during the "countdown" of the excited species, if it cannot occur in that period of time, it will not be effective despite of being thermodynamically favored. Therefore both analyses should be taken into account to understand the mechanism involved in a photoredox process and optimize it.[6]

The study of the kinetics usually requires spectroscopic and fast kinetic tools such as steady-state and time-resolved fluorescence emission spectroscopy, to study the processes that involve the singlet, and phosphorescence emission and laser flash photolysis (LFP), to study the processes involving the triplet. In general terms, upon steady state fluorescence experiments, the emission of the excited species is measured upon addition of the quencher; therefore, if there is an interaction between the ground state or the singlet state of the photocatalyst and the quencher, the emission intensity will decrease. To determine the kinetic constant of such process, the Stern-Volmer equation is employed:

$$\textbf{Eq. 4.}\quad \frac{I_0}{I_i} = 1 + K_{SV} \cdot [Q]_i$$

$$\textbf{Eq. 5.}\quad k_q = \frac{K_{SV}}{\tau_0}$$

Where $I_0$ is the emission of the photocatalyst (in arbitrary units), $I_i$ is the emission of the photocatalyst (in arbitrary units) after adding a specific concentration of the quencher, $[Q]_i$ is the quencher concentration at each specific addition (M) , $K_{SV}$ is the steady-state Stern Volmer constant ($M^{-1}$), $\tau_0$ is the lifetime of the excited species in the

absence of the quencher (s) and $k_q$ is the kinetic constant ($M^{-1} \cdot s^{-1}$). This experiment is useful as indicating if a process has taken place. However, this information is not unequivocal since any formed complex involving the ground state of the photocatalyst may provide a decrease in the fluorescence emission that does not correspond to a real quenching of the singlet excited state. Therefore, time-resolved experiments obtained from time-resolved fluorometer (to evaluate participation of the singlet) and LFP experiments (to evaluate participation of the triplet) are needed. In this kind of experiments, the lifetime of the excited species is measured upon addition of increasing concentration of quencher. To determine the kinetic constant, the Stern-Volmer equation is applied:

$$\text{Eq. 6.} \quad \frac{1}{\tau_i} = \frac{1}{\tau_0} + k_q \cdot [Q]_i$$

Where $\tau_i$ (s) is the lifetime of the excited species after adding a specific amount of quencher. Although these experiments provide the kinetic constant of the quenching process, a more valuable piece of evidence of a photoredox reaction will be given by the absorption spectrum of any of the intermediates formed in the process from LFP experiments if their lifetime is long enough. These spectra can act as an unequivocal proof of the photoredox process.

Finally, in the case of a ground state complex formation, Job's plot experiments can be carried out in order to investigate the stoichiometry of the complex ($PC^{+\delta}$--$Q^{\delta'+}$). [8, 9] In these experiments, the UV absorption is recorded at a specific wavelength for several solutions, keeping the total concentration [PC + Q] constant, while varying the corresponding molar fraction. For an unknown stoichiometry, the equilibrium complex will be described as:

$$PC + nQ \underset{}{\overset{K}{\rightleftharpoons}} PC\text{--}Q_n$$

Thus, the equilibrium constant will be given by:

$$\text{Eq. 7.} \quad K = \frac{[PC\cdots Q_n]}{([PC]_0 - [PC\cdots Q_n])([Q]_0 - n[PC\cdots Q_n])^n}$$

Where $[PC]_0$ is the initial concentration of photocatalyst, $[Q]_0$ is the initial concentration of quencher and $[PC{-}{-}{-}Q_n]$ is the concentration of complex formed in the equilibrium.

In the common case of a 1:1 stoichiometry, the Benesi-Hildebrand relationship [8, 9] can be used to determine the complexation constant from the steady-state fluorescence data previously obtained.

$$\text{Eq. 8. } \frac{1}{I_o - I} = \frac{1}{I_o} + \frac{1}{I_0 K[Q]}$$

Where Q represents the quencher (M), I is the fluorescence emission intensity and K is the resulting complexation constant ($M^{-1}$).

An overall analysis of the described experiments is needed to understand the mechanism involved in a photoredox process. However, these valuable tools are not available in every laboratory and despite the huge advance that the photoredox field is living, little attention has been paid to the examination of the kinetic feasibility of the involved processes. Therefore, the mechanisms involved are not always clear enough or they are uncomplete. The group of Prof. Scaiano in Ottawa, among others, has pointed the lack in the field, and, as a result, several articles have been published as "tutorials" that explain how to analyze thermodynamically and kinetically this kind of systems, in which photocatalysis is applied to develop synthetic routes. [6, 10]

Attending now to the nature of the photocatalysts it is worth mentioning that in the last decades, the most commonly employed visible-light photocatalysts are metal complexes based on Ru or Ir. Though advantageous in terms of stability and activity, these metals are expensive and scarce on Earth, which leads into difficulties with respect to large-scale application and sustainability for industry. [11] Maybe that is why photocatalysis, despite demonstrating to be a top tool, is still regarded as a process confined to the laboratory. Thus, the use of organic molecules, able to absorb visible light, as photocatalysts, may provide a deep understanding of the mechanisms and will contribute to the current state of art.

## 1.4. Application of photochemistry and photocatalysis

Photochemistry has been applied to many different fields.[12] Some of them include the development of photochemical devices, such as irradiation sources for photochemical reactors, LEDs, etc.; the study of new synthetic routes in chemistry; the branch known as photoelectrochemistry, which involves solar cells, photocatalytic water splitting for $H_2$ production or harvesting light as an artificial photosynthesis for biofuel production; the biomedical field, in which applications are mainly focused on deleterious effects of light, photoprotection or therapeutic uses of light; several techniques such as fluorescence microscopy, lithography, imaging, electro-generated chemiluminescence, etc. Besides, the area known as environmental photochemistry covers topics such as degradation of pollutants through advanced oxidation processes (AOP), in which the use of organic photocatalysis has demonstrated to be a potential alternative. The study of all of them is obviously out of the scope of the present dissertation. Herein, Part I and II, are devoted to photocatalysis for wastewater remediation, and Part III, describes the application of photocatalysis to synthetic chemical purposes. Nevertheless, since one of the main goals of this work is the study of the mechanisms involved in a photoredox process, it will be demonstrated how such two different fields can be rationally analysed with the tools above described.

## 1.5. Contaminants of Emerging Concern and Photocatalysis as an Advanced Oxidation Process (AOP)

### 1.5.1. Contaminants of Emerging Concern

Water is essential for life on Earth; however, about 15% of the world's population lives in areas of water stress,[13] caused mainly by anthropogenic activities. Within the European Community, water resources are under growing pressure due to the increasing demand, need of good quality and enough quantity for all uses.

Under this context, the European Union created in 2000, a common legislation, the Water Framework Directive, WFD (2000/60/CE), to ensure the water quality and also, to establish homogeneous environmental goals among the State Members. Within this Directive, the formulation of a list of 33 compounds known as Priority Substances was achieved. A Priority Substance is a compound that can be risky for the aquatic media due

to several aspects: an intrinsic danger related to the nature of the substance, as aquatic eco-toxicity and human toxicity, or due to proofs obtained from a wide environmental exposure. The 2013/39/UE Directive updated this list up to 45 substances and established that the Environmental Quality Standards, EQS, must be achieved before the end of 2027 for all the 45 substances. These substances include metals such as cadmium, lead or mercury, benzylic compounds or halogenated compounds, among others. The directive specifies their maximum concentration permitted in water, and highlights that wastewater treatments can be expensive, thus, suggests the development of innovative technologies to obtain cheaper treatments.

In parallel to this, a new concept has been introduced in the last years in the field of water treatment, that is Contaminants of Emerging Concern, CECs, also known as Emerging Pollutants, EPs. This term usually refers to compounds of different origin and chemical composition, whose presence in the environment is not significant in terms of distribution or concentration, therefore they may have passed unnoticed,[14] and there is little information about their potential impact in the environment. However, the highly specialized detection equipment available nowadays allows detecting these substances,[15] therefore their presence is becoming a concern.[16, 17] Among them, there are pesticides, pharmaceutical compounds, illegal drugs, steroidal hormones, personal care products, surfactants, flame retardants, food additives or "lifestyle products" like caffeine or nicotine.[14] They usually reach the environment through domestic or industrial wastewaters,[15, 18] hospital effluents,[19] and agricultural and farming activity.[20] Their massive production and use introduce constantly these compounds in the environment, therefore irrespective to whether they are persistent or not, they could have a negative impact. Due to the lack of information of these substances, a new directive (2015/495/CE) was published in 2015. This directive stablishes a first observation list with 10 substances which are required to be monitored in the Union, in order to provide solid knowledge for future priority assignation. The observation list substances have been selected among those which current available information points out that may be significantly risky at the Union for the aquatic systems. To be included at the observation list, substances must represent a risk for the aquatic media, used at the State members and poured to the aquatic media, but rarely

monitored. Therefore, at present, there is no regulation for these compounds, but they are potential candidates to be included in future regulations, depending on their effect on health and on aquatic organisms.

Conventional wastewater treatment plants are not properly designed to remove CECs.[21, 22] Moreover, pollutants such as pharmaceuticals or personal care products exhibit a great variety of chemical properties, therefore the success in their removal will depend on their particular properties.[14] All these precedents have encouraged scientific community to investigate new treatments for the removal of the so-called CECs. Some of them are ultrafiltration, use of adsorbents or membranes, biological treatments, direct photolysis, advanced oxidation processes or a combination of them. However, it is worth mentioning that these protocols are not fully established and are on preliminary steps of research.[23, 24] Up to date, no effective removal technology has been developed to simultaneously remove all the CECs, although some technologies have demonstrated potential.[25]

### 1.5.2. Photocatalysis as an Advanced Oxidation Process

In 1987, Glaze *et al.* contributed with one of the first references about Advanced Oxidation Processes, AOP's, defining them as processes that mainly use hydroxyl radical ($OH^{\cdot}$), generated through different pathways, to oxidize hardly degradable matter at mild conditions of pressure and temperature.[26] Hydroxyl radical is a very oxidizing reactive oxygen species (ROS) with an oxidation potential of 2.8 V (at pH 0) or 1.95 (at pH 14) *vs* SCE; therefore, it rapidly reacts non-selectively with other compounds with rate constants in the order of $10^8 – 10^{10}$ $M^{-1}s^{-1}$. [27] Due to its short lifetime, hydroxyl radical is *in situ* produced through different methods.[27] Moreover, other AOP's, that may include hydroxyl radical, have been developed during the last decades. Roughly, AOP's are currently defined as physico-chemical processes able to produce transient reactive species which are highly efficient in the oxidation of the hardly degradable matter, and, in principle, this matter is transformed in innocuous derivatives that are then treatable with further processes. Current AOP's are mainly based on $UV/O_3$, $UV/H_2O_2$, Fenton, photo-Fenton, nonthermal plasmas, sonolysis, photocatalysis, radiolysis, supercritical water oxidation processes or the generation of other reactive oxygen species, such as

superoxide anion radical, hydrogen peroxide and singlet oxygen.[28-32] All the generated transient species are highly oxidizing, such as the hydroxyl radical, and therefore, non-selective, being able to oxidize mixtures of compounds that would remain stable under other conditions. Therefore, the main advantage that they offer remains in their low selectivity, and, in principle, in the generation of non-dangerous by-products. Furthermore, several of them can be activated by UV-vis light, making them very interesting processes regarding to environmental sustainability criteria.[24] All these characteristics, convert these methodologies in potential processes to remove the so-called CECs in order to depurate wastewaters,[33] as an alternative for conventional treatments.[34-37] Nowadays, several AOP have been applied for the decontamination of waters, gases or soils.[38-40]

In the case of heterogeneous photocatalysis, the most widely used photocatalyst is $TiO_2$. This photocatalyst exhibits great activity, high stability, low cost and nonenvironmental impact. It is commercially found as anatase and rutile, being anatase the most active one.

Upon UV irradiation, $TiO_2$ promotes one of its electrons from the valence band to the conduction band (band gap of 3.2 eV), becoming a very reactive species.[41] Subsequently, it can mainly experience two different reactions: hydroxyl radical formation (reaction with water) and superoxide radical anion formation (reaction with oxygen).[42] Many works using $TiO_2$ have been reported, such as the photodegradation of 3,4-dichloropropionamide,[43] paraquat,[44] carbetamide,[45] carbaryl[46] and other carbamates,[47-49] imidacloprid and other neonicotinoid insecticides,[50, 51] imazalil,[52] phenols and chlorophenols,[53-56] nitrophenols,[57] lindane[58, 59], several organophoosphorous pesticides,[49, 60-66] pyrimethanil,[67], phenylurea herbicides,[68] isoproturon,[69] etc.

Despite all these pros in the use of $TiO_2$, there are other practical problems associated to it. It is only able to absorb light in the UV-A and UV-B regions; therefore, only around 7% of the solar spectrum is used, see Figure 8. Besides, it needs appropriate electron acceptors to avoid recombination of the electron and hole, since in their absence, it is the most effective process. Finally, despite being heterogeneous, $TiO_2$ is

generally used as a thin powder, and at large scale, the catalyst-recovering step is not easy due to the small particle size.[24]

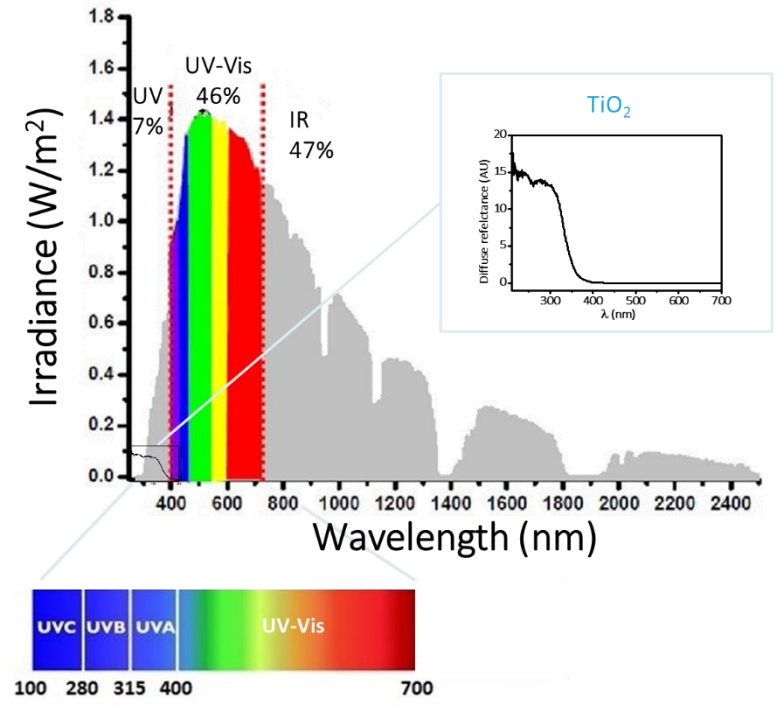


**Figure 8**: Intensity and ranges of the Solar emission spectrum. Inset: $TiO_2$ diffuse reflectance.

A less explored field in the decontamination of toxic effluents, as an alternative to other more stablished AOP, is the use of organic photocatalysts.[70] Under this context, some examples are the photodegradation of pollutants such as mercaptodimethur and ethiofencarb using anthraquinone,[71] chloroaromatic pesticides using *N,N,N',N'*-tetramethylbenzidine,[72] fenitrothion and organophosphorous pesticides using acetone,[73, 74] organophosphorous pesticides, phenylamide fungicides, sulfonylurea and chlorpyrifos using humic and fulvic materials,[75-78] 2-mercaptobenzothiazole using methylene blue,[79] phenols and other pesticides with a variety of photocatalysts [80-85], etc.

The main advantage of using organic dyes as photocatalysts remains in the fact that they do not contain metals and normally exhibit strong absorption bands in the UV-vis range, being able to more efficiently use the visible portion of the solar irradiation, see Figure 8.[70] Therefore they take advantage of the range that Sun mainly offers

(Visible light) in comparison with $TiO_2$ which only uses UV-B and UV-A, see Figure 8. The present thesis will be focused on the use of organic dyes as photocatalysts for wastewater remediation, therefore, only this procedure will be deeply commented below.

The excited states of organic photocatalysts present better redox properties than ground states; therefore, they will be able to oxidize the compounds present in the media through electron transfer mechanism. Besides, some of these photocatalysts can also generate reactive oxygen species (ROS). [70, 86, 87] For this reason, the mechanism underlying these photodegradations deserves a deeper investigation.

Regarding to the classification of the oxidizing reactions that involve photocatalysts able to act trough electron transfer processes and also to generate any kind of ROS, a very active controversy has been found in the literature.[88] The probably most cited work related to this topic is that presented by Foote in 1991, which accumulates more than one thousand citations.[89] In this work, the author classifies as Type I reactions those which involves either hydrogen atom or electron transfer, between the photocatalyst, from any of its excited states, and any substrate or solvent, yielding radicals. Meanwhile, Type II reaction corresponds to the reaction between the excited photocatalyst and oxygen. For the present thesis, Foote's classification has been completed with other works.[90] Therefore, an electron transfer mechanism between the excited photocatalyst and a substrate that may be oxygen, resulting in the corresponding radicals would be considered a Type I photoreaction. Meanwhile, a Type II photosensitization will happen through energy transfer from the excited photocatalyst to oxygen, generating singlet oxygen, see Scheme 1.

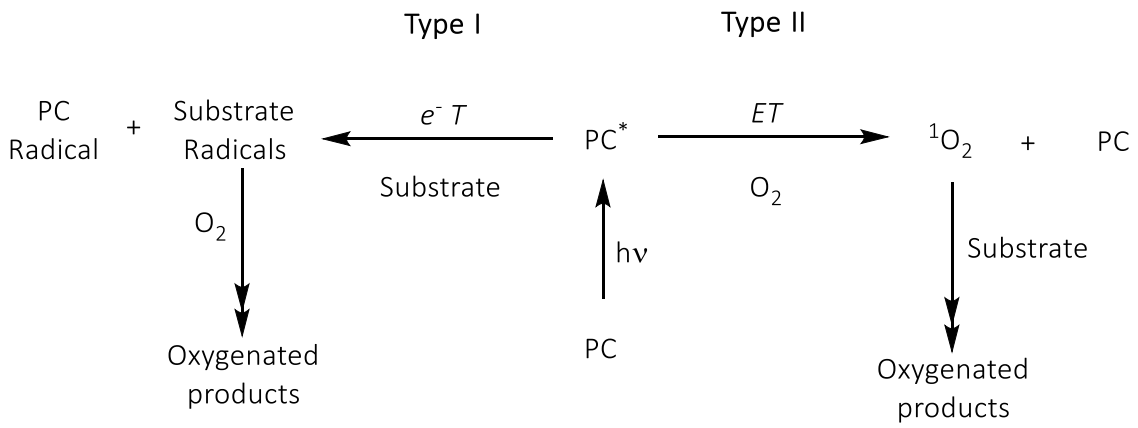


**Scheme 1:** Classification of processes as Type I and Type II, where PC represents the photocatalyst.

When a photocatalyst is able to react through both Type I and Type II mechanisms, elucidation of the involved pathway is not trivial. Several experiments have to be performed to determine if singlet oxygen is being formed and to elucidate if is actually working as an oxidant for the pollutants. In the present thesis, time resolved phosphorescence measurements using laser flash photolysis will be employed to determine the phosphorescence emission (at 1270 nm) of $^1O_2$ and the shorten of its lifetime upon addition of the substrates. Results will be analyzed together with direct reaction between excited states of the photocatalysts and the pollutants.

Nevertheless, the use of organic photocatalysts in pollutants' degradation also comprises several limitations. Among them, it is difficult to recover them after the reaction and they could present potential toxicity. To overcome these drawbacks, heterogenization by supporting the organic photocatalysts onto solid materials such as adsorption into zeolites or covalent linkage to different inorganic supports is desirable. Nevertheless, understanding their behavior in the homogeneous phase is crucial prior to heterogenization.[12] Under this context, the present dissertation will be focused on the use of several photocatalysts as homogeneous photoredox process mediators to study both, the viability of their potential and more interestingly, the elucidation of the involved mechanisms.

More recently, a novel class of treatments, called Advanced Reduction Processes (ARPs), are being developed alone, or in combination with the more common oxidation

techniques under the name of Advanced Oxidation and Reduction Processes (AO/RPs). The basis of ARPs is similar to that of AOPs, but in this case highly reducing radicals are applied for degradation of contaminants. Therefore, the difference between AOPs and ARPs relies in the nature of the reactive species which react with the pollutants to degrade them.[91] Different reducing agents have been used, such as, sulfur dioxide radical anion ($SO_2^{\cdot-}$) obtained from dithionite ($S_2O_4^{2-}$);[92] sulfite radical anion ($SO_3^{\cdot-}$) and hydrated electron ($e^-_{eq}$) [93-95] obtained from sulfurous acid ($H_2SO_3$), bisulfite ($HSO_3^-$) and sulfite ($SO_3^{2-}$). In the case of sulfite radical anion, it could act as reductant (donating an electron and reacting with water to form sulfate), or as an oxidant (accepting an electron to return to sulfite);[91] and also metals such as elemental (zero valent) iron (ZVI) [96, 97] with a redox potential of -0.45 V. [98]

$S_2O_4^{2-} \rightarrow 2SO_2^{\cdot-}$

$SO_3^{2-} + h\nu\ (315nm) \rightarrow SO_3^{\cdot-} + e_{eq}$

However, in general, reduction processes are used in combination as AO/RPs. AO/RPs usually involve the formation of hydroxyl radicals ($OH^{\cdot}$) as oxidizing species and hydrated electrons ($e^-_{aq}$) as reducing species.[99, 100] A studied process to generate these species is through Vacuum UV (VUV; 185 + 254 nm) in which $OH^{\cdot}$ and $e^-_{eq}$ are formed through photoionization and homolysis:[101, 102]

Photoionization:

$H_2O + VUV\ (\lambda = 185\ nm) \rightarrow OH^{\cdot} + H^+ + e^-_{eq}$

Homolysis:

$H_2O + VUV\ (\lambda = 185\ nm) \rightarrow OH^{\cdot} + H^{\cdot}$

$H^{\cdot} + H_2O \rightarrow H_3O^+ + e^-_{eq}$

These procedures are in a first stage of study and deserve research to develop the potential of ARPs and/or AORPs.[91, 98]

## 1.6. Background and collaborations within our research group

Recent results directly related with this Thesis come from the projects that have been developed within the Photochemistry Group at the Institute of Chemical Technology from the Universitat Politècnica de València, as independent studies or in collaboration with other groups. The most relevant are summarized in this section.

1) As starting point, a deep study on the potential of 2,4,6-triphenylpyrylium tetrafluoroborate ($TPP^+$) as an electron-transfer photosensitizer was performed. Thus,

$TPP^+$ was fully characterized and several applications of this photocatalyst were explained. This study was published as a review which accumulates around 230 cites.[86]

2) A wide compilation of the properties of different photocatalysts used in wastewater remediation. This study resulted in a review that summarizes the main photophysical data from the typical photocatalysts used in this field and accumulates more that 140 cites. [70]

3) A study on the role of $OH^{\cdot}$ as species responsible for the photodegradation of several pesticides under different oxidative conditions.[103, 104]

4) A doctoral thesis entitled "*Efecto de distintas especies reactivas generadas fotoquímicamente sobre la eliminación de contaminantes presentes en aguas naturales*" by Juan Gomis. In this thesis, the reactivity of a model mixture of pollutants was studied through several advanced oxidation processes. Among them, the use of $TPP^+$ and $TPTP^+$ (2,4,6-triphenylthiapyrylium) as photocatalysts to photodegrade them were evaluated. These photochemical preliminary results worked as starting point for Chapters 4 and 5 of the present Thesis.

With this background, the present Thesis is divided in three parts. The first part is devoted to Oxidative Electron Transfer, the second part is about Type I *vs* Type II processes, and the third part is entitled Reductive Electron Transfer. For the oxidative electron transfer processes for wastewater remediation, two photocatalysts ($TPP^+$ and $TPTP^+$) have been employed with different objectives. For the investigation of Type I *vs* Type II processes, three photocatalysts (*N*-methylquinolinium, rose bengal and perinaphthenone) were evaluated for wastewater remediation as photocatalysts able to act trough the two different pathways. Finally, for reductive electron transfer processes, riboflavin has been used as a photocatalyst able to photochemically give rise to a reduced species that subsequently act as a reductant of several halogenated compounds.

# 2. Objectives

The general objective of this Thesis is to use organic photocatalysts to gain a deep understanding of different photoredox processes. Under this context, the specific objectives of the present Thesis are:

- To study the viability of organic photocatalysts as photoredox process initiators for wastewater remediation.
- To provide evidence for the formation of intermediates to elucidate the mechanisms involved in the photoredox reactions.
- To investigate the contribution of Type I *vs* Type II mechanisms in the photodegradation of pollutants.
- To investigate the kinetics of the intermediates involved in photocatalytic processes with chemical purposes.

*PART I:*

# *OXIDATIVE ELECTRON TRANSFER PROCESSES*

# Preamble

The use of organic photocatalysis as an advanced oxidation process (AOP) is an alternative that has demonstrated high efficiency for removal of recalcitrant organic contaminants.[24, 105-108] The photodegradation occurs through the formation of highly reactive species that subsequently react with the pollutants. Therefore, organic photocatalysts have been widely employed to oxidize pesticides,[82, 103] or emerging pollutants, such as drugs in wastewaters effluents.[109-111] One of the main advantages of organic photocatalysts is that they exhibit absorption bands in the UV-vis region, which can be excited to generate transient species able to interact with the substrates.[70, 112] Among them, solar-driven ones are particularly interesting since they could be considered as green methodologies.[107] A complete analysis of these systems requires the possibility of monitoring the derived-excited species which usually exhibit short lifetimes. Thus, the difficult detection of these short-lived primary key species involved in the photocatalytic processes has hampered the elucidation of the reaction mechanisms behind these reactions.[104] Interestingly, photophysical techniques based on emission and UV-vis absorption spectroscopy, provide time-resolved data in the nano or microsecond scale. They allow direct monitoring and quantification of reactive species; therefore, they can be applied to gain insight into the mechanistic aspects of the photo-redox reactions.[70]

Under this context, organic photocatalysts, such as 2,4,6-triphenylpyrylium ($TPP^+$) and 2,4,6-triphenylthiapyrylium ($TPTP^+$) salts, see Figure 9, have been reported as good oxidants from their excited states, see section 1.3. Both photocatalysts are able to absorb UV-vis light and have been employed to produce the photodegradation of pesticides under real solar irradiation mainly through electron transfer mechanisms.[85, 113-115]

More specifically, upon irradiation, both can oxidize contaminants from their singlet and triplet excited states and also through the formation of ground-state complexes. Their photophysical properties are shown in Table 1.[103, 111, 116, 117]

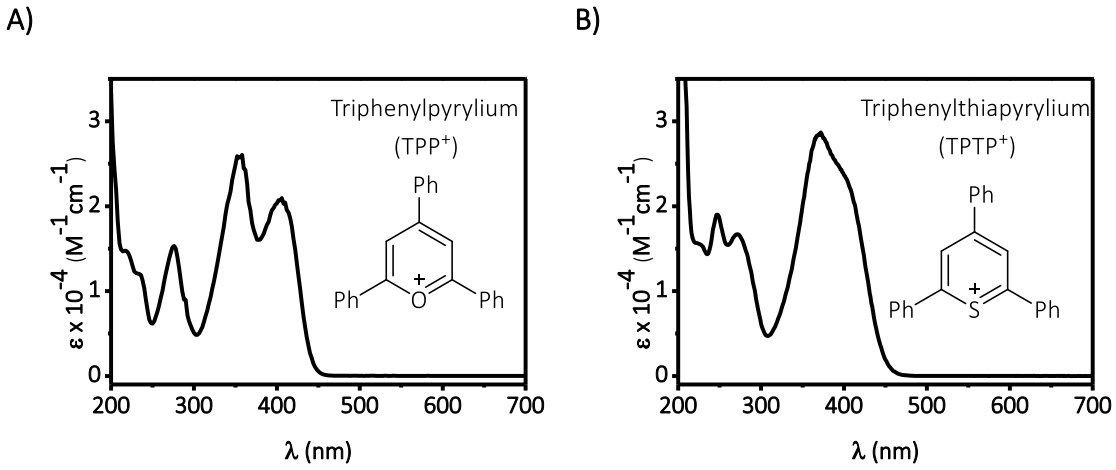


**Figure 9**: Chemical structure and UV-vis absorption spectra of 2,4,6-triphenylpyrylium ($TPP^+$) salt (**A**) and 2,4,6-triphenylthiapyrylium ($TPTP^+$) salt (**B**) in acetonitrile.

**Table 1**: Main photophysical properties of $TPP^+$ and $TPTP^+$.[70]

| Parameter | $TPP^+$ | $TPTP^+$ |
|---|---|---|
| $\Phi_F$ | 0.47 | 0.06 |
| $\Phi_{ISC}$ | 0.53 | 0.94 |
| $\tau_S$ | $4.4 \times 10^{-9}$ s | $4.4 \times 10^{-9}$ s |
| $\tau_T$ | $6.3 \times 10^{-6}$ s | $4.4 \times 10^{-6}$ s |
| $E_S$ | 66 kcal $mol^{-1}$ | 66 kcal $mol^{-1}$ |
| $E_T$ | 53 kcal $mol^{-1}$ | 52 kcal $mol^{-1}$ |
| $^1O_2$ | none | none |
| $O_2^{\cdot-}$ | none | none |

On these bases, these photocatalysts have been selected herein with three different purposes:

i) In the first project, the viability of the photodegradation of two pollutants from cork industry, gallic acid and 2,4,6-trichloroanisole, and the involved mechanisms, have been evaluated using both photocatalysts.

ii) In the second study, direct detection of all the $TPP^+$ derived short-lived intermediates in the photocatalyzed oxidation of a mixture of pollutants using $TPP^+$ was proposed as a methodology to assess the photodegradation extent.

iii) In the last study, the role of singlet and triplet excited states in the photocatalytic treatment of a mixture of pollutants, at different concentrations, was evaluated using $TPTP^+$ as photocatalyst.

# 3. Photocatalytic Treatment of Cork Wastewater Pollutants. Degradation of Gallic Acid and Trichloroanisole using Triphenyl(thia)pyrylium salts.

## 3.1. Introduction

This chapter is focused on investigating the photocatalytic degradation of real pollutants present in wastewaters coming from a typical industry in Spain. Wine production in Spain involves a parallel cork stoppers industry to guarantee the quality of the product until consumption. The production of cork stoppers includes a post-harvest treatment of raw material with water at high temperatures to improve their plastic properties. However, the generated dark complex liquor contains suspended solids and also a high concentration of organic matter, see Table 2,[118, 119], being polyphenolic compounds the most representative organic pollutants.[120, 121] This kind of effluent exhibits low biodegradability, reducing the effectiveness of conventional biological treatments; [122-124] therefore the application of photocatalytic tools for their degradation offers good expectations.

Table 2: Typical composition of cork boiling and bleaching wastewaters.[119]

| Parameter | Cork boiling wastewater | Cork bleaching wastewate |
|---|---|---|
| Chloride (mg/L) | 0.7 | 2.5 |
| Sulphate (mg/L) | 42.0 | 1549 |
| Nitrate (mg $NO_3^-$/L) | 57.0 | 4.1 |
| Nitrite (mg $NO_2^-$/L) | < 0.01 | 0.24 |
| Phosphates (mg P/L) | 5.1 | 3.0 |
| Potassium (mg K/L) | 1582 | 123 |
| Sodium (mg Na/L) | 51 | 3954 |
| Calcium (mg Ca/L) | 35 | 21.5 |
| Magnesium (mg Mg/L) | 6.4 | 5.1 |
| Iron (mg Fe/L) | 1.7 | 1.4 |
| Phenols (mg/l) | 73.9 | 12.7 |
| Polyphenols (mg caffeic acid/L) | 740 | 24 |

Under this context, the aim of the present chapter is to investigate the photocatalytic degradation of gallic acid (GA) and 2,4,6-trichloroanisole (TCA), Figure 10, two typical pollutants present in the cork industry wastewaters, using $TPP^+$ and $TPTP^+$ as

organic photocatalysts, see Figure 9 and Table 1 in the Preamble of Part I. In addition, the involved mechanisms will be investigated to deeper explain the behavior of the involved transient species in the presence of each pollutant.

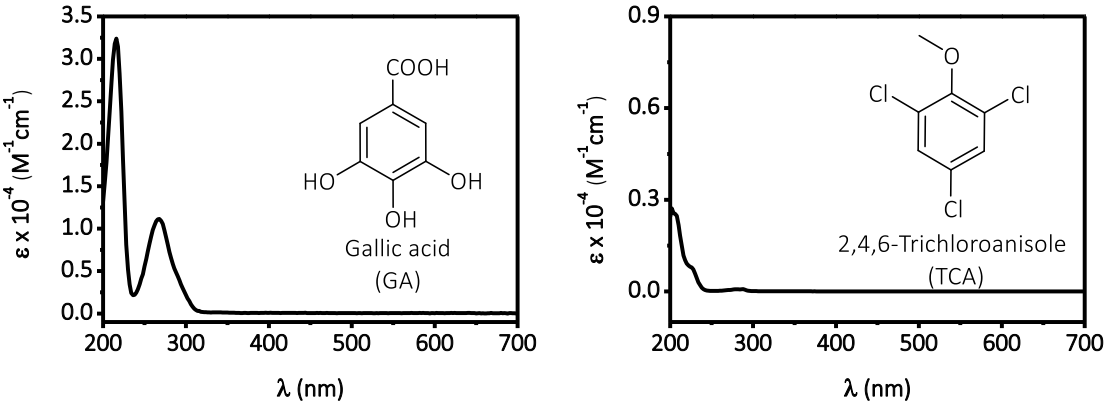


Figure 10: Chemical structures of the selected cork wastewater pollutants together with their corresponding UV-visible absorption spectra in acetonitrile.

## 3.2. Results and discussion

The efficiency of the degradation of GA and TCA through homogeneous photocatalysis using $TPP^+$ or $TPTP^+$ acting *via* electron transfer [86, 125] was evaluated in organic media, under $N_2$ and air. Lamps centred at 420 nm were used to ensure selective excitation of $TP(T)P^{+\cdot}$, and HPLC or GC analysis were used to monitor the disappearance of GA or TCA, respectively.

Figure 11 shows complete removal of GA in less than one hour, while TCA was more reluctant to degradation. More specifically, in the case of TCA, the reaction rate decreased considerably after 20 hours, although 90% of TCA removal was only achieved after 50 hours using $TPTP^+$ under air. This decrease in the photodegradation rate after 20 hours, is attributed to the partial solvolysis of the central heterocyclic ring of the photocatalysts, which has been observed previously and was eventually solved upon adsorption onto inorganic supports.[114] Aerobic photodegradations were more efficient, regardless the photocatalyst used, than the anaerobic ones; however, GA was more efficiently removed with $TPP^+$, while $TPTP^+$ gave higher removal yields in the case of TCA.

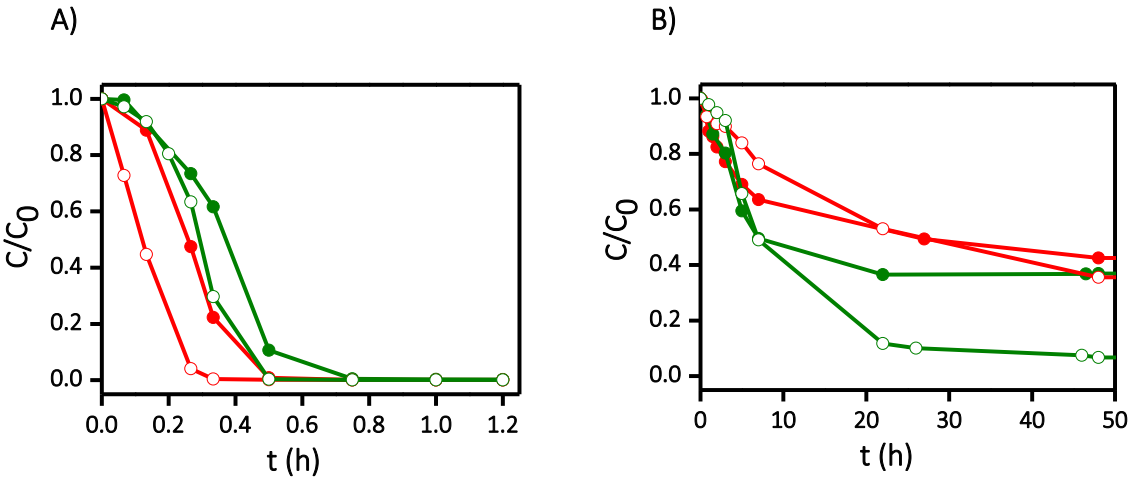


**Figure 11:** Plot of the relative [GA] (**A**) or [TCA] (**B**) upon irradiation times under air (blank) or $N_2$ (solid), using $TPP^+$ (red) or $TPTP^+$ (green) as photocatalysts ($\lambda_{exc}$ = 420 nm), monitored by HPLC (GA) or GC (TCA). $[GA]_o = [TCA]_o$ = 5 mg/L, $[TP(T)P^+]_o$ = 10 mg/L.

Mass spectral analysis of the complex photolysis mixtures revealed formation of minor amounts of decarboxylated and oxygenated products from GA, while in the case of TCA the only identified product was 2,4,6-trichlorophenol.

Control experiments to determine the extent of direct photolysis and the potential reaction occurring without light were carried out in the absence of photocatalyst and in the absence of light, respectively. Under these conditions, no significant degradation was observed after 1 h (in the case of GA) or 60 h (in the case of TCA), see Figure 12.

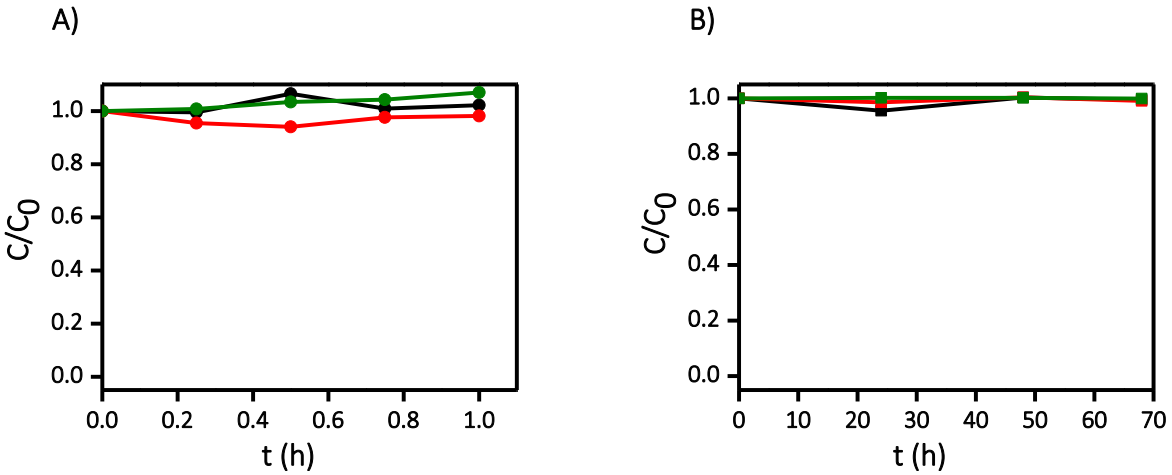


**Figure 12**: Plot of the relative [GA] (**A**) or [TCA] (**B**) upon irradiation times in the absence of photocatalysts (black), and in the presence of $TPP^+$ (red) or $TPTP^+$ (green) but in the absence of light, $[GA]_o=[TCA]_o$ = 5 mg/L, $[TP(T)P^+]_o$ = 10 mg/L.

Both photocatalysts are known for acting *via* electron transfer; nevertheless, examples of participation of $^1(TPP^+)^*$,[114] $^3(TPP^+)^*$,[116] or a non-emissive ground state complex[103] in the removal of contaminants can be found in the literature. In the case of $TPTP^+$, despite its high intersystem crossing quantum yield ($\Phi_{ISC}$ = 0.93)[70] involvement of $^1(TPTP^+)^*$ was proposed in the removal of pyrimethanil or alachlor.[117] Therefore, it was necessary to perform a full mechanistic analysis of the participation of all the transient species to find out which one is responsible for the photodegradation of the selected contaminants.

To investigate the participation of the singlet and/or the ground state of $TPP^+$ or $TPTP^+$ in the photodegradation of GA and TCA, fluorescence experiments were performed. First, steady-state fluorescence emission of $TPP^+$ decreased upon increasing amounts of GA or TCA; while, emission of $TPTP^+$ only decreased after adding TCA, remaining unchanged upon addition of increasing concentrations of GA, see Figure 13. From the Stern-Volmer relationships, Figure 13D, and the reported lifetime for the singlet excited state of $TPP^+$ and $TPTP^+$ (4.4 ns),[126] the corresponding quenching rate constants were obtained: 2.4 x $10^{10}$, 3.3 x $10^{10}$ and 5.9 x $10^{10}$ $M^{-1}s^{-1}$, for the quenching of $TPP^+$ by GA, $TPP^+$ by TCA and $TPTP^+$ by TCA, respectively.

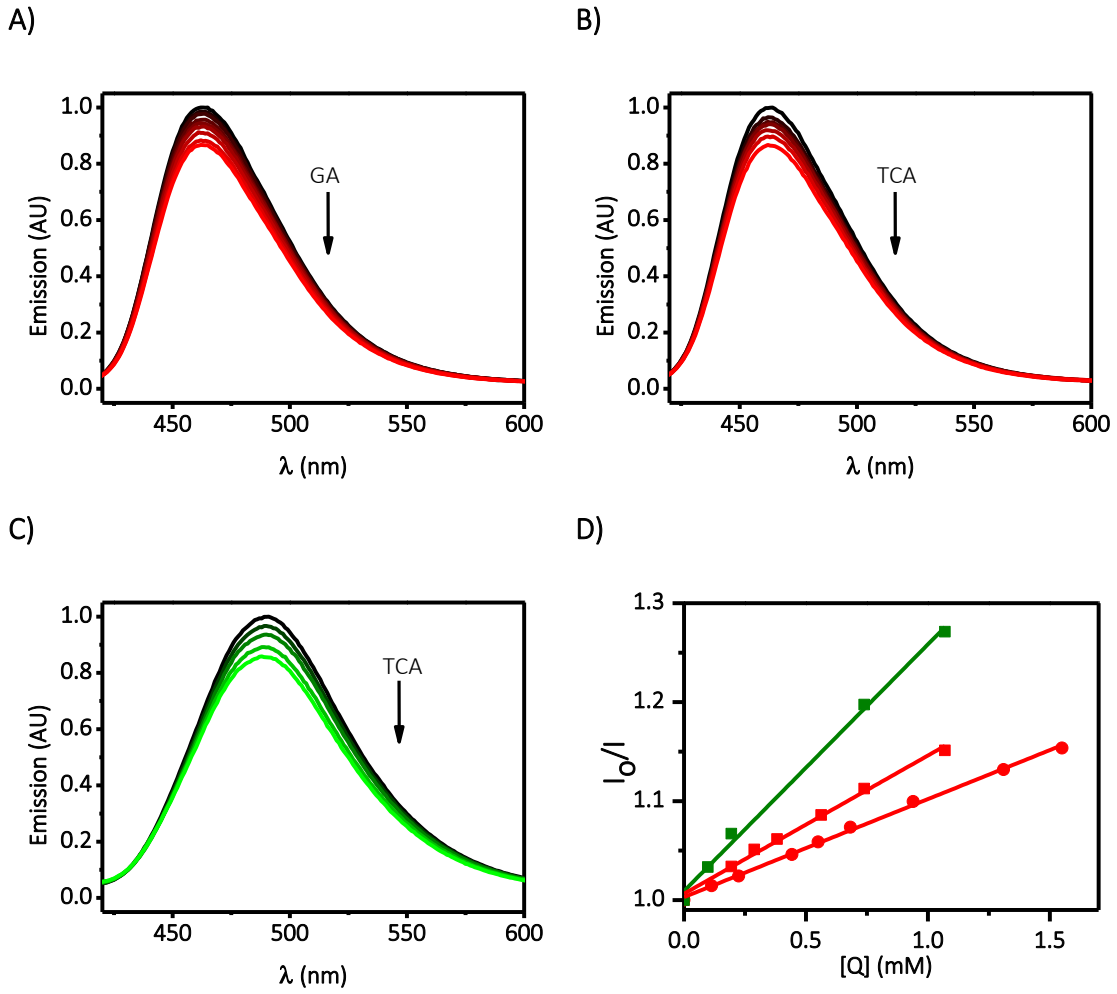


**Figure 13**: Steady-state fluorescence quenching of $^1(TPP^+)^*$ by GA (**A**), $^1(TPP^+)^*$ by TCA (**B**) and $^1(TPTP^+)^*$ by TCA (**C**), and their corresponding Stern-Volmer plots (**D**), $TPP^+$ and GA (●), $TPP^+$ and TCA (■) and $TPTP^+$ and TCA (■) in aerated acetonitrile solutions ($\lambda_{exc}$ = 405 nm).

Secondly, time-resolved fluorescence measurements were performed to check the real involvement of the singlet excited species. In every case, the lifetime of both $^1(TPP^+)^*$ and $^1(TPTP^+)^*$ remained constant upon increasing concentrations of GA or TCA, revealing that the singlet excited states of the photocatalysts are not involved in these reactions. Therefore, fluorescence experiments clearly pointed to the formation of ground-state complexes as the species responsible for the observed fluorescence emission quenching.

The next step was to determine the stoichiometry of those ground state complexes, through Job's plot experiments.[127, 128] Thus, binary solutions of

photocatalyst and pollutant at a constant total concentration of 1 x $10^{-5}$ M were prepared varying the pollutant molar fraction and their UV-Vis spectra were recorded, see Figure 14A, B and C. Then, the product of the absorption at 406 nm and the pollutant concentration was plotted against the molar fraction of the pollutant, and a curve was obtained in the three cases. The maxima of these parabolas were found at $X_{pollutant}$ = 0.5, which corresponds to a 1:1 stoichiometry, Figure 14D.

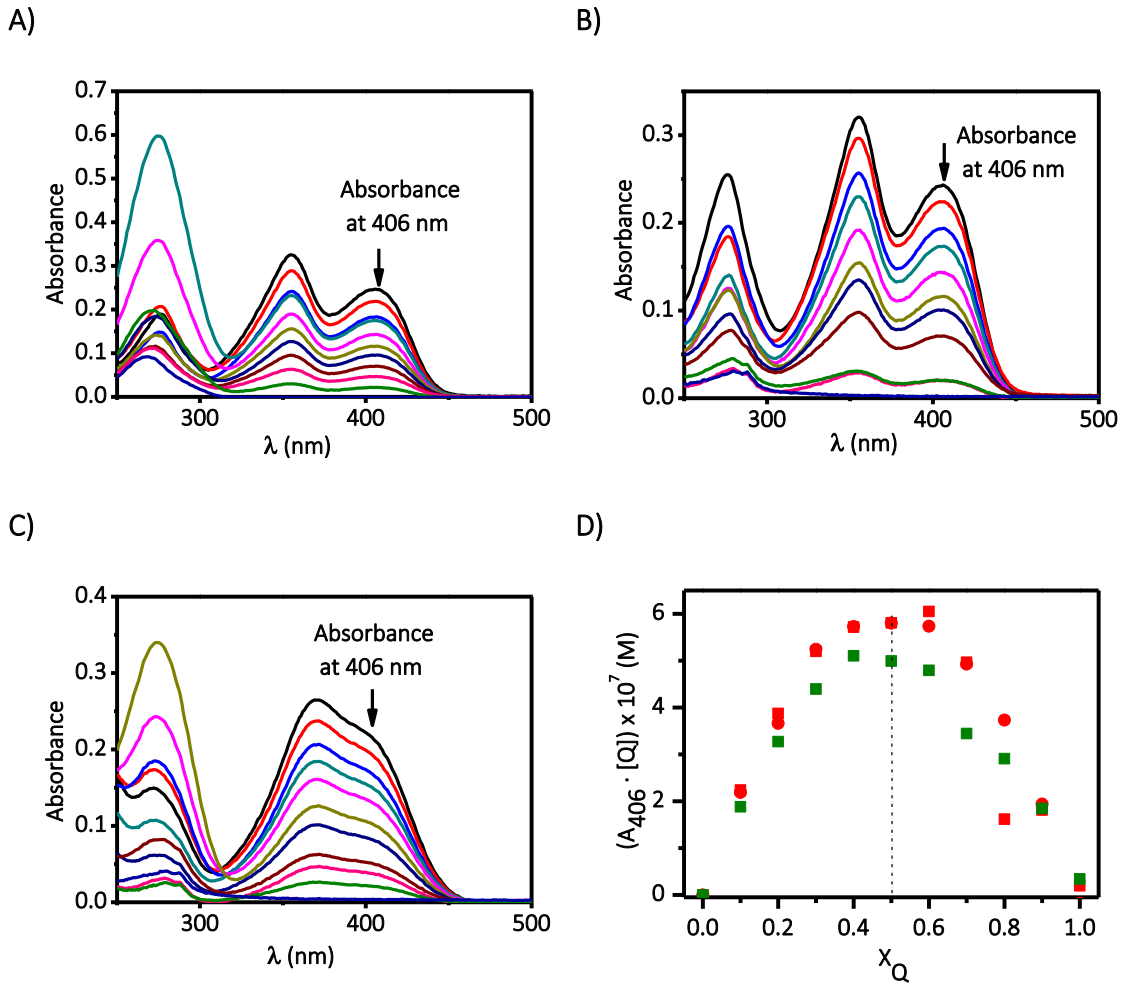


**Figure 14**: UV-visible spectra of mixtures of $TPP^+$ and GA **(A)** or TCA **(B)** and of $TPTP^+$ and TCA **(C)**, [TP(T)P + GA/TCA] = 1x$10^{-5}$M. Black traces: pure TP(T)P, dark blue traces: pure GA or TCA. Job's plots for $TPP^+$ *versus* GA (●), $TPP^+$ *versus* TCA (■) and $TPTP^+$ *versus* TCA (■) molar fractions ($X_Q$), **(D).**

The corresponding complexation constants were calculated from the slopes and intercepts of each fitting using the emission data obtained from the steady-state fluorescence experiments, Figure 15, according to the Benesi-Hildebrand relationship,

Eq. 8, section 1.3. [8, 9] The determined values were: $K_{TPP\text{-}GA}$= 468.4 $M^{-1}$, $K_{TPP\text{-}TCA}$ = 528.0 $M^{-1}$ and $K_{TPTP\text{-}TCA}$ = 657.1 $M^{-1}$.

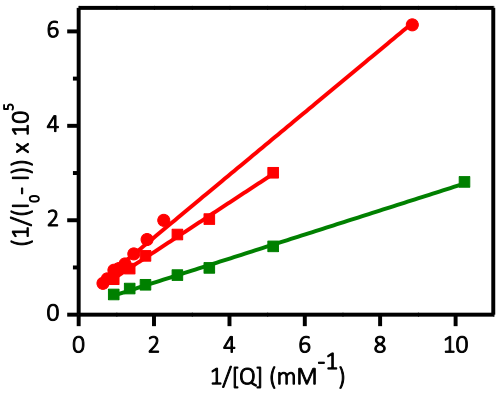


**Figure 15**: Benesi-Hildebrand relationships for the formation of different complexes: $TPP^+$ with GA (●), $TPP^+$ with TCA (■) and $TPTP^+$ with TCA (■).

Finally, the possible involvement of the triplet excited state of the photocatalysts in the photodegradation of the pollutants was evaluated by laser flash photolysis (LFP) experiments with excitation wavelength at 355 nm. First, transient absorption spectra for the triplet excited states of each photocatalyst were recorded in deaerated acetonitrile, obtaining their typical broad absorption bands (400-600 nm) in the case of $TPP^+$ and a sharp band centred at 470 nm for $TPTP^+$, in agreement with data previously reported.[70, 125] Then, the traces corresponding to the triplets were recorded (at 470 nm and 620 nm for $TPP^+$ and $TPTP^+$, respectively) upon addition of increasing concentrations of the pollutants.

In the case of GA, increasing concentration of the pollutant produced a decrease in the lifetime of the triplet excited states of both photocatalysts, see Figure 16A and Figure 16B for $TPP^+$ - GA and $TPTP^+$ - GA, respectively. The corresponding quenching constants were determined from the Stern Volmer linear relationships (Eq. 6), see the corresponding insets in Figure 16. Thus, the determined quenching constant values were: $k_q$ = 5.8 x $10^9$ $M^{-1}s^{-1}$ and 9.8 x $10^9$ $M^{-1}s^{-1}$, for the quenching of $^3(TPP^+)^*$ and $^3(TPTP^+)^*$ by GA.

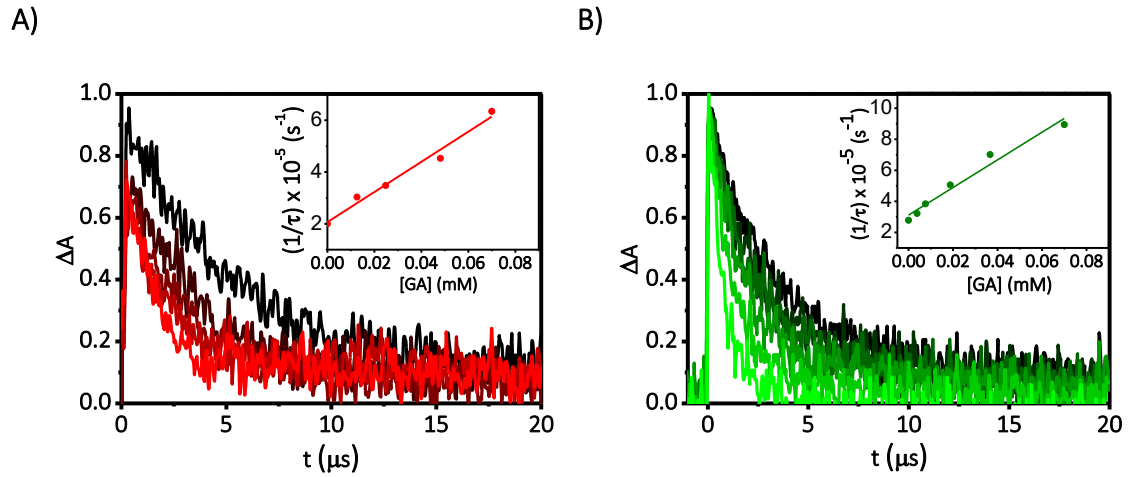


**Figure 16**: Kinetic traces obtained upon irradiation ($\lambda_{exc}$ = 355 nm) of deaerated acetonitrile solutions (7 x $10^{-5}$ M) of $TPP^+$ (**A**) or $TPTP^+$ (**B**) in the presence of increasing concentrations of GA (0 – 7 x $10^{-5}$ M), recorded at 470 nm (**A**) or 620 nm (**B**). Insets: Stern–Volmer plots for the reverse triplet lifetime of $TPP^+$ (**A**) or $TPTP^+$ (**B**) *versus* GA concentration.

To get further evidence of the electron transfer process, the transient absorption spectra of $TPP^+$ and of $TPTP^+$ were recorded in the presence of GA (7 x $10^{-5}$ M), and compared to the corresponding spectra of the $^3(TPP^+)^*$ and $^3(TPTP^+)^*$ obtained in the absence of GA, see Figure 17. In the case of $TPP^+$, the typical band corresponding to the semireduced pyranyl radical ($TPP^{\cdot}$) centred at 550 nm was observed, see Figure 17A. In the case of $TPTP^+$, the spectrum also changed to a broad band between 450 and 575 nm approximately, see Figure 17B. This band can be attributed to the reduced species of $TPTP^+$, which, to the best of our knowledge, remains undescribed in literature.

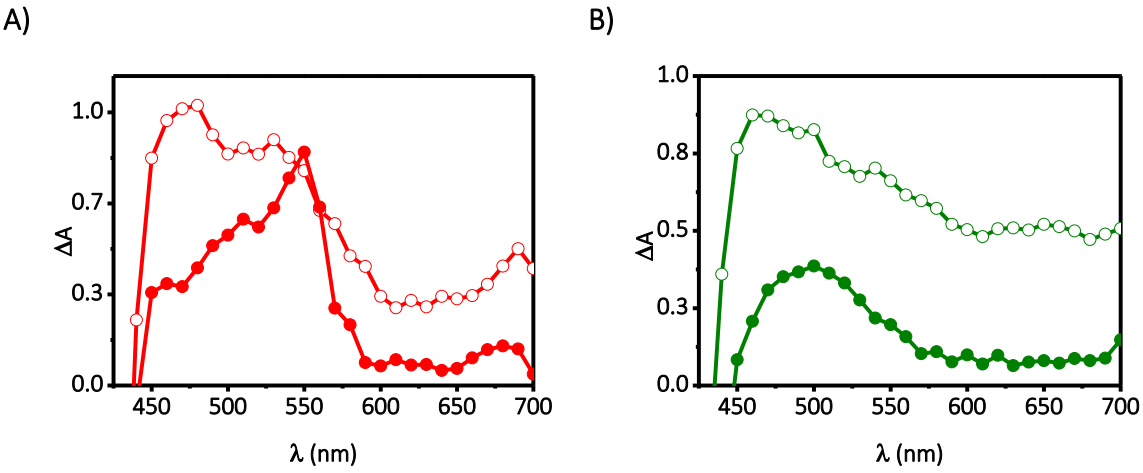


**Figure 17**: Transient absorption spectra obtained upon laser flash photolysis of deaerated acetonitrile solutions of $TPP^+$ (**A**) and $TPTP^+$ (**B**) (7 x $10^{-5}$ M) in the absence (blank) and in the presence (solid) of GA (7 x $10^{-5}$ M) recorded 2.4 µs after the pulse.

When analogous experiments were performed using TCA, addition of increasing amounts of TCA did not have any effect on the lifetimes of $^3(TPP^+)^*$ nor $^3(TPTP^+)^*$. Besides, the transient absorption spectra recorded immediately after the laser pulse upon addition of TCA revealed a decrease in the intensity of the signals corresponding to the triplets but without any change in their shapes, see Figure 18. This decrease could be attributed to the consumption of the photocatalysts in the formation of the ground state complexes.

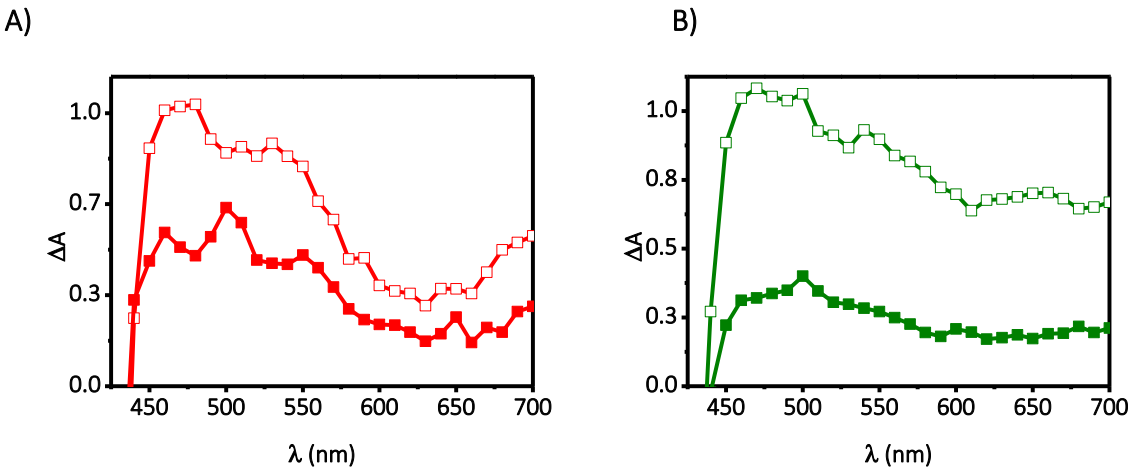


**Figure 18:** Transient absorption spectra obtained upon laser flash photolysis of deaerated acetonitrile solutions of $TPP^+$ (**A**) and $TPTP^+$ (**B**) (7 x $10^{-5}$ M) in the absence (blank) and in the presence (solid) of TCA (7 x $10^{-5}$ M) recorded 0.8 µs after the pulse.

The results from the photophysical studies are summarized in Table 3.

Table 3: Experimental constants between the photocatalysts and the pollutants obtained from the photophysical measurements.

| | Ground state complex K ($M^{-1}$) | Quenching of the triplet $k_{qt}$ ($M^{-1}s^{-1}$) |
|---|---|---|
| $TPP^+$ - GA | 468.4 | $5.8 \times 10^9$ |
| $TPP^+$ - TCA | 528.0 | - |
| $TPTP^+$ - GA | - | $9.8 \times 10^9$ |
| $TPTP^+$ - TCA | 657.1 | - |

Once the involvement of all the potential species has been evaluated, the thermodynamics of the photoinduced electron transfer from GA to the triplet excited state of both $TPP^+$ and $TPTP^+$ was evaluated using the photoinduced Gibbs free energy equation, Eq.9.[7]

Eq.9:

$$\Delta G^0_{et}\ (kcal\ mol^{-1}) = -23.06\ [E^0_{red}(TP(T)P^+/TP(T)P^{\cdot}) - E^0_{red}(Q^{\cdot+}/Q)\ ] - E^*_T(TP(T)P^+)$$

The corresponding values for each parameter of Eq.9 are summarized in Table 4.

Table 4: Thermodynamic values for the species involved in the electron transfer between $TPP^+$ and/or $TPTP^+$ and GA or TCA.

| Parameter | $TPP^+/TPP^{\cdot}$ | $TPP^+$ | $TPTP^+/TPTP^{\cdot}$ | $TPTP^+$ | $GA^{+\cdot}/GA$ | $TCA^{+\cdot}/TCA$ |
|---|---|---|---|---|---|---|
| $E_{red}$ (V) *vs* SCE | -0.37[129] | - | -0.29[129] | - | +0.80[115] | +1.9* |
| $E^*_T$ (kcal $mol^{-1}$) | - | 53[70] | - | 52[70] | - | - |

*Experimentally measured, see Figure 19.

Using the reported values from Table 4, the estimated ΔG values calculated for the reaction from the triplet excited states of $TPP^+$ and $TPTP^+$ with GA are -26.0 and -26.9 kcal $mol^{-1}$, respectively, indicating that electron transfer is indeed exergonic. In the case of TCA, the lack of singlet/triplet quenching could be associated with a thermodynamically less favored process, with values of -0.7 and -1.5 kcal $mol^{-1}$ for the

electron transfer from TCA to $^3(TPP^+)^*$ and $^3(TPTP^+)^*$ respectively, due to the high redox potential of TCA, see Table 4.

Nevertheless, photodegradation of GA and TCA in the presence of $TPP^+$ and/or $TPTP^+$ has been achieved, being the reactions rates higher in the case of GA. Scheme 2 shows the proposed mechanism for the reactions between GA and TCA and $TP(T)P^+$, were $\delta^+$ and $\delta^{+'}$ represent the charge distribution between any of the photocatalysts and any quencher (GA or TCA).

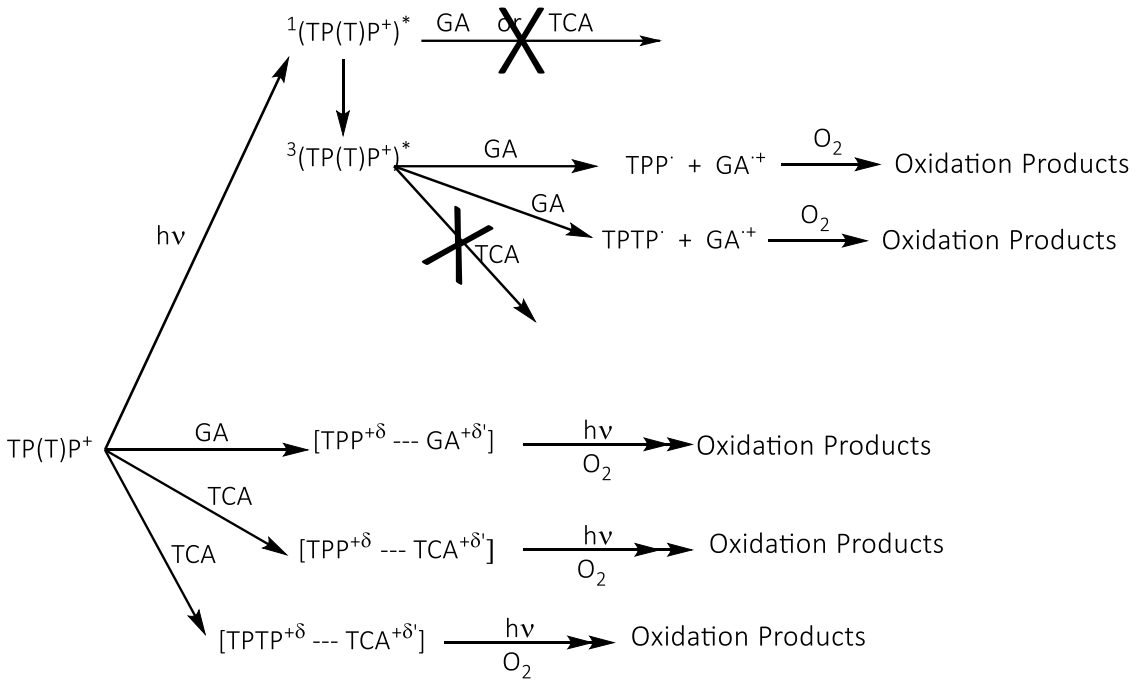


Scheme 2: Mechanistic proposal for the photodegradation of GA and TCA in the presence of $TP(T)P^+$.

The involvement of the singlet excited states of both photocatalysts in the photodegradation of GA or TCA was ruled out since no changes in the fluorescence lifetime of $TPP^+$ or $TPTP^+$ were observed after adding increasing concentrations of the pollutants. These results together with the decrease of the steady-state fluorescence emission in the cases of $TPP^+$ with GA, $TPP^+$ with TCA and $TPTP^+$ with TCA pointed to the formation of ground-state complexes between the photocatalysts and the pollutants in these three cases. The stoichiometry of these complexes was calculated based on the Job's plots and the values of the complexation constants for the complexes were calculated using the Benesi–Hildebrand relationship: $K_{TPP\text{-}GA}$= 468.4 $M^{-1}$, $K_{TPP\text{-}TCA}$= 528.0

$M^{-1}$and $K_{TPTP\text{-}TCA}$= 657.1 M. Moreover, in the case of GA, quenching of the triplet excited states of both photocatalysts was demonstrated, with kinetic constants close to the diffusion limit ($k_{diff}$= 1.9 × $10^{10}$ $M^{-1}s^{-1}$ in $CH_3CN$)[130]: $k_q$ = 5.8 x $10^9$ $M^{-1}s^{-1}$ and 9.8 x $10^9$ $M^{-1}s^{-1}$ for the quenching of $^3(TPP^+)^*$ and $^3(TPTP^+)^*$, respectively. In addition, the formation of the corresponding reduced species of $TP(T)P^+$, the (thia)pyranyl radical ($TP(T)P^{\cdot}$) was observed. Thermodynamic calculations also support the participation of the triplet excited states in the oxidation of GA.

The relative contribution of the photocatalyst-derived species involved in the photooxidations were also estimated on the basis of Eq. 13 and Eq. 20.

First, a photocatalyst (PC) from its ground state, may form a complex with the pollutant (Q), the percentage of photocatalyst involved in it (for 1:1 stoichiometry) is shown in Eq. 13.

$$PC + Q \underset{}{\overset{K}{\rightleftharpoons}} PC^{\delta+}\text{--}Q^{\delta'+}$$

$$\text{Eq. 10: } K = \frac{[PC^{\delta+}\cdots Q^{\delta\prime+}]}{([PC]-[PC^{\delta+}\cdots Q^{\delta\prime+}])([Q]-[PC^{\delta+}\cdots Q^{\delta\prime+}])}$$

Assuming that:

$$\text{Eq. 11: } [PC^{\delta+}\cdots Q^{\delta\prime+}] \ll [PC] \; and \; [PC^{\delta+}\cdots Q^{\delta'+}] \ll [Q]$$

$$\text{Eq. 12: } [PC^{\delta+}\cdots Q^{\delta\prime+}] \cong K \times [PC] \times [Q]$$

Dividing Eq. 12 by the initial concentration of photocatalyst ([PC]), the percentage of complex formation will be obtained:

$$\text{Eq. 13: } [PC^{\delta+}\cdots Q^{\delta\prime+}](\%) \cong K \times [Q] \times 100$$

According to this, Eq. 14 describes the percentage of photocatalyst able to reach the singlet excited state:

$$\text{Eq. 14:}$$

$$^1(PC)^* \; formation \; (\%) = \; 100 - [PC^{\delta+}\cdots Q^{\delta'+}](\%) \approx 100 - K \times [Q] \times 100 = \\ = (1 - K \times [Q]) \times 100$$

From the singlet excited state, three processes can happen: emission $(\Phi_F/\tau_S)$, intersystem crossing $(\Phi_{ISC}/\tau_S)$ and quenching by the pollutant $\left(k_{qs}[Q]\right)$, as described by Eq. 15.

$$\text{Eq. 15: } \sum Processes\ from\ {}^1(PC)^* = \frac{\Phi_F}{\tau_S} + \frac{\Phi_{ISC}}{\tau_S} + k_{qs}[Q]$$

Thus, quenching of the singlet excited state by the pollutant is shown by Eq. 16, and formation of the triplet excited state is obtained by Eq. 17.

Eq. 16:

$$Quenching\ of\ {}^1(PC)^*\ (\%) = {}^1(PC)^*\ formation(\%) \times \frac{k_{qs}[Q]}{\frac{\Phi_F}{\tau_S}+\frac{\Phi_{ISC}}{\tau_S}+k_{qs}[Q]}$$

$$\text{Eq. 17: } {}^3(PC)^*\ formation(\%) = {}^1(PC)^*\ formation\ (\%) \times \frac{\frac{\Phi_{ISC}}{\tau_S}}{\frac{\Phi_F}{\tau_S}+\frac{\Phi_{ISC}}{\tau_S}+k_{qs}[Q]}$$

Moreover, the triplet excited state can also follow two different pathways: intrinsic decay $(1/\tau_T)$ and quenching by the pollutant $\left(k_{qT}[Q]\right)$, as shown in Eq. 18:

$$\text{Eq. 18: } \sum Processes\ from\ {}^3(PC)^* = \frac{1}{\tau_T} + k_{qT}[Q]$$

Thus, quenching of the triplet excited state by the pollutant is shown by Eq. 20, and its intrinsic deactivation is described by Eq. 21.

$$\text{Eq.19: } Quenching\ of\ {}^3(PC)^*\ (\%) = {}^3(PC)^*\ formation\ (\%) \times \frac{k_{qT}[Q]}{\frac{1}{\tau_T}+k_{qT}[Q]}$$

Eq. 20:

$$Quenching\ of\ {}^3(PC)^*\ (\%) = {}^1(PC)^*\ formation\ (\%) \times \frac{\frac{\Phi_{ISC}}{\tau_S}}{\frac{\Phi_F}{\tau_S}+\frac{\Phi_{ISC}}{\tau_S}+k_{qs}[Q]} \times \frac{k_{qT}[Q]}{\frac{1}{\tau_T}+k_{qT}[Q]}$$

Eq. 21:

$$Deactivation\ of\ {}^3(PC)^*\ (\%) = {}^1(PC)^*\ formation\ (\%) \times \frac{\frac{\Phi_{ISC}}{\tau_S}}{\frac{\Phi_F}{\tau_S}+\frac{\Phi_{ISC}}{\tau_S}+k_{qs}[Q]} \times \frac{\frac{1}{\tau_T}}{\frac{1}{\tau_T}+k_{qT}[Q]}$$

Taking into account the described equations, the initial concentration of each compound ([GA] =[TCA] = 5 mg/L) and the experimentally obtained constants (Table 3),

the percentage of photocatalysts involved in each pathway can be calculated. More specifically, the percentage of photocatalyst involved in the formation of a ground state complex can be determined with Eq. 13, the percentage of photocatalyst involved in the quenching of the triplet excited state can be calculated from Eq. 20, see Table 5. For the case of $TPP^+$ and GA, only 1.4% of the initial $TPP^+$ is employed in the formation of the ground-state complex, while *ca*. 27% of the initially excited $TPP^+$ follow the electron transfer pathway from the triplet excited state. For the case of $TPTP^+$ and GA, 43.5% of the initially excited $TPTP^+$ follows the electron transfer pathway from its triplet excited state to oxidize the compound. Attending now to TCA, 41.7% of the initial $TPP^+$ is employed in the formation of the ground-state complex, while, the formation of ground-state complex with $TPTP^+$ represents 44%.

Table 5: Distribution (in percentage) of the different alternative pathways followed by $TPP^+$ and $TPTP^+$ in the photodegradation of GA and TCA.

| | $TPP^+$ | | $TPTP^+$ | |
|---|---|---|---|---|
| Q | % Complex formation (Eq. 13) | % Quenching of the triplet (Eq. 20) | % Complex formation (Eq. 13) | % Quenching of the triplet (Eq. 20) |
| GA | 1.4 | 27 | - | 43.5 |
| TCA | 41.7 | - | 44.0 | - |

## 3.3. Conclusions

Photodegradation of two representative wastewaters pollutants from cork industry can be achieved in the presence of (thia)pyrylium salts as organic photocatalysts. Photocatalytic degradations reveal fast removal of gallic acid while degradation of the reluctant 2,4,6-trichloroanisole is much slower. These results are in agreement with the thermodynamic calculations for the photoredox processes. Photophysical experiments indicate that for gallic acid, oxidative electron transfer occurs mainly from the triplet excited state, while for 2,4,6-trichloroanisole formation of ground state complexes is the operating pathway.

## 3.4. Experimental

Photodegradations were carried out according to the general methodology explained in section 9.3.1. In this case, photodegradation mixtures were prepared in 100

mL of $CH_3CN$ containing 5 mg/L of GA or TCA and 10 mg/L of the photocatalysts $TPP^+$ or $TPTP^+$.

The photodegradation of GA was monitored by HPLC. The mobile phase was an isocratic mixture of water pH 3 (80 %) and acetonitrile (20 %) at the flow rate of 0.7 mL $min^{-1}$; detection wavelength was fixed at 275 nm and 2-nitrobenzoic acid (5 mg/L) was used as internal standard. The photodegradation of TCA was monitored by GC. Samples were subjected to an isothermal period of 1 min (100ºC), followed by a thermal gradient of 6 minutes (up to 280ºC) and a final isothermal period of 3 minutes. The internal standard was pentadecane (5 mg/L).

All the photophysical measurements were carried out according to section 9.3.4. For the steady-state and time-resolved fluorescence experiments, the final concentrations of each pollutant were up to 1.6 x $10^{-3}$ M or 1.1 x $10^{-3}$ M for GA or TCA, respectively, the excitation wavelength was fixed at 410 nm and 365 nm for $TPP^+$ and $TPTP^+$, respectively, and all the measurements were performed under aerobic atmosphere.

For the Job's plot experiments, the general procedure explained at section 9.3.4 was followed, the absorbance changes were measured at 406 nm.

For the laser flash photolysis experiments, the final concentrations of each pollutant were up to 7 x $10^{-5}$ M for GA and TCA and the concentration of the photocatalysts were of 7 x $10^{-5}$ M for $TPP^+$ or $TPTP^+$. The excitation wavelength was fixed at 355 nm.

The redox potential measurement for TCA was carried out according to 9.3.3.

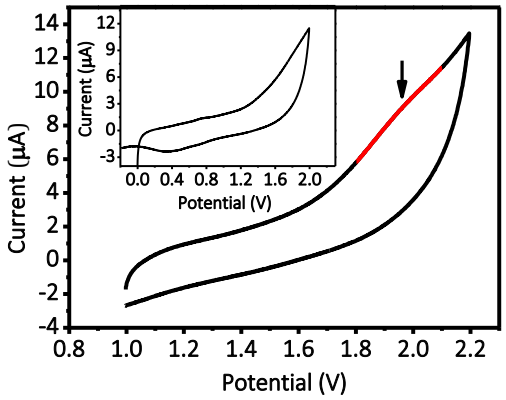


| ELECTRODE | E ($TCA^{\cdot+}$/TCA) |
|---|---|
| AgCl/Ag (sat. KCl) | 1.97 V |
| SCE* | 1.93 V |

**Figure 19**: Cyclic voltammetry of TCA (30 µM) measured in tetrabutyl ammonium perchlorate (TBA) solution (0.1 M) as electrolyte at 0.1 V $s^{-1}$. Inset: Cyclic voltammetry of the electrolyte TBA (0.1 M). *The obtained data from the AgCl/Ag (sat KCl) was converted into redox potential value *vs* SCE as follows: E (vs SCE, in V) = E (vs AgCl/Ag, in V) -0.045.

# 4. Direct Detection of all the Triphenylpyrylium-Derived Short-Lived Intermediates in the Photocatalyzed Oxidation of Aqueous Contaminants

## 4.1. Introduction

One of the challenges in the field of photoredox catalysis is the detection of the species involved in the processes, mainly due to their short lifetime. Therefore, specific equipment that provides time resolved data in the time-scale of the lifetimes of these intermediates is required.

Under this context, $TPP^+$ looks as an appropriate candidate to be used as a model to provide direct evidence for the electron transfer mechanism in a photoredox process for several reasons: i) its photophysical properties are deeply described in the literature, see Table 1 in the Preamble of Part I; ii) it has demonstrated to be a good oxidant from its excited states, see results described in Chapter 3 and previous results of the group; [82, 85, 103, 111] and iii) the spectra of its triplet excited state and the corresponding reduced species (pyranyl radical) after the redox process are well reported in the literature and have been experimentally obtained in Chapter 3.

The formation of the reduced species can be exploited to quantify the amount of the triplet excited state and the radical species involved in the photoredox process. This analysis should be based on the lifetimes and molar absorption coefficients of these two species and will require a biexponential analysis due to the partial overlap of both signals, see Figure 20. This analysis can act as a proof of the electron transfer pathway, and more important, it could be correlated to the extent of the photodegradation process.

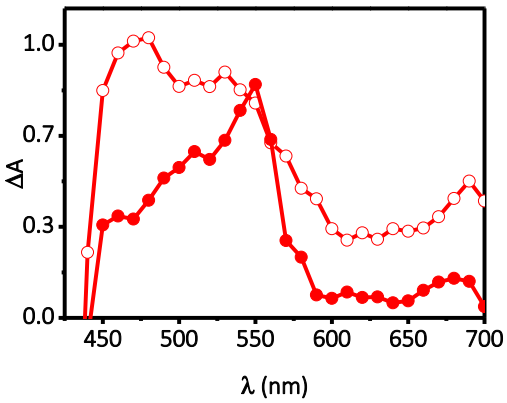


**Figure 20**: Transient absorption spectra obtained upon laser flash photolysis of deaerated acetonitrile solutions of $TPP^+$ (○) and $TPP^+$ in the presence of GA (●), recorded 2.4 μs after the pulse ($[TPP^+] = 7x10^{-5}M$, $[GA] = 7x10^{-5}M$).

With this background, the aim of the present chapter is to provide a direct and quantitative piece of evidence for the photooxidation of a group of common pollutants, as well as to correlate the concentration of the primary reduced species ($TPP^{\cdot}$) with the extent of the photodegradation *via* electron transfer mechanism.

To carry out this task, steady-state photolysis was first carried out under simulated solar irradiation in the presence of $TPP^+$, and then photophysical measurements based on emission spectroscopy (steady-state and time-resolved fluorescence) and on transient absorption spectroscopy (laser flash photolysis) were used to provide fast kinetic data.

In addition, the selected pollutants: acetaminophen (ACF), acetamiprid (ACP), caffeine (CAF) and carbamazepine (CBZ), see Figure 21, present a variety of chemical structures and different redox potentials, which where experimentally measured or obtained from the literature. Therefore, they can serve as examples to demonstrate the applicability and general scope of the proposed methodology. Furthermore, they belong to the family of emerging pollutants, which are of increasing environmental concern.[131, 132]

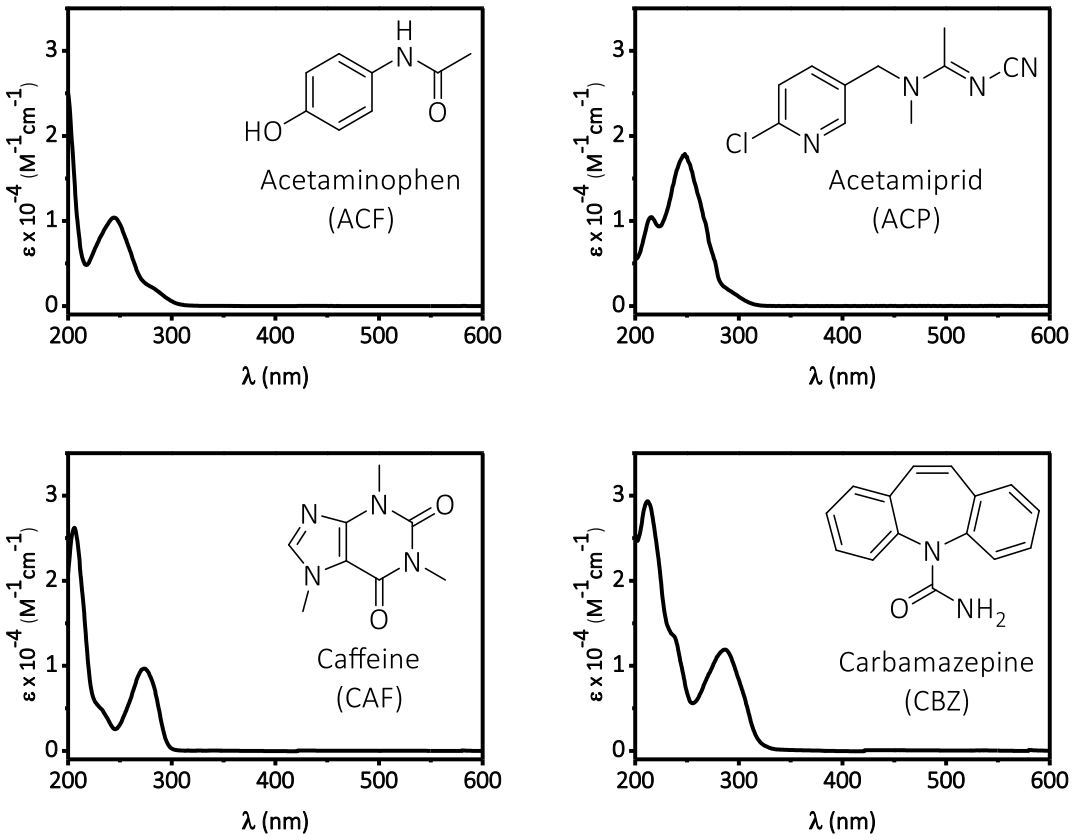


**Figure 21**: UV-vis spectra in $CH_3CN$ and chemical structures of the selected pollutants.

## 4.2. Results and discussion

$TPP^+$ is well known for its ability as oxidant from its singlet and its triplet excited states; the redox potentials of these excited species are $E_{red}\ ^1(TPP^+)^*$ = +2.5 V and $E_{red}\ ^3(TPP^+)^*$ = +2.0 V *vs* SCE, respectively.[86] Therefore, to analyse the thermodynamics of the photooxidations, the redox potentials of the pollutants were measured, see Table 6. Then, with the photoinduced Gibbs free energy changes (Eq. 2), the exergonicity of the process was calculated. Table 6 reveals that the oxidation of all the pollutants from both excited states, singlet and triplet, is highly exergonic except in the case of the triplet excited state and ACP.

Table 6: Reduction potentials for each pollutant and the corresponding photoinduced Gibss free energy for the oxidative processes from the singlet and triplet excited states of $TPP^+$.

| | ACF | ACP | CAF | CBZ |
|---|---|---|---|---|
| $E_{red}(Q^{\cdot+}/Q)$ *vs* SCE (V) | 0.9* | 1.8* | 1.1* | 1.4[133] |
| $\Delta G_{SINGLET}$ (kcal·mol$^{-1}$) | -36.7 | -16.0 | -32.1 | -25.2 |
| $\Delta G_{TRIPLET}$ (kcal·mol$^{-1}$) | -23.7 | -3.0 | -19.1 | -12.2 |

* Experimentally measured, see Figure 26.

Then, the first step was to evaluate the evolution of the relative concentration of each pollutant in the presence of $TPP^+$ *vs* irradiation time upon solar irradiation. For this purpose, an aerated aqueous solution containing the photocatalyst and the four selected pollutants was acidified to ensure the stability of $TPP^+$ [134] and treated under different experimental conditions, see Figure 22.

Removal of ACP was negligible, while CBZ and CAF were not so reluctant. Conversely, ACF suffered photodegradation to a high extent under the employed experimental conditions. More specifically, removal of ACF was completely achieved after 90 minutes of irradiation in the presence of $TPP^+$, however, only *ca.* 20% of CAF and CBZ were removed after 180 minutes. Control experiments in darkness or in the absence of $TPP^+$ showed no reaction, see Figure 22B and C.

In the case of ACF, further investigation of the oxidation reaction was performed upon detection of the formation of $CO_2$. A new batch containing ACF and $TPP^+$ was submitted to solar irradiation upon continuous flow of $O_2$, that subsequently was bubbled through a saturated aqueous solution of $Ba(OH)_2$. The $Ba(OH)_2$ in the presence of $CO_2$ was converted into $BaCO_3$ that precipitated at the bottom. After irradiating during 24 hours the precipitate was filtered. Elemental analysis of the precipitate unequivocally demonstrated the formation of $BaCO_3$, confirming that mineralization was achieved from the oxidation process.

A)

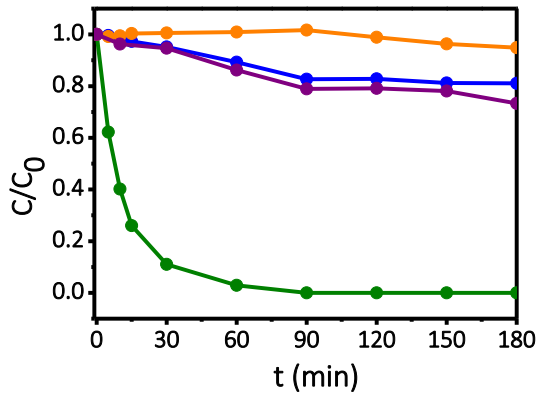


B)

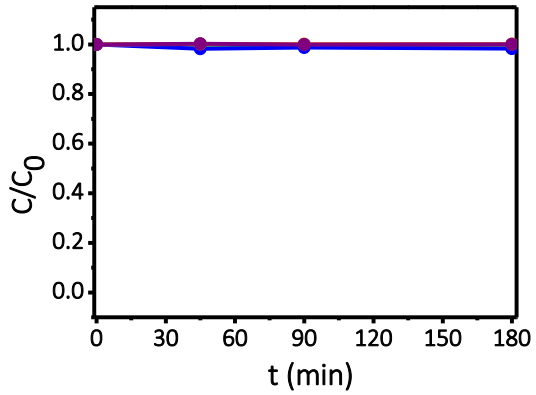


C)

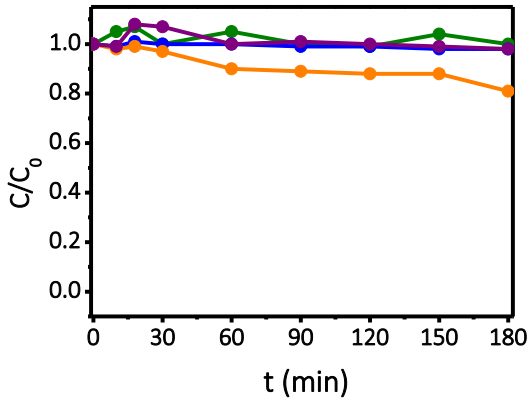


**Figure 22**: Plot of the relative concentration of ACF (●), ACP (●), CAF (●) and CBZ (●) at $C_o$= 5 mg $L^{-1}$ each (0.1 mM in global concentration) in aerated acidic (pH = 3) aqueous media *vs*. time under different conditions: **A)** solar simulated irradiation in the presence of 10 mg $L^{-1}$ (0.03 mM) of $TPP^+$; **B)** in the presence of 10 mg $L^{-1}$ (0.03 mM) of $TPP^+$, but in the absence of light (darkness control experiment); **C)** solar simulated irradiation, in the absence of $TPP^+$ (direct photolysis control experiment)

Next, fluorescence experiments (steady-state and time-resolved) were performed in deaerated acetonitrile to investigate the involvement of $^1(TPP^+)^*$ in the photodegradation of the pollutants, Figure 23. A decrease in the emission and also in the lifetime of $^1(TPP^+)^*$ was observed in all cases upon addition of the pollutants. Then, applying the Stern-Volmer relationship between the reciprocal lifetime and contaminants concentration, the corresponding quenching rate constants were determined. The values are summarized in Table 7, all of them are in the order of $\approx 10^{10}$ $M^{-1}$ $s^{-1}$, what confirms the

dynamic involvement of the singlet excited state in all cases, with values in the range of the diffusion limit ($k_{diff}$ = 1.9 x $10^{10}$ $M^{-1}s^{-1}$ in $CH_3CN$).[135]

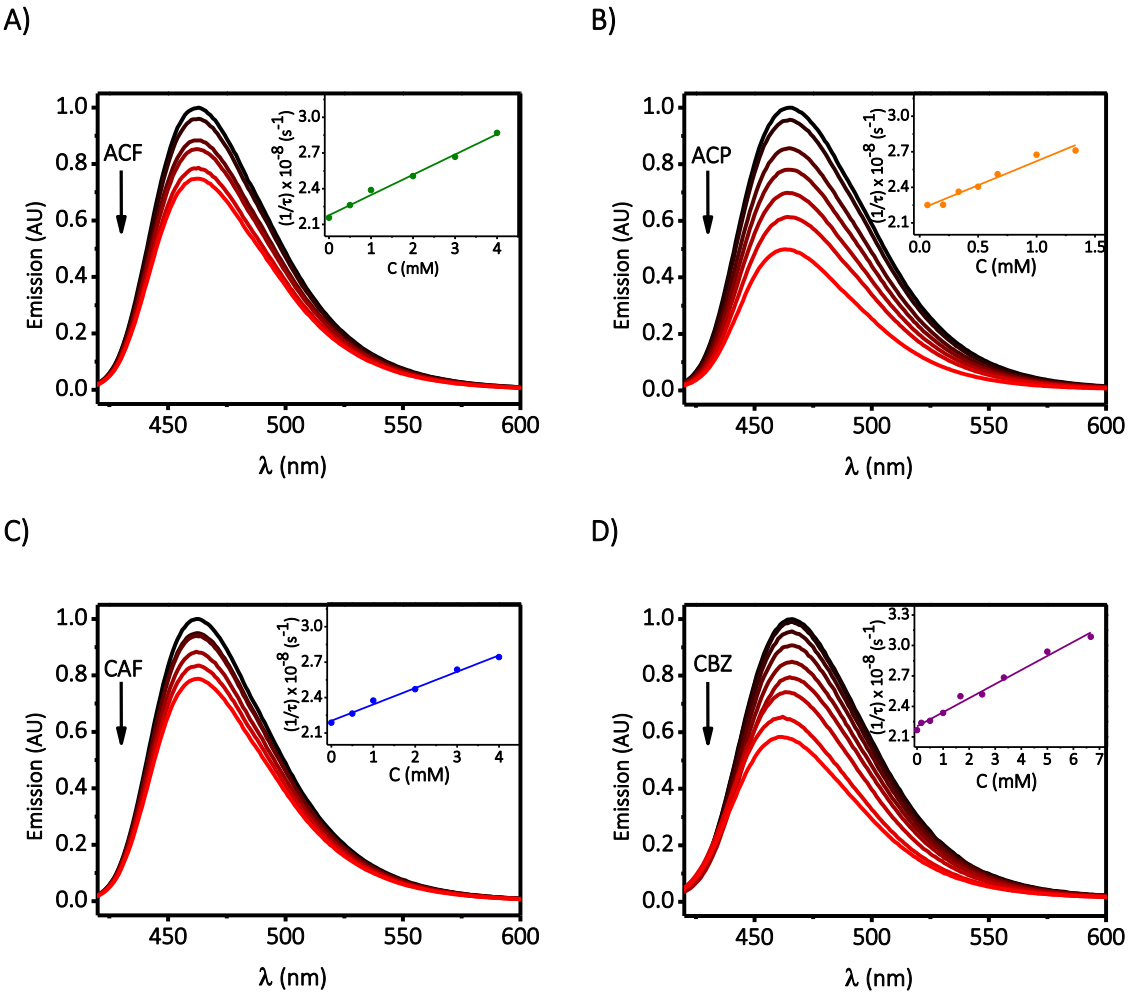


**Figure 23**: Steady-state $^1(TPP^+)^*$ fluorescence quenching ($\lambda_{exc}$ = 405 nm) and Stern-Volmer plots, obtained from the time-resolved experiments (insets), upon increasing concentration of contaminants in deaerated $CH_3CN$: ACF (**A**), ACP (**B**), CAF (**C**) and CBZ (**D**).

**Table 7**: Rate constants for the quenching of the singlet excited state of $TPP^+$ by each pollutant obtained from time-resolved experiments.

| | ACF | ACP | CAF | CBZ |
|---|---|---|---|---|
| $k_{qs}$ ($M^{-1}s^{-1}$) | 1.8 x $10^{10}$ | 3.6 x $10^{10}$ | 1.4 x $10^{10}$ | 1.5 x $10^{10}$ |

Next, laser flash photolysis (LFP) experiments were performed in the presence of increasing concentrations of the contaminants upon excitation of $TPP^+$ at 355 nm. Kinetic traces were recorded at 550 nm, where both the triplet excited state and the reduced species of the photocatalyst absorb, see Figure 24.

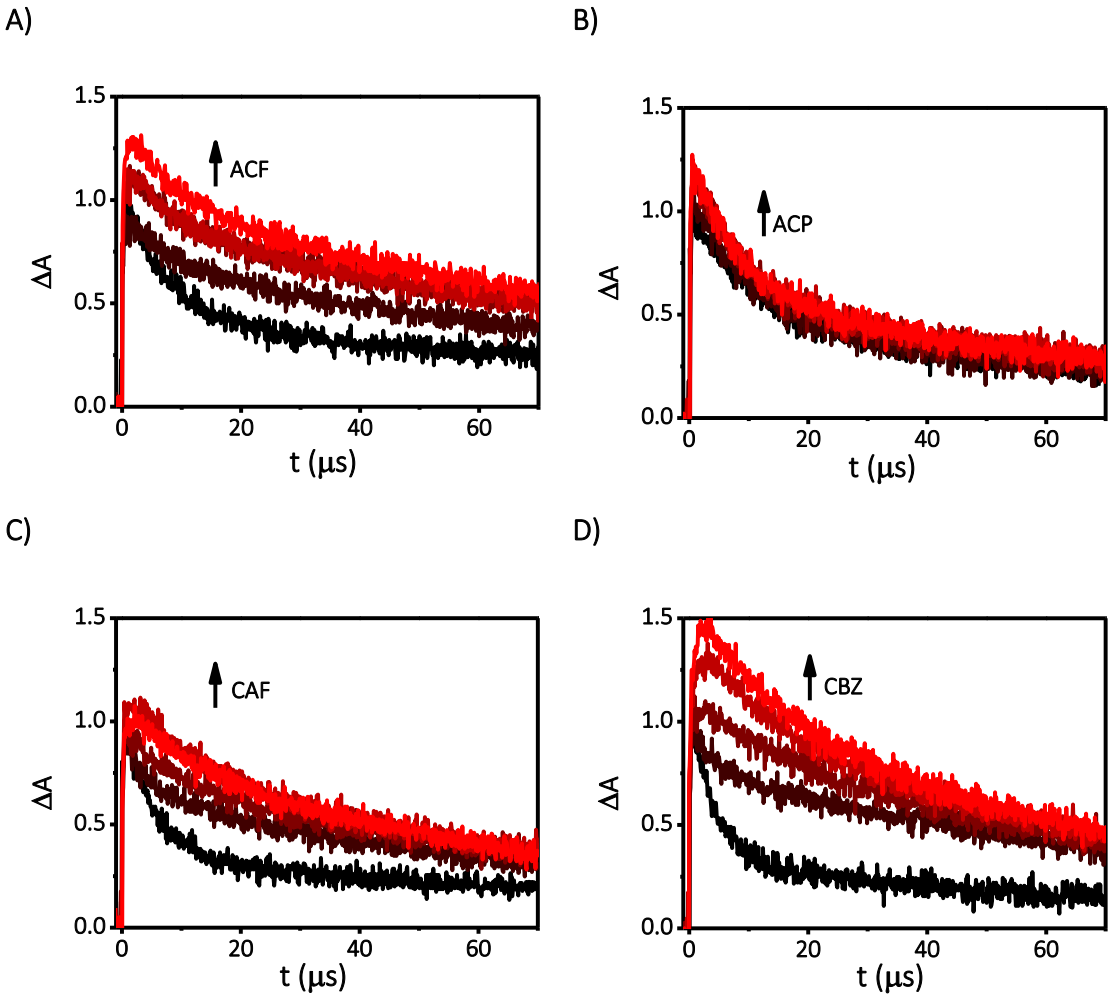


**Figure 24**: Kinetic traces recorded at 550 nm, obtained upon LFP excitation ($\lambda_{exc}$ = 355 nm) of deaerated acetonitrile solutions of $TPP^+$ ($7 \times 10^{-5}$ M) upon increasing pollutant concentrations ($0 - 7 \times 10^{-5}$ M): ACF (**A**), ACP (**B**), CAF (**C**) and CBZ (**D**).

The traces shown in Figure 24 provide the first piece of evidence to support the electron transfer mechanism. The first absorption decay recorded in the absence of contaminants at 550 nm (initial trace in the four cases, in black) is due exclusively to the characteristic absorption of the triplet excited state of TPP, $^3(TPP^+)^*$. Upon addition of increasing concentration of the pollutants, the absorption at the initial recording time and the lifetime of the observed traces increase in the case of ACF, CAF and CBZ. The

higher absorption can only be attributed to the contribution of a species different from the triplet which absorbs at the same wavelength but with a higher molar absorption coefficient, thus the reduced pyranyl radical, TPP· (see Figure 20). The appearance of the TPP· within the laser pulse in the presence of the pollutants is in good agreement with the observed quenching of the singlet excited state in these three cases (see above). The existence of both species at the recorded wavelength of 550 nm needed a two monoexponential terms to accurately fit the decay trace. As a result, the pre-exponential factor (amplitude), which is the population decaying with a specific lifetime, was obtained for each species. These values allowed quantifying the concentration of the two species, as shown on Figure 25 for the triplet (A) and for the pyranyl radical (B), see section 9.3.5 for details.

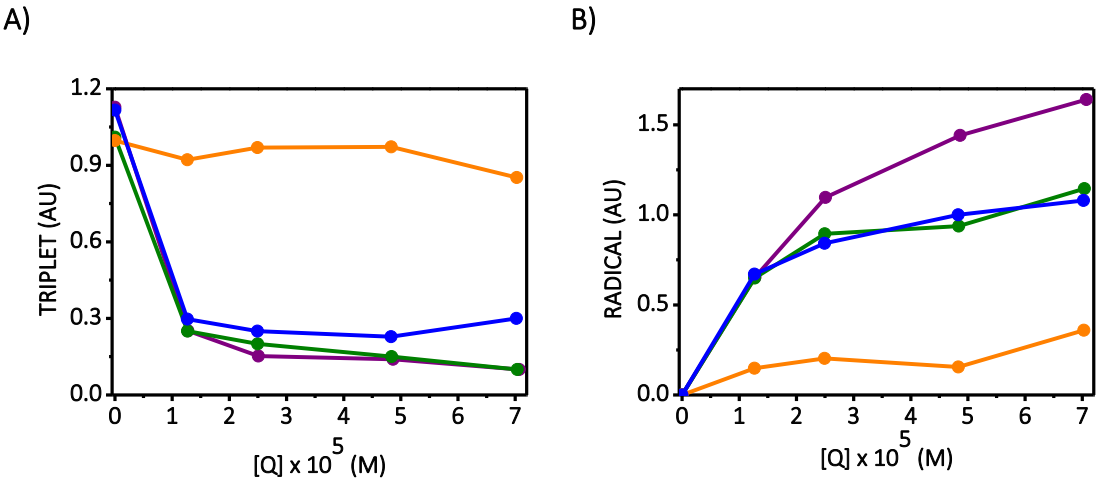


**Figure 25**: Evolution of the concentration of the triplet excited state (**A**) and pyranyl radical (**B**) upon increasing amounts of ACF (●), ACP (●), CAF (●) and CBZ (●).

From these results we can conclude that the appearance of the reduced TPP· acts as a proof of the first step of the photooxidation process, since the corresponding pollutant radical cations are not revealed in the available UV-vis spectral window (300-700 nm). Moreover, the lack of photodegradation of ACP shown in Figure 22 is in good agreement with the very low formation of the pyranyl radical found upon the analysis of the LFP experiments. Therefore, the fluorescence quenching observed at Figure 23B can be attributed to an efficient electron transfer followed by an also efficient back electron transfer (BET) since no pyranyl radical formation was observed.

Scheme 3 shows the postulated mechanism for the photooxidation of the contaminants with $TPP^+$. The detection and quantification of the primary reduced pyranyl radical species demonstrates that the electron transfer mechanism is the initial step to carry out the oxidation process from the excited states of the photocatalyst. After the $e^-$ transfer, the resulting photooxidized radical cations react with $O_2$ giving rise to a different extent of the overall photodegradation process. The fact that after only 90 min of irradiation ACF was completely removed could be attributed to a more efficient reaction pathway occurring from the resulting phenoxyl radical.

A) Initiation step:

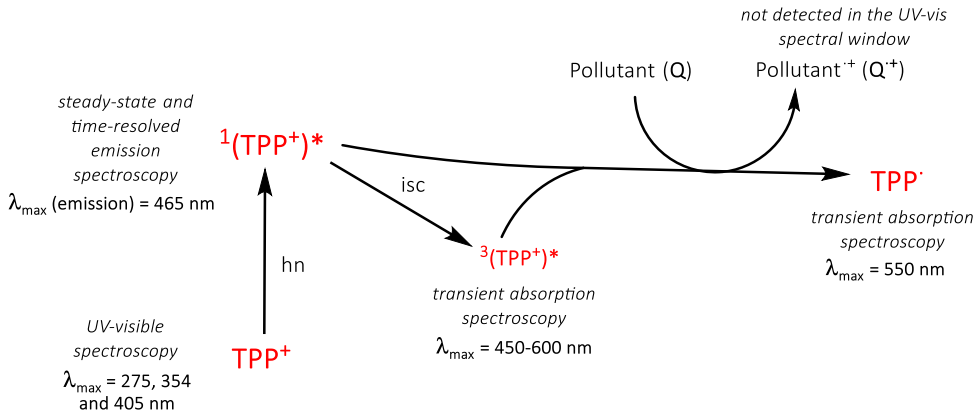


B) Propagation step:

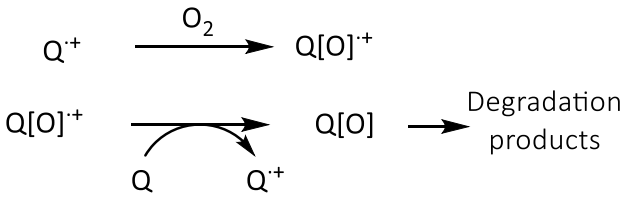


**Scheme 3**: **A)** Electron transfer mechanism to explain the photodegradation of the pollutants in the presence of $TPP^+$, happening from either the singlet or the triplet excited states. The primary reduced pyranyl radical and oxidyzed pollutant radical cation are indicated. The detection technique applied for each species is specified. **B)** Further oxidation of the pollutants that may happen after the photocatalytic step.

## 4.3. Conclusions

The photocatalyzed oxidation of acetaminophen, acetamiprid, caffeine and carbamazepine with triphenylpyrylium ($TPP^+$) can be correlated with direct detection of the short-lived intermediates derived from the photocatalyst. Thus, steady-state and

time-resolved fluorescence measurements allow characterizing the reaction from the $^1(TPP^+)^*$; whereas, complementary information about $^3(TPP^+)^*$ and $TPP^{\cdot}$ is provided by laser flash photolysis experiments. Oxidation of the contaminants goes in parallel with the $TPP^+$ reduction, and subsequent formation of the pyranyl radical ($TPP^{\cdot}$). The reduced radical can be directly detected by laser flash photolysis; its detection constitutes a fingerprint of the redox process and can be correlated with its efficiency.

## 4.4. Experimental

Photodegradations were carried out according to the general methodology explained in section 9.3.1. In this case, photodegradation mixtures were prepared in 250 mL of aqueous solutions containing 5 mg/L of each pollutant (0.1 mM global concentration) and 10 mg/L (0.03 mM) of $TPP^+$. To increase stability of the photocatalyst, the pH was adjusted to 3 by dropwise addition of sulfuric acid, and water was periodically added to compensate for the evaporation loss.

For the detection by HPLC, aliquots were firstly filtered through polypropylene (0.45 μm). The HPLC mobile phase was a gradient mixture containing acetonitrile (from 3 to 70%) and 0.1% aqueous formic acid at a flow rate of 0.3 mL/min.

Mineralization of ACF was evaluated upon trapping the formed carbon dioxide as $BaCO_3$, according to the general procedure explained at 9.3.2. For this purpose, an aqueous solution (80 mL) containing acetaminophen (1.0 g) and $TPP^+$ (2.5 mg) was irradiated for 24 hours under continuous flow of $O_2$.

The photophysical measurements were performed according to the general procedure 9.3.4.

For the steady-state and time-resolved fluorescence experiments, the final concentrations were up to $7 \times 10^{-3}$ M for each pollutant, the excitation wavelength was fixed at 405 nm and the measurements were performed under anerobic atmosphere.

For the laser flash photolysis experiments, the final concentration of each pollutant was $7 \times 10^{-5}$ M, and the concentration of the photocatalysts was of $7 \times 10^{-5}$ M. The measurements were recorded in deaerated $CH_3CN$ upon 355 nm excitation.

Redox potential measurements were carried out according to 9.3.3.

A)

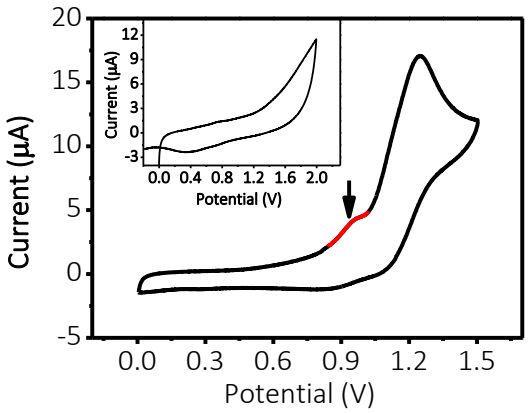


| ELECTRODE | E ($ACF^{\cdot+}$/ACF) |
|---|---|
| AgCl/Ag (sat KCl) | 0.95 V |
| SCE* | 0.91 V |

B)

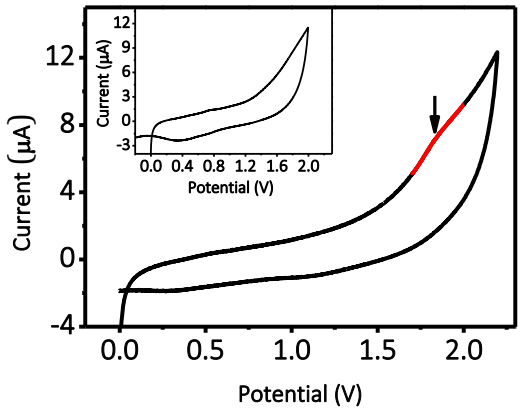


| ELECTRODE | E ($ACP^{\cdot+}$/ACP) |
|---|---|
| AgCl/Ag (sat. KCl) | 1.83 V |
| SCE* | 1.79 V |

C)

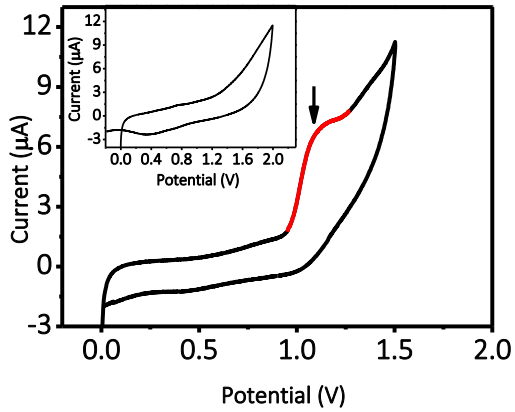


| ELECTRODE | E ($CAF^{\cdot+}$/CAF) |
|---|---|
| Ag Cl Ag (sat. KCl) | 1.10 V |
| SCE* | 1.06 V |

**Figure 26**: Cyclic voltammetry of ACF (**A**), ACP (**B**) and CAF (**C**) (30µM) measured in PBS, in the case of ACF, or tetrabutyl ammonium perchlorate (TBA), for ACP and CAF, solution (0.1 M) as electrolyte at 0.05 (ACF and CAF) or 0.1 (ACP) V $s^{-1}$. (**D**) Cyclic

voltammetry of the corresponding electrolytes PBS or TBA. * The obtained data from the AgCl/Ag (sat KCl) were converted into redox potential values *vs* SCE as follows: E (*vs* SCE, in V) = E (*vs* AgCl/Ag, in V) -0.045.

# 5. Time-resolved Kinetic Assessment of the Role of Singlet and Triplet Excited States in the Photocatalytic Treatment of Pollutants at Different Concentrations

## 5.1. Introduction

Photochemical processes are getting importance in the field of Green Chemistry since, in general, they involve milder conditions than conventional ones. However, photochemical systems are not simple, as they involve excited states, hydroxyl radical, singlet oxygen, superoxide anion and/or organic/inorganic radicals.[104, 112, 136-138] Therefore, in order to fully understand such a system, two complementary aspects should be taken into account: the thermodynamics and the kinetic viability of all the competing pathways. Firstly, thermodynamic estimations based on the redox potentials of the involved species could help to discard those pathways that result highly endergonic and to identify the thermodynamically allowed key steps. Secondly, an overall analysis of the lifetime of the involved transient species would help to elucidate the role of each photoactive species and thus to assess whether the processes are competitive at that time scale and, therefore, which are the key species. In addition, a further parameter to be evaluated is the efficiency of each competitive process as a function of the substrate concentration.[70]

Under this context, $TPTP^+$ could work as a model to perform a full analysis of a photoredox system, due to several reasons: i) its redox potentials from the singlet and the triplet excited states, $E^*(TPTP^+/TPTP^{\cdot})$, are. 2.5 and 2.0 V *vs* SCE, respectively, therefore is an extremely good oxidant; ii) it is able to absorb UV-vis light (Figure 9 and Table 1 in the Preamble of Part I).[70]

With this background, the main goal of the present chapter is to provide a kinetic-based analysis to assess the role of the singlet and triplet excited states in the photodegradation of real pollutants at different concentrations. These pollutants were previously used in Chapter 4: acetaminophen (ACF), acetamiprid (ACP), caffeine (CAF)

and carbamazepine (CBZ), Figure 21; in addition clofibric acid (CLOF), Figure 27, which is used as a pharmaceutical compound,[139] was added to this study.

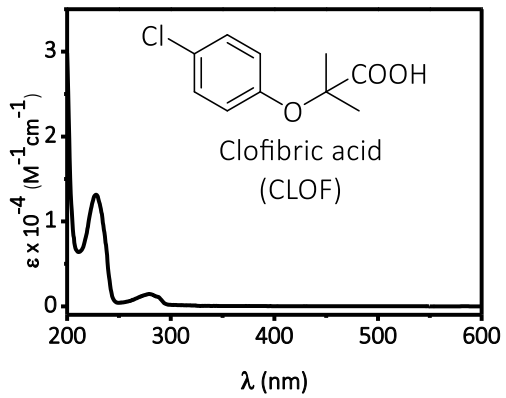


**Figure 27**: UV-vis spectrum in $CH_3CN$ and chemical structure of the selected pollutant clofibric acid (CLOF).

First, photochemical oxidation of the pollutants was carried out under solar irradiation in the presence of $TPTP^+$; next, photophysical measurements (fluorescence and laser flash photolysis) provided fast kinetic data; and finally, a mathematical analysis allowed evaluating the role of the concentration of pollutants on the relative contribution of the different excited states to the overall photodegradation.

## 5.2. Results and discussion

$TPTP^+$ is known for being a good oxidant from both, its singlet and its triplet excited states, with $E^*_{TPTP+/TPTP^\cdot}$ *ca*. 2.5 and 2.0 V *vs* SCE, respectively.[86] Attending to the reported redox potentials for the pollutants measured in our hands, see Figure 26A, B and C and Figure 33, and those reported in the literature, the photooxidation of the five pollutants is thermodynamically favoured in every case, see Table 8.

**Table 8:** Redox potentials for each pollutant and the corresponding values of the photoinduced Gibbs free energy for the oxidation processes from the singlet and triplet excited state of $TPTP^+$.

| | ACF | ACP | CAF | CBZ | CLOF |
|---|---|---|---|---|---|
| $E_{red}$ ($Q^{\cdot+}/Q$) *vs* SCE (V) | +0.9 | +1.8 | +1.1 | +1.4[133] | +1.5 |
| $\Delta G_{SINGLET}$ (kcal·mol$^{-1}$) | -38.6 | -18.0 | -33.9 | -27.0 | -24.7 |
| $\Delta G_{TRIPLET}$ (kcal·mol$^{-1}$) | -24.6 | -4.0 | -19.9 | -13.0 | -10.7 |

Then, an aerated aqueous solution containing the five pollutants was irradiated with a solar simulator in the presence of $TPTP^+$. Figure 28A shows the relative concentration of each pollutant vs. irradiation time: removal of ACP was negligible, as expected from the thermodynamic analysis; CBZ and CAF were degraded in *ca.* 50% after 180 min; and CLOF and ACF showed the highest photodegradation percentages. In fact, CLOF was completely removed after only 10 min irradiation, while *ca.* 60 min were required in the case of ACF, under the studied experimental conditions. The fast degradation in the case of CLOF could be attributed to the formation of stable by-products that may favour the degradation reaction or to direct photolysis, see Figure 28B.

Direct photolysis control experiments (in the absence of $TPTP^+$) showed almost no reaction apart from CLOF, which suffered some direct photodegradation although much more slowly (Figure 28B).

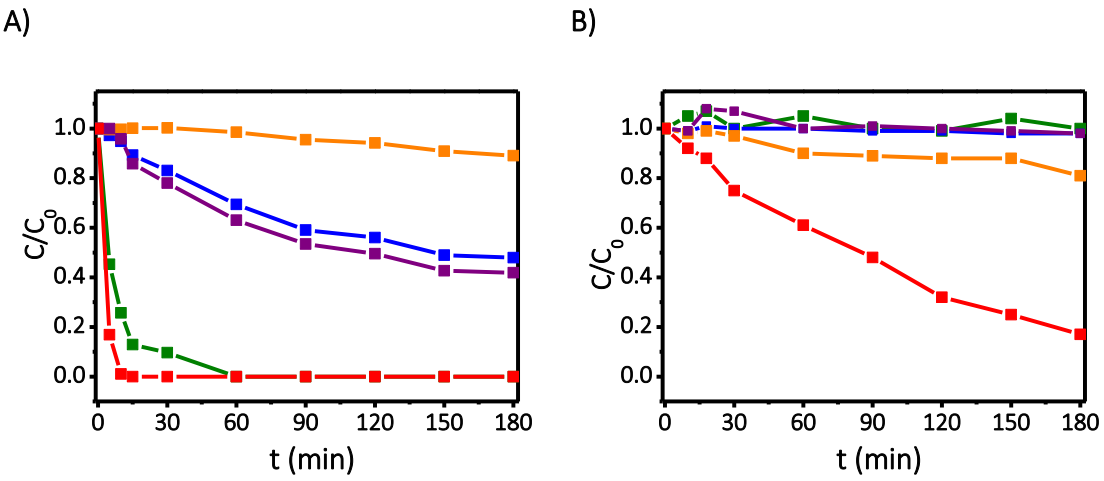


**Figure 28**: Plot of the relative concentration of ACF (■), ACP (■), CAF (■), CBZ (■)and CLOF (■) at $C_o$= 5 mg $L^{-1}$ each (1.3x10$^{-4}$ M global concentration)in aerated acidic

(pH = 3) media, *vs*. time under solar simulated irradiation, in the presence of 10 mg $L^{-1}$ ($2x10^{-5}$ M) of $TPTP^+$ (A) and in the absence of photocatalyst (B).

The next step was the evaluation of the electron transfer from the singlet and from the triplet excited states of $TPTP^+$ and the formation of photoactive ground-state complexes, since previous studies have demonstrated that this photocatalyst is also able to act through all those pathways[103, 111, 116, 117, 140]. Therefore, every potential species that may participate in the photodegradation has to be evaluated for every pollutant and the combined results have to be analysed for each pollutant at different concentrations.

First, fluorescence experiments (steady-state and time-resolved) were performed in deaerated acetonitrile to investigate the involvement of $^1(TPTP^+)^*$ in the photodegradation of the pollutants, (Figure 29). A decrease in the emission and also in the lifetime of $^1(TPTP^+)^*$ was observed in all cases upon increasing concentration of every pollutant. Then, applying the Stern-Volmer relationship for the time-resolved results, ($1/\tau$ *vs* contaminants' concentration), the corresponding quenching rate constants were determined. The obtained values are summarized in Table 9, all of them are in the order of ≈ $10^{10}$, what confirms the dynamic involvement of the singlet excited state in all cases, with values in the range of the diffusion limit ($k_{diff}$ = 1.9 x $10^{10}$ $M^{-1}s^{-1}$ in $CH_3CN$).[135]

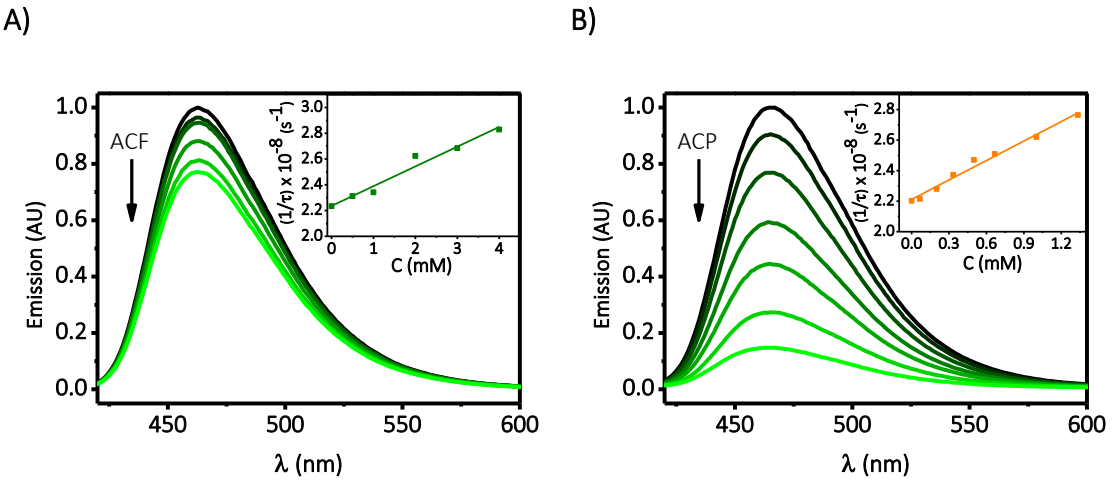

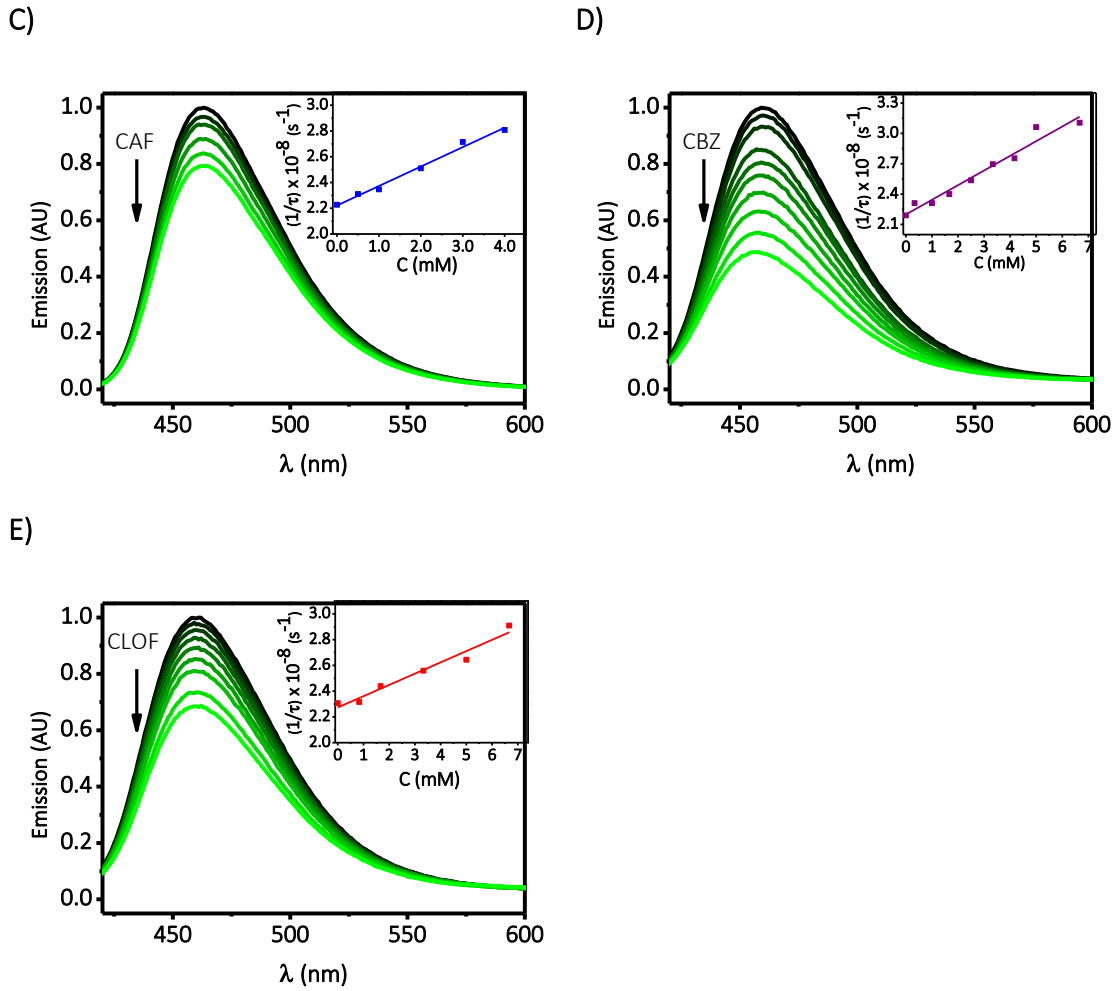


**Figure 29**: Steady-state $^{1}(TPTP^{+})^{*}$ fluorescence quenching by every pollutant; Insets: Stern-Volmer plots obtained from time-resolved experiments; all upon increasing pollutant concentration (in the millimolar range) in deaerated $CH_3CN$ ($\lambda_{exc}$ = 400 nm).

Moreover, it is worth mentioning that in the case of ACP, while the Stern-Volmer relationship revealed a linear behaviour (inset of Figure 29B), results obtained from the steady-state experiments did not follow a linear trend (Figure 29B). In fact, when $I_0/I$ was plotted *vs* ACP concentration (Figure 30A) the observed deviation from a linear fitting in the Stern-Volmer relationship, pointed to the formation of a non-emissive ground state complex. The stoichiometry of the so called complex ($TPTP^{\delta+}$--$ACP^{\delta'+}$) calculated from a Job's plot experiment [128, 141], see Figure 30 B, was 1:1, and its corresponding complexation constant, K, was determined on the basis of the Benesi-Hildebrand relationship (K=503 $M^{-1}$), see Figure 30 C.[8, 9] Formation of this kind of ground-state complexes could in principle influence positively on the photocatalytic oxidation of a substrate, since the pre-association could result in an "intramolecular-like" reaction

proceeding at much higher rate (not-controlled by diffusion) and therefore offering a much more competitive degradation pathway. On the contrary, back electron transfer could also be much more favored, resulting in a lower photodegradation efficiency.

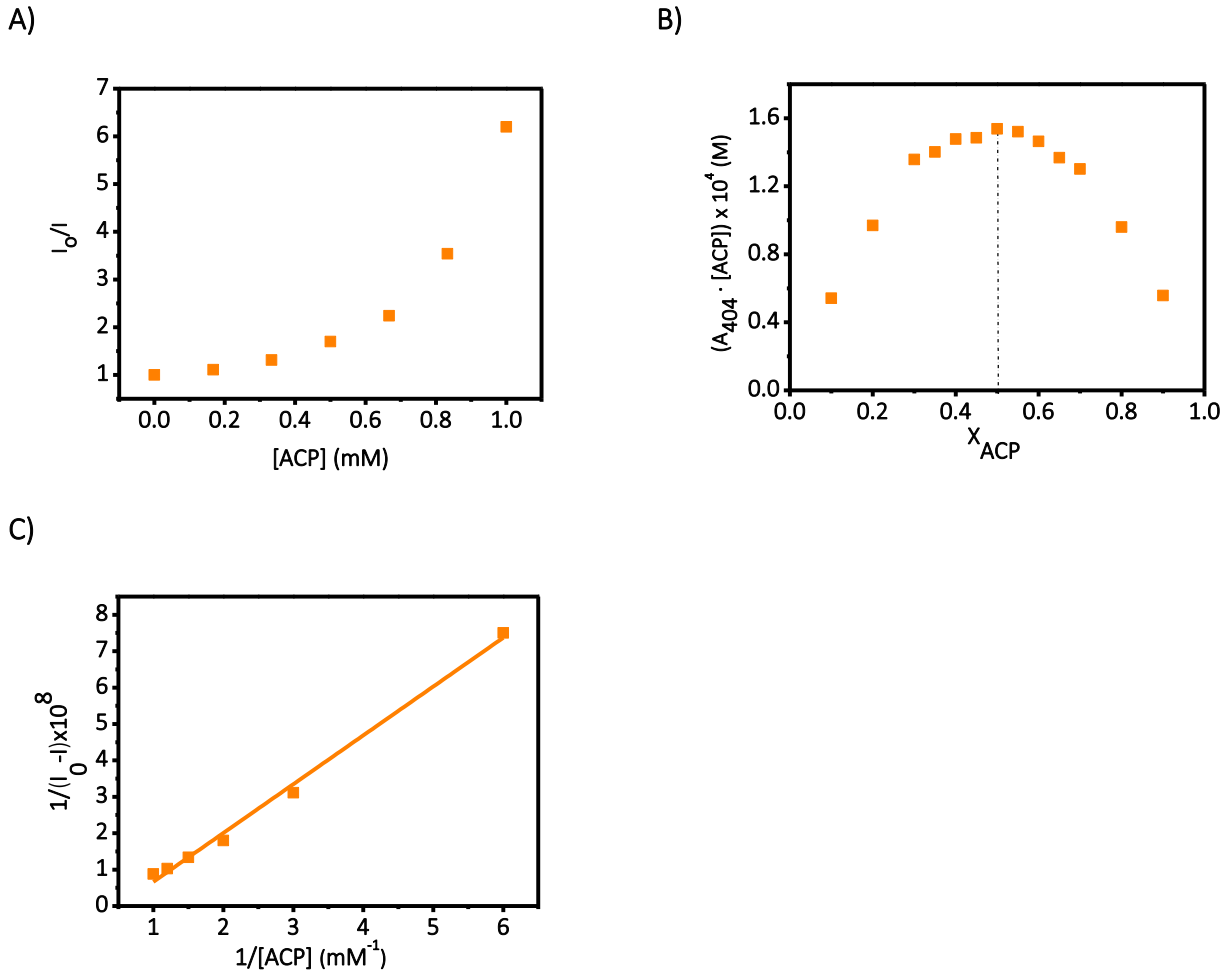


**Figure 30: A)** Plot of the relative steady-state $^1$(TPTP$^+$)* fluorescence emission upon increasing ACP concentration in deaerated $CH_3CN$ ($\lambda_{exc}$ = 400 nm). **B)** Job's plot for TPTP$^+$ *vs* ACP molar fraction at total concentration of 50 μM. **C)** Benesi-Hildebrand fitting for $^1$(TPTP)* with ACP.

Next, the participation of the triplet excited state of TPTP$^+$ was investigated on the basis of laser flash photolysis (LFP) experiments. Therefore, deaerated acetonitrile solutions of TPTP$^+$ were submitted to laser flash excitation (355 nm) and its triplet lifetime was monitored at 620 nm. The lifetime of the triplet excited state of TPTP$^+$ clearly decreased in every case (Figure 31) and the corresponding quenching constants were

determined from the Stern-Volmer linear relationships. The values of the kinetic constants are summarized in Table 9.

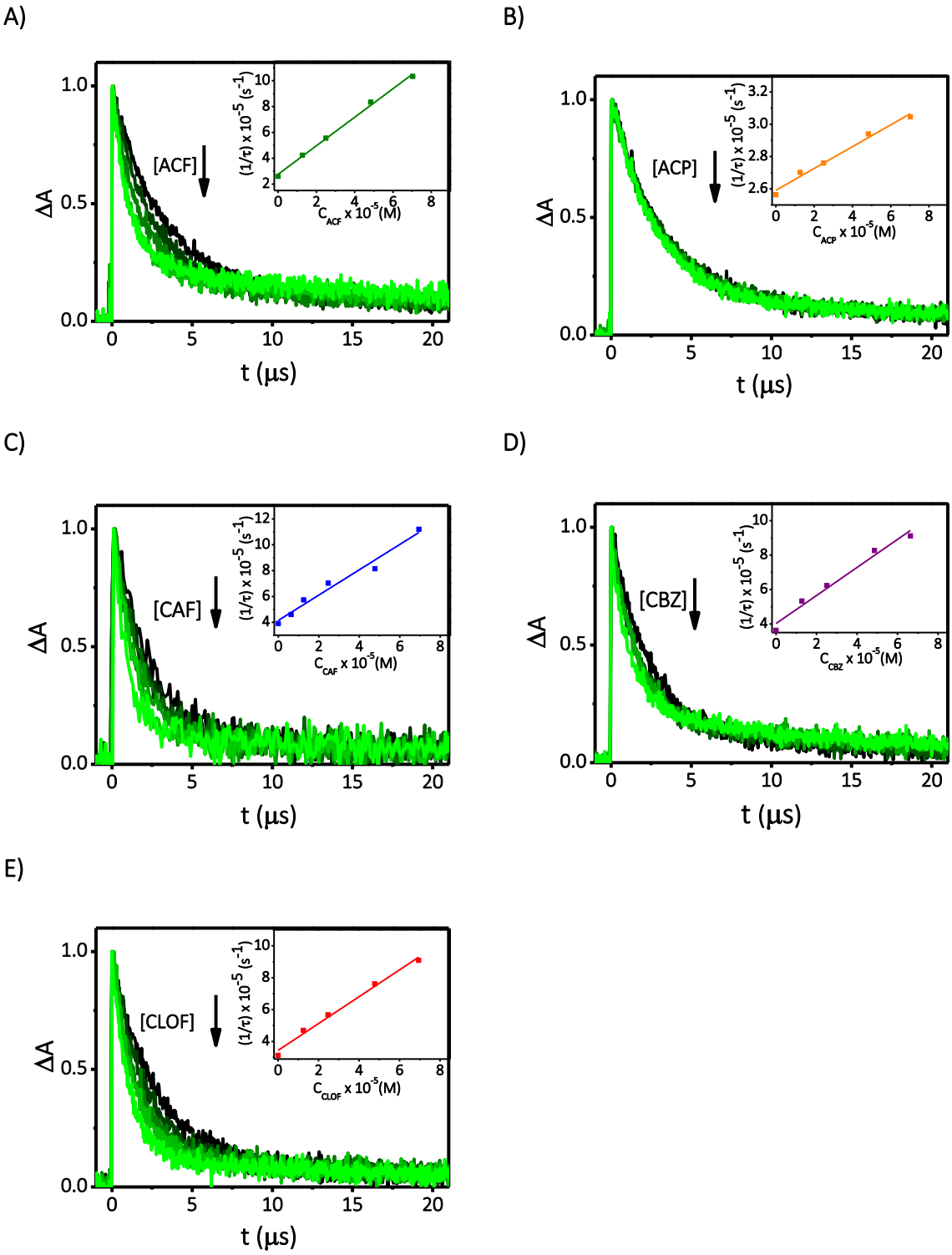


**Figure 31**: Normalized kinetic traces recorded at 620 nm obtained upon LFP excitation (355 nm) of deaerated acetonitrile solutions (7 x $10^{-5}$ M) of $TPTP^{+}$ upon increasing pollutant concentrations. Insets: Corresponding Stern-Volmer plots.

Table 9: Rate constant values ($k_{qS}$ and $k_{qT}$) for the quenching of $^1(TPTP^+)^*$ and $^3(TPTP^+)^*$ by the pollutants determined from time-resolved fluorescence and laser flash photolysis experiments, respectively.

| POLLUTANT | $k_{qS}$ x $10^{-10}$ ($M^{-1}s^{-1}$) | $k_{qT}$ x $10^{-8}$ ($M^{-1}s^{-1}$) |
|---|---|---|
| | $^1(TPTP^+)^*$ | $^3(TPTP^+)^*$ |
| ACF | 1.5 | 110 |
| ACP | 4.4 | 6.8 |
| CAF | 1.5 | 98 |
| CBZ | 1.5 | 81 |
| CLOF | 0.8 | 84 |

Finally, quenching of the excited states of $TPTP^+$ through an energy transfer mechanism was ruled out attending to the UV-visible spectra of the photocatalyst and the pollutants (Figure 9, Figure 21 and Figure 27). $TPTP^+$ absorbs up to 450 nm while the pollutants absorb at much shorter wavelength, all below 320 nm, which allows predicting much more energetic excited states in the case of the pollutants than in the case of $TPTP^+$. Therefore, an energy transfer from the photocatalyst to each pollutant looks unlikely.

A further piece of evidence supporting the electron transfer mechanism was obtained, using CAF as example, from the results of the quenching experiments performed in solvents of different (relative) permittivity since a correlation should be found with the quenching constants if the process happens through an electron transfer mechanism. Thus, the quenching of the triplet excited state of $TPTP^+$ was performed in tetrahydrofuran ($\varepsilon$ = 7.58) and the result was compared to the result obtained in acetonitrile ($\varepsilon$ = 35.94). The obtained quenching constants were 6.0 x $10^8$ $M^{-1}s^{-1}$ and 9.8 x $10^9$ $M^{-1}s^{-1}$ in tetrahydrofuran and acetonitrile, respectively; thus, supporting the photoxidation occurring through an electron transfer process, Figure 32.

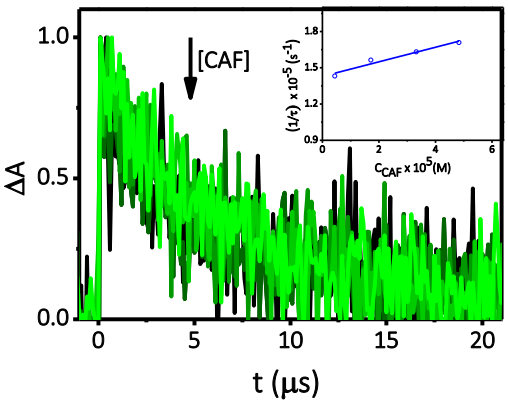


**Figure 32**: Normalized kinetic traces recorded at 620 nm, obtained upon LFP excitation (355 nm) of deaerated THF solutions of $TPTP^+$ (7 x $10^{-5}$ M) upon increasing concentration of CAF. Inset: Corresponding Stern-Volmer plot.

With this background, the overall electron transfer mechanistic pathway to explain the observed photodegradation of ACF, ACP, CAF, CBZ and CLOF in the presence of $TPTP^+$ is postulated in Scheme 4, were $^{+}\delta$ and $^{+}\delta'$ represents the charge transfer distribution between $TPTP^+$ and a pollutant. As a summary, quenching of the singlet and of the triplet excited states of $TPTP^+$ was observed in every case. In addition, in the case of ACP, formation of a complex was also demonstrated.

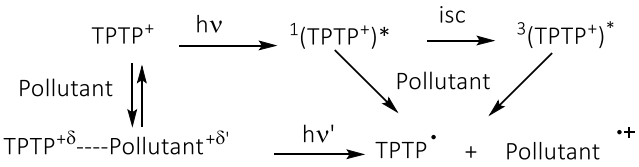


**Scheme 4**: Overall mechanistic pathways to explain photodegradation of pollutants by oxidative $e^-$ transfer to $(TPTP^+)^*$.

Once the mechanism has been postulated, the contribution of each species can be calculated on the basis of the equations of Chapter 3, Eq. 10 to Eq. 20. Moreover, the efficiency in the use of a photocatalyst to carry out the photodegradation of the pollutants can be correlated with the pollutants concentration. In order to facilitate the understanding, the main equations are summarized again:

Formation of a ground-state complex:

$$\text{Eq. 13: } \left[PC^{\delta+}\cdots Q^{\delta\prime+}\right](\%) \cong K \times [Q] \times 100$$

Formation of the singlet excited state:

Eq. 14:

$$^{1}(PC)^{*}\ formation\ (\%) = \ 100 - \left[PC^{\delta+}\cdots Q^{\delta'+}\right](\%) \approx 100 - K \times [Q] \times 100 = \\ = (1 - K \times [Q]) \times 100$$

Thus, quenching of the singlet excited state by the pollutant is shown by Eq. 16 , and formation of the triplet excited state is described by Eq. 17:

Eq. 16: $$Quenching\ of\ \ ^{1}(PC)^{*}\ (\%) = \ \ ^{1}(PC)^{*}\ formation(\%) \times \frac{k_{qs}[Q]}{\frac{\Phi_F}{\tau_S}+\frac{\Phi_{ISC}}{\tau_S}+k_{qs}[Q]}$$

Eq. 17: $$^{3}(PC)^{*}\ formation(\%) = \ ^{1}(PC)^{*}\ formation\ (\%) \times \frac{\frac{\Phi_{ISC}}{\tau_S}}{\frac{\Phi_F}{\tau_S}+\frac{\Phi_{ISC}}{\tau_S}+k_{qs}[Q]}$$

Finally, the reaction from the triplet excited state is given by Eq. 20 and the intrinsic triplet decay by Eq. 21:

Eq. 20:

$$Quenching\ of\ \ ^{3}(PC)^{*}\ (\%) = \ ^{1}(PC)^{*}\ formation\ (\%) \times \frac{\frac{\Phi_{ISC}}{\tau_S}}{\frac{\Phi_F}{\tau_S}+\frac{\Phi_{ISC}}{\tau_S}+k_{qs}[Q]} \times \frac{k_{qT}[Q]}{\frac{1}{\tau_T}+k_{qT}[Q]}$$

Eq. 21:

$$Deactivation\ of\ \ ^{3}(PC)^{*}\ (\%) = \ ^{1}(PC)^{*}\ formation\ (\%) \times \frac{\frac{\Phi_{ISC}}{\tau_S}}{\frac{\Phi_F}{\tau_S}+\frac{\Phi_{ISC}}{\tau_S}+k_{qs}[Q]} \times \frac{\frac{1}{\tau_T}}{\frac{1}{\tau_T}+k_{qT}[Q]}$$

The equations described above, explain how the relative contribution of the different deactivation channels of the photocatalyst depends on the intrinsic properties of the photocatalyst, on the experimentally determined quenching constants and on the pollutant concentration.

From the results obtained in this chapter, formation of a photoactive ground-state complex, singlet and triplet excited states are considered as species participating in the photodegradation. Therefore, attending to the kinetic quenching constants of the pollutants (Table 9) and with the photophysical data reported for the photocatalyst (Table 1), [70] the determined relative contribution of every pathway is determined for every pollutant and the results are shown in Table 10 .

**Table 10:** Relative contribution of the ground-state complex formation, singlet and triplet excited states quenching, together with fluorescence and intrinsic triplet deactivation, in the photocatalytic degradation of the pollutants, at different concentrations, using $TPTP^+$ (10 mg $L^{-1}$ or 0.02 mM).

| [Q] (M) | Pollutant | Complex formation (%) | Quenching of $^1$(TPTP)* (%) | $^1$(TPTP)* intrinsic decay (%) | Quenching of $^3$(TPTP)* (%) | $^3$(TPTP)* intrinsic decay (%) |
|---|---|---|---|---|---|---|
| $10^{-3}$ | ACF | - | 3.2 | 5.8 | 89.2 | 1.8 |
| | ACP | 50.6 | 1.6 | 2.9 | 33.7 | 11.3 |
| | CAF | - | 3.2 | 5.8 | 89.0 | 2.1 |
| | CBZ | - | 3.2 | 5.8 | 88.6 | 2.4 |
| | CLOF | - | 3.2 | 5.8 | 88.6 | 2.5 |
| $10^{-5}$ | ACF | - | <0.1 | 6.0 | 30.7 | 63.2 |
| | ACP | 0.5 | <0.1 | 6.0 | 2.7 | 90.8 |
| | CAF | - | <0.1 | 6.0 | 28.3 | 65.7 |
| | CBZ | - | <0.1 | 6.0 | 25.4 | 68.6 |
| | CLOF | - | <0.1 | 6.0 | 24.8 | 69.2 |
| $10^{-8}$ | ACF | - | 0.0 | 6.0 | 0.0 | 94.0 |
| | ACP | - | 0.0 | 6.0 | 0.0 | 94.0 |
| | CAF | - | 0.0 | 6.0 | 0.0 | 94.0 |
| | CBZ | - | 0.0 | 6.0 | 0.0 | 94.0 |
| | CLOF | - | 0.0 | 6.0 | 0.0 | 94.0 |

Table 10 shows that when quenching of singlet and triplet occurs, the relative contribution of the singlet is negligible compared to that of the triplet. This is in good agreement with the lifetime of both species, the shorter the lifetime of the excited species, the more difficult to be quenched. Moreover, the kinetic constants obtained for the quenching of the triplet are in good agreement with the photodegradation extent, (Figure 28) except for the case of CLOF, whose oxidation is even faster than predicted by the photophysical experiments. Therefore, it can be stated that, in general, quenching of the triplet is more efficient than quenching of the singlet; or, in other words, the higher the intersystem crossing quantum yield, the better.

In addition, it should be highlighted that the pollutant concentration is also a parameter to be considered. It could be observed how efficient the quenching of the excited photocatalyst can be when the concentration of the pollutants is in the order of $10^{-3}$ M. Comparing this situation with another one in which the pollutants are much more

diluted (for instance $10^{-5}$ M), it can be seen (Table 10, top and middle) that the relative contribution of the excited species decreases in favor of the intrinsic decay of the excited state. This fact is even clearer at lower concentrations, as for example at $10^{-8}$ M, in which the intrinsic decay of the triplet is the major deactivation pathway, making the photodegradation of the pollutants clearly negligible. This reveals that the efficiency of a photocatalyst is higher as higher is the concentration of the pollutant. In other words, the energy employed in activating the photocatalyst is best invested when the concentration of the pollutants is high.

## 5.3. Conclusions

Results obtained using $TPTP^+$ as organic photocatalyst allow stating that efficiency of the triplet excited state is higher than the one of the singlet when both are quenched. Furthermore, the concentration of the pollutants plays a key role; in fact, below micromolar concentration, the lifetime of the excited species hampers encountering with the pollutants.

## 5.4. Experimental

Photodegradations were carried out according to the general methodology explained in section 9.3.1. In this case, photodegradation mixtures were prepared in 250 mL of aqueous solutions containing 5 mg/L of each pollutant ($1.3x10^{-4}$ M global concentration) and 10 mg/L (0.02 mM) of $TPTP^+$. To increase stability of the photocatalyst, the pH was adjusted to 3 by dropwise addition of sulfuric acid and water was periodically added to compensate for the evaporation loss.

For the detection by HPLC, aliquots were firstly filtered through polypropylene (0.45 µm). The HPLC mobile phase was a gradient mixture containing acetonitrile (from 3 to 70%) and 0.1% aqueous formic acid at a flow rate of 0.3 mL/min.

The photophysical measurements were performed according to general procedure 9.3.4.

For the steady-state and time-resolved fluorescence experiments, the final concentrations were in the millimolar range for each pollutant, the excitation wavelength

was fixed at 400 nm and the measurements were performed under deaerated atmosphere.

For the Job's plot experiment, the general procedure explained in section 9.3.4 was followed, the absorbance changes were measured at 404 nm.

For the laser flash photolysis experiments, the final concentration of each pollutant was up to 7 x $10^{-5}$ M and the concentration of the photocatalyst was 7 x $10^{-5}$ M.

The redox potential measurement was carried out according to 9.3.3.

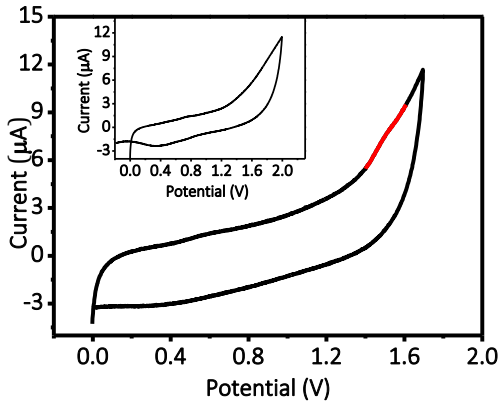


| ELECTRODE | E ($CLOF^{\cdot+}$/CLOF) |
|---|---|
| Ag Cl /Ag (sat. KCl) | 1.50 V |
| SCE | 1.46 V |

**Figure 33**: Cyclic voltammetry of CLOF (30 µM) measured in tetrabutyl ammonium perchlorate (TBA) solution (0.1 M) as electrolyte at 0.05 V $s^{-1}$. Inset: Cyclic voltammetry of the electrolyte TBA. The obtained data from the AgCl/Ag (sat KCl) was converted into redox potential value *vs* SCE as follows: E (*vs* SCE, in V) = E (*vs* AgCl/Ag, in V) -0.045.

*PART II:*

*TYPE I VS TYPE II PROCESSES*

# Preamble

Molecular oxygen, which exhibits a triplet ground state configuration, is essential to support life on Earth. Moreover, in the presence of light, a molecule acting as photocatalyst could give rise to the formation of the *reactive oxygen species* (ROS). The name of ROS comprises several reactive oxygen species such as $^1O_2$, $OH^{\cdot}$, $HO_2^{\cdot}$, $O_2^{\cdot-}$ and $H_2O_2$. These species can be undesirable side-products that could inhibit pursued reactions, but they are also considered of great importance in materials degradation or as oxidative stressors in damaged living systems such as tumors. In the context of the present thesis, ROS are considered as species able to oxidize hardly degradable matter from aqueous effluents.[3]

In water remediation field, when photocatalysts able to generate singlet oxygen or superoxide anion have been employed, photooxidation of the organic matter has been attributed to these species.[142] Accordingly, many studies have been carried out to study the formation of these ROS from several dyes, and their subsequent reaction with different pollutants. Some of the typical photocatalysts used in wastewater remediation, due to their ability to form singlet oxygen and superoxide anion, are rose bengal, methylene blue or riboflavin, among others. Rose bengal has been used for the removal of, for example, hydroxypyridines,[143-145] hydroxypyrimidines,[146] phenols,[80] chlorophenols,[147-150] butylparaben,[151] etc.; methylene blue has been used in the removal of chlorophenols[149]or anthocyanines[152] among others; and riboflavin has been used, for example, in the removal of hydroxyquinolines,[153] carbendazim and other related benzimidazoles.[84] Besides, other singlet oxygen or superoxide anion generators, such as humic acids, have been used in literature to degrade drugs as sulphamethoxazole, clofibric acid, ofloxacin and propranolol; [154] or humic acids combined with Cu (II) for the removal of atrazine, [155] or spin-coated on a polycarbonate plate for the photodegradation of carbocyanine dyes.[156]

However, when the photocatalyst is also able to react *via* an electron transfer mechanism, the only participation of $^1O_2$ could not be assumed, and the role of Type II *versus* Type I mechanism has to be evaluated.

With this background, the second part of this thesis will be mainly focused in evaluating the involvement of Type I *versus* Type II mechanism in the photodegradation of several pollutants. More specifically, in Chapter 6, a typical photocatalyst used in wastewater remediation, known for working presumably *via* Type II mechanism (rose bengal) was studied together with a second photocatalyst that exhibits a singlet oxygen quantum yield close to the unit (perinaphthenone). Finally, in Chapter 7, a singular photocatalyst able of generate singlet oxygen from its singlet excited state (*N*-methylquinolinium salt) was employed in the photodegradation of pollutants, and the contribution of Type I *vs* Type II from the singlet excited state was also evaluated.

# 6. Type I vs Type II Photodegradation of Pollutants

## 6.1. Introduction

Rose bengal (RB) (Figure 34) is a photocatalyst with high quantum yield of singlet oxygen ($^1O_2$) formation ($\Phi_\Delta$ = 0.76-0.83).[70, 142, 157-159] It has been widely used for wastewater remediation and its activity has been attributed to the Type II mechanism.[80, 147, 160, 161] However, based on its redox potential (-0.95 V *vs* SCE) [162] it could also be able to react *via* electron transfer (Type I mechanism).[11, 163, 164]

Moreover, in aqueous media, Type I reactions are more favored than Type II, due to several reasons: i) the high value of the relative permittivity for water ($\varepsilon_{H2O}$ = 80.16); ii) the low concentration of $O_2$ in aqueous media (0.29 mM); and iii) the short lifetime of $^1O_2$ in water (*ca.* 2 μs).[165, 166] Furthermore, RB exhibits a high $\Phi_{ISC}$ (Figure 34), and, as discussed in Chapter 5, electron transfer happens more efficiently from the triplet excited states, due to their longer lifetime compared to that of the corresponding singlets.[167] Therefore, when using RB as a photocatalyst, competition between the two described pathways (Type I and II) deserves further investigation to establish the real mechanism involved in the photodegradation.

In the present Chapter, two commonly used drugs, such as diclofenac (DCF), which is included in the 2015/495/CE directive (see section 1.5.1), and acetaminophen (ACF), Figure 35, found in real wastewaters at low concentrations have been selected, and the mechanism behind their photodegradations when using RB as photocatalyst has been analysed. In addition, for a better understanding of the competition between Type I and Type II mechanisms, a second photocatalyst, perinaphthenone (PN), Figure 34, has also been evaluated using the same representative pollutants. PN has not been so widely employed in this field, but offers a higher $^1O_2$ quantum yield formation ($\Phi_\Delta$ *ca* 1) and a $E_{PN/PN^{\cdot-}}$ = -0.62 V *vs* SCE; therefore, in principle, it should give even better results if Type II is the acting mechanism.[168, 169]

To evaluate the role of the species involved in the photodegradation, laser flash photolysis of RB/PN and behavior of $^1O_2$ by transient emission spectroscopic experiments in the presence of the contaminants, will be performed. As a result, the determined

quenching rate constants will shed light on the contribution of Type I/Type II mechanisms in the photodegradation of the selected contaminants and a general conclusion will be drawn.

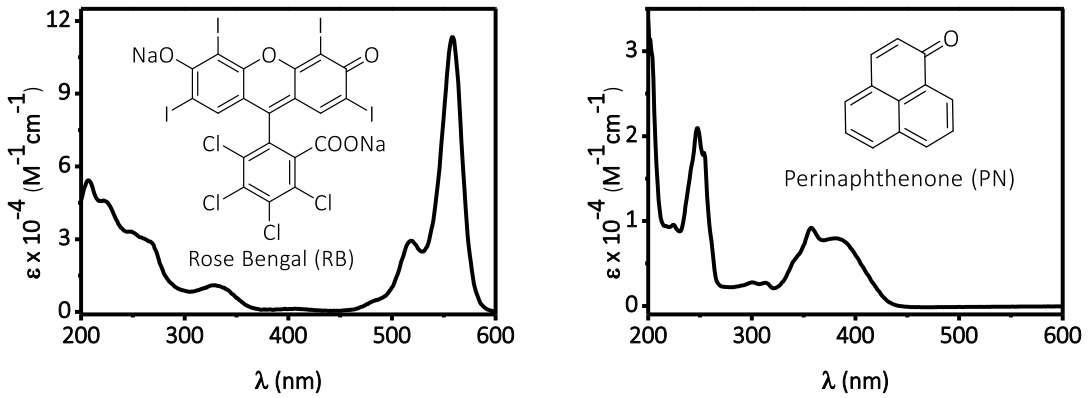


| Data | RB[11] | PN[169] |
|---|---|---|
| $\Phi_{isc}$ | 0.77 | 1 |
| $E_T$ (eV) | 1.8 | 1.9 |
| $E_{red}$ ($PC/PC^{\cdot-}$) (V *vs* SCE) | -0.95 | -0.62 |

**Figure 34**: Top: UV-visible spectra in ACN:$H_2O$ (4:1) and chemical structures of the selected photocatalysts; bottom: photophysical (intersystem crossing quantum yield and energy of the triplet) and electrochemical (redox potential) properties of the selected photocatalysts.

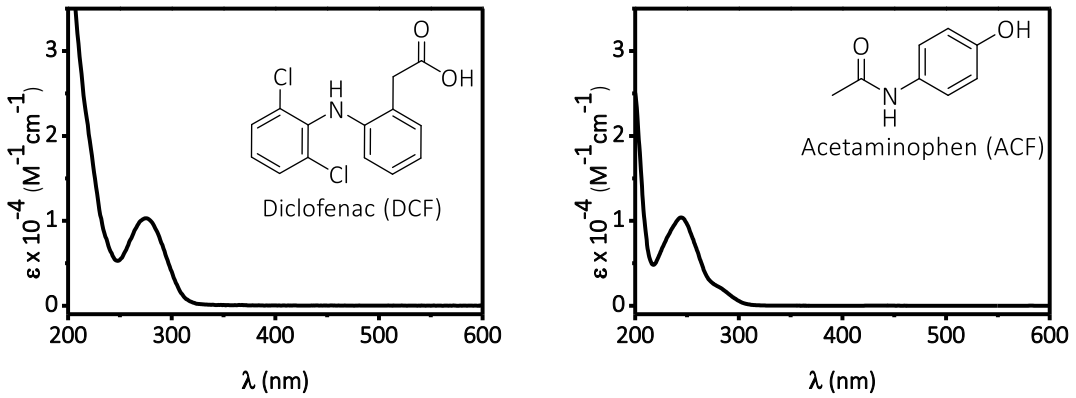


**Figure 35**: UV-visible spectra in ACN:$H_2O$ (4:1) and chemical structures of the selected drugs.

## 6.2. Results and discussion

First, photodegradation of a mixture of both pollutants upon selective excitation of the photocatalyst (530 or 420 nm for RB or PN, respectively) was carried out in aqueous aerobic and anaerobic media and was monitored up to 9.5 hours, see Figure 36. DCF was

easily removed when using PN regardless the atmosphere. However, when RB was used, complete removal was only achieved under $N_2$, see Figure 36A. In the case of ACF, it was fully degraded in the presence of PN, under air or nitrogen, but when using RB, total degradation was not achieved (*ca*. 50% and 40% in aerobic and anaerobic media, respectively), see Figure 36B. For the case of PN, the removal achieved for both pollutants was indeed higher than the one found when using RB as the photocatalyst. However, the results obtained in the absence of oxygen are similar to those in aerobic media; therefore, the involvement of $^1O_2$ as the species responsible for the removal of the pollutants does not seem to be the major pattern.[170]

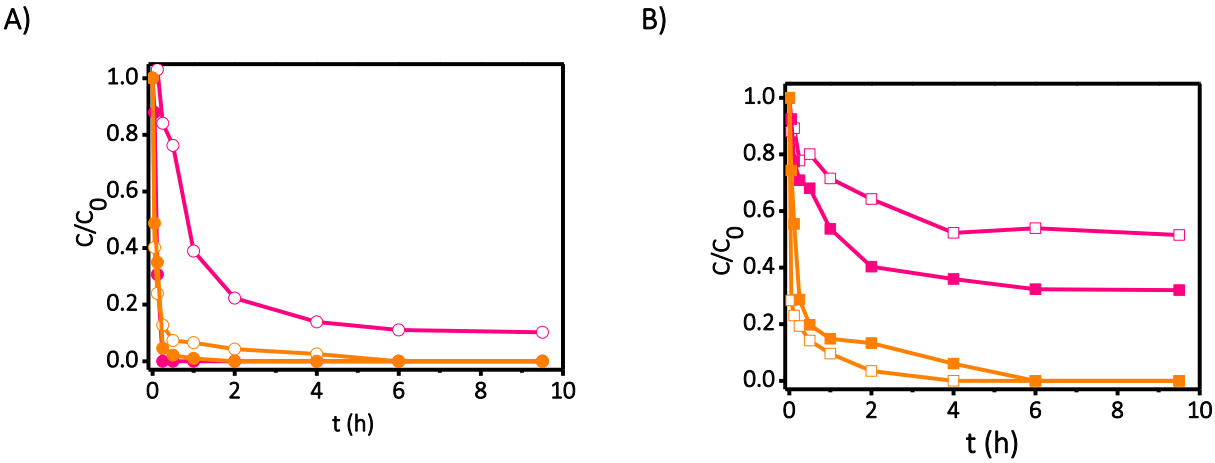


**Figure 36**: Plot of the relative concentration of DCF (**A**) or ACF (**B**), $C_0$= 0.05 mM each, *vs*. irradiation time with light centred at 530 or 420nm for RB or PN, respectively, in the presence of 10 mg $L^{-1}$ of RB (pink) or PN (orange) (0.01 mM and 0.06mM for RB and PN, respectively), in aerobic (blank) and anaerobic (solid) media.

Direct photolysis only produced *ca* 20% of degradation in the case of DCF, after 6 hours of irradiation, Figure 37A. Moreover, mixtures containing RB or PN and both pollutants under dark conditions did not produce any effect, Figure 37B.

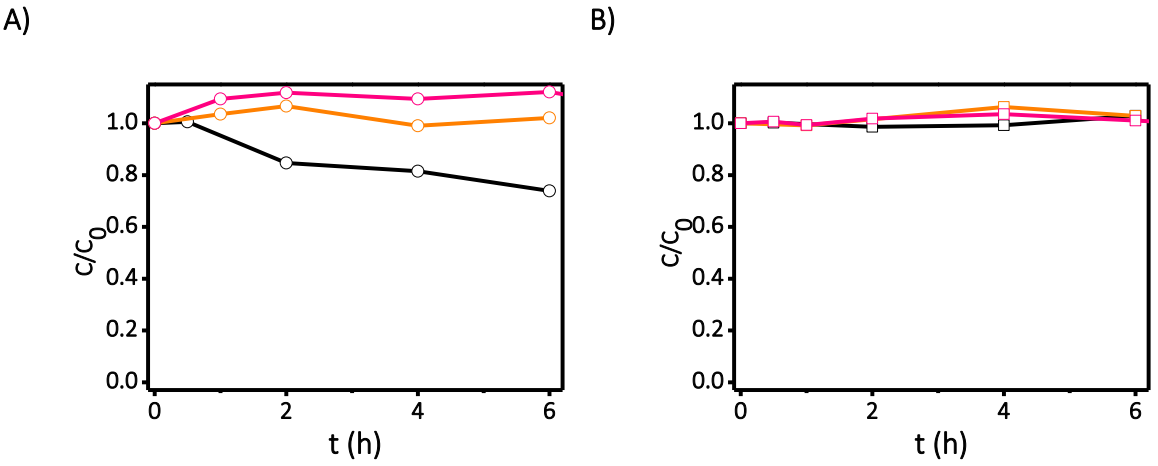


**Figure 37**: Plot of the relative concentration of DCF (**A**) or ACF (**B**), $C_o$= 5 x $10^{-5}$ M each, *vs*. irradiation time, in the absence of RB or PN (black) with light centered at 420 nm; and in the presence of RB (pink) or PN (orange) at 10 mg·$L^{-1}$ (or 0.01 mM and 0.06mM for RB and PN, respectively) but in the absence of light.

To elucidate the mechanism involved in the photodegradation, participation of both, Type I and Type II mechanisms was investigated. Starting from the Type I, the involvement of the triplet excited state of each photocatalyst was analyzed on the basis of LFP. First, the transient absorption spectra of both RB and PN were recorded, Figure 38A and B. Then, the lifetime of the triplet excited state of RB and PN were recorded at 610 and 390 nm, respectively, upon addition of the contaminants, in ACN:$H_2O$ (4:1) (in order to achieve the needed concentration), see Figure 38C, D, E and F. The obtained kinetic constants for the $^3RB^*$ quenching were in the order of $10^7$ - $10^8$ $M^{-1}s^{-1}$, see Figure 39 and Table 11. In the case of $^3PN^*$, quenching was even more efficient, (Figure 39 and Table 11). The observed quenching is attributed to an electron transfer from the drugs to the triplet excited states of the photocatalysts.

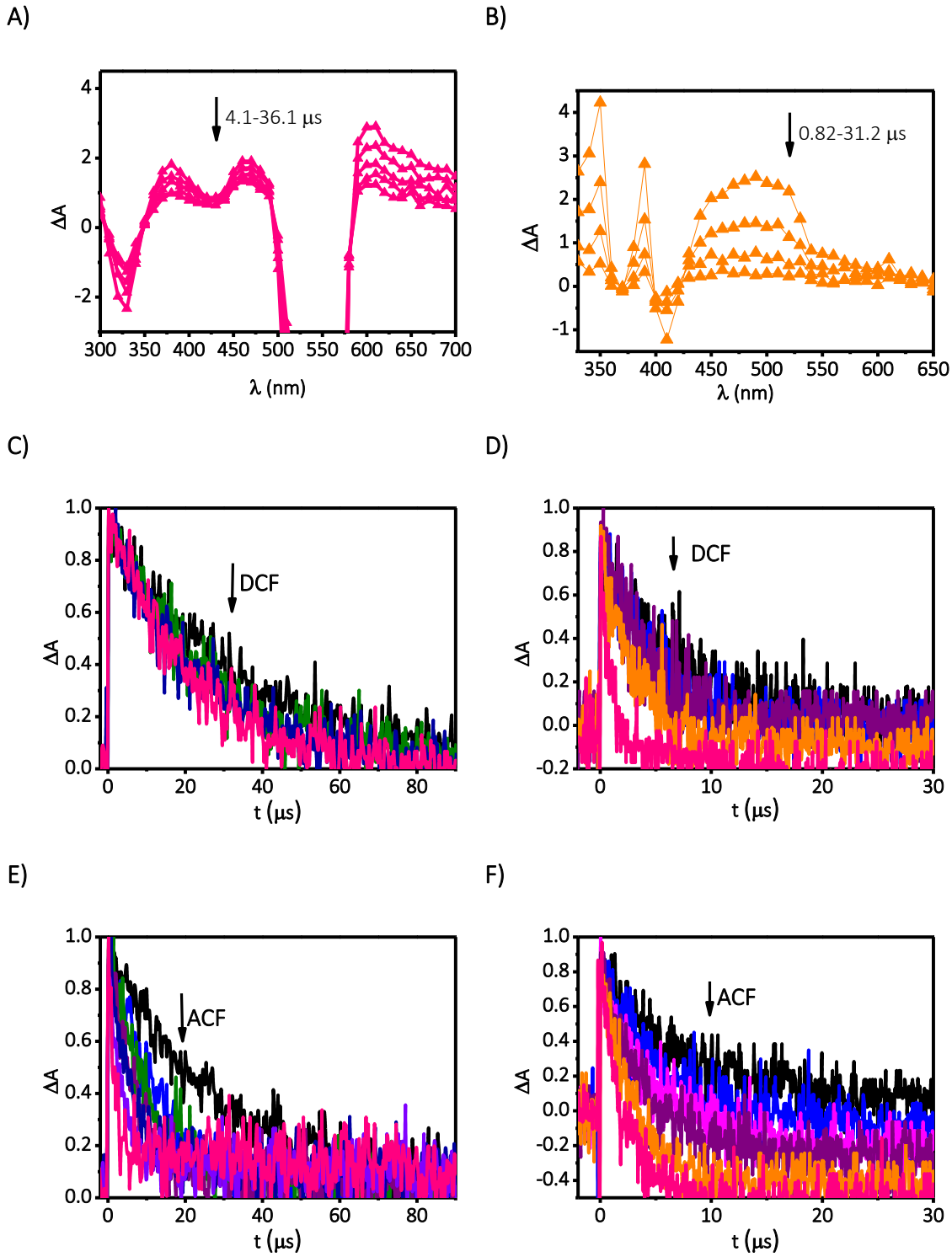


**Figure 38**: Transient absorption spectra of RB (**A**) and PN (**B**) obtained at different times after the laser pulse. Traces recorded at 610 or 390 nm for $^3$RB* (left) or $^3$PN* (right), respectively, upon increasing amounts of DCF (**C**, **D**) or ACF (**E**, **F**) (Abs ≈ 0.3 at $\lambda_{exc}$ = 532 nm or $\lambda_{exc}$ = 355 nm, for RB or PN, respectively, all the experiments were performed in deaerated ACN:$H_2O$ (4:1).

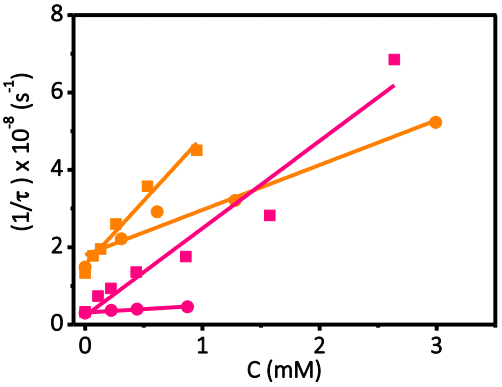


**Figure 39**: Stern-Volmer fittings corresponding to the quenching of $^3$RB* (pink) or $^3$PN* (orange) by DCF (circles) and ACF (squares) in ACN:$H_2O$ (4:1).

**Table 11**: Quenching rate constants of $^3RB^*$, $^3$PN* and $^1O_2$ by the two pollutants.

| | $^3RB^*$ | $^3PN^*$ | $^1O_2$ |
|---|---|---|---|
| | $k_q$ ($M^{-1}s^{-1}$) | $k_q$ ($M^{-1}s^{-1}$) | $k_q$ ($M^{-1}s^{-1}$) |
| DCF | $1.8 \times 10^7$ | $1.2 \times 10^8$ | $9.7 \times 10^6$ |
| ACF | $2.3 \times 10^8$ | $3.3 \times 10^8$ | $2.3 \times 10^7$ |
| $O_2$ | $7.4 \times 10^9$ (1) | $2.1 \times 10^9$ | - |

(1) Diffusion control in water.[135]

Moreover, in the case of PN, the spectra of the corresponding reduced species of PN ($PN^{\cdot-}$) formed in the photoredox process, which exhibits an intense band located at 350 nm and a second band at 440 nm,[171] was recorded after addition of the pollutants. Figure 40A and C, reveal the formation of $PN^{\cdot-}$ upon addition of DCF and ACF, respectively. Besides, the formation of the new band at 350 nm was monitored upon addition of increasing amounts of both, DCF and ACF, see Figure 40B and D.

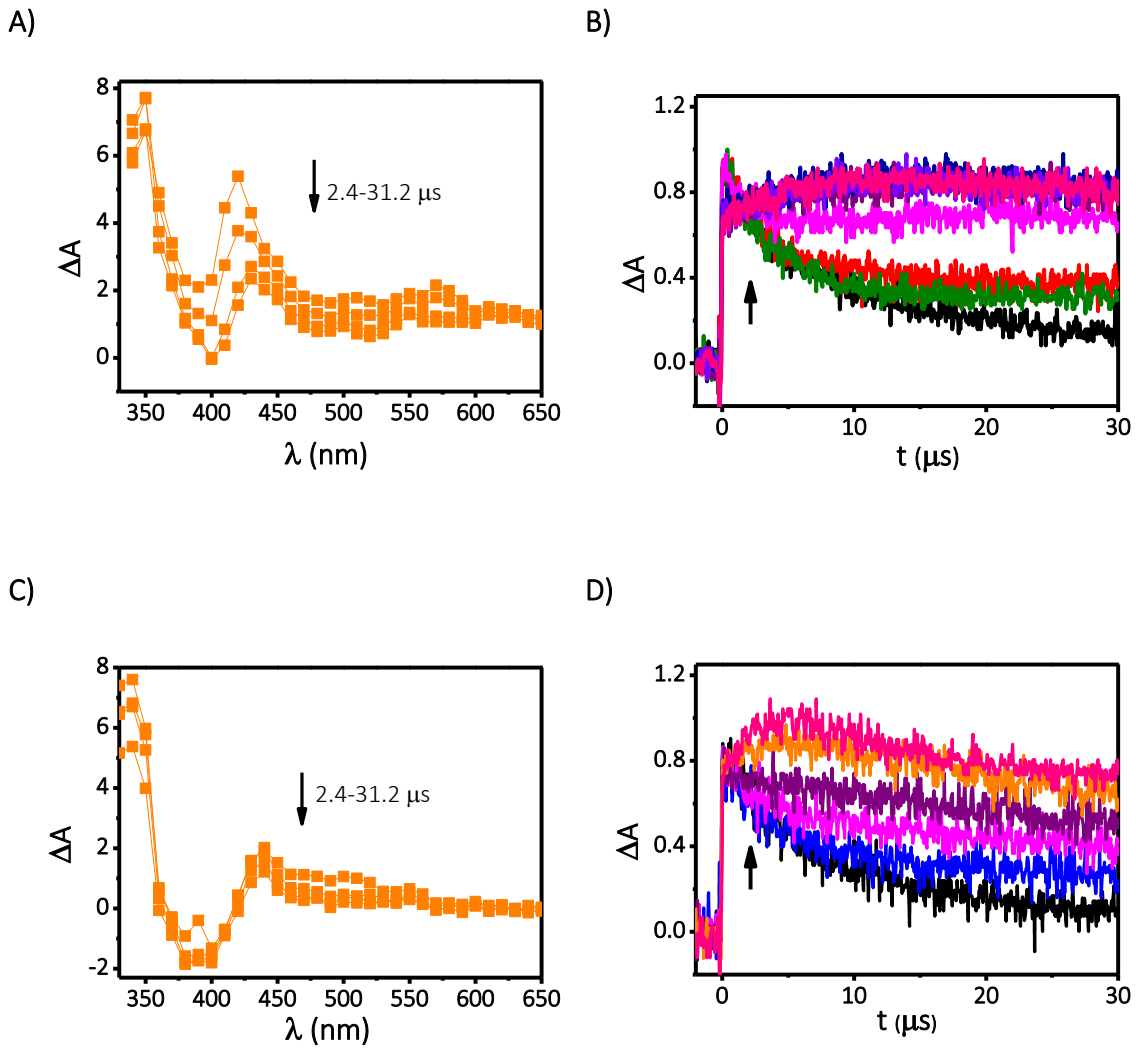


**Figure 40**: Transient absorption spectra of PN obtained at different times after the laser pulse in the presence of DCF (**A**) or ACF (**C**) at 1 mM. Decay traces recorded at 350 nm upon increasing concentrations of DCF (**B**) and ACF (**D**) up to 1 mM. Laser flash photolysis experiments were performed in deaerated ACN:$H_2O$ (4:1), $A_{PN}$ *ca.* 0.3 at $\lambda_{exc}$ = 355 nm.

On the other hand, both triplet excited states were also efficiently quenched by $O_2$. To perform this experiment, traces at 610 or 390 nm for RB and PN, respectively, were recorded under different atmospheres: $N_2$ ($[O_2]_{WATER}$ = 0 M), air ($[O_2]_{WATER}$ = 0.29 mM)[135] and $O_2$ ($[O_2]_{WATER}$ = 1.39 mM).[135] In the case of RB, quenching of $^3RB^*$ with oxygen was completed just in the presence of air; therefore, it was not possible to obtain an accurate value for the quenching constant, and then, the diffusion control value was employed for the calculations.[135] In the case of PN, the experimentally obtained kinetic constant value was $k_q$ = 2.1 x $10^9$ $M^{-1}s^{-1}$.

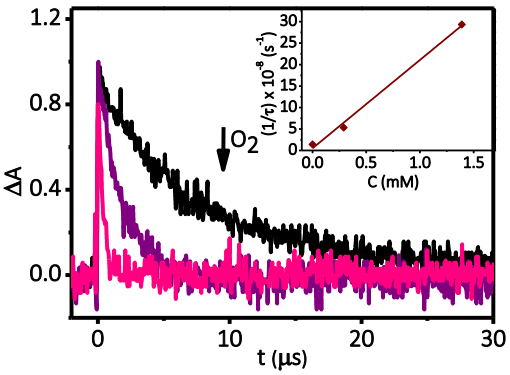


**Figure 41**: PN triplet traces recorded at 390 nm in $H_2O$, upon increasing concentration of $O_2$ ($Abs_{PN}$ ≈ 0.3 at $\lambda_{exc}$ = 355 nm). Inset: Stern – Volmer fitting for the corresponding quenching.

Once the electron transfer mechanism had been investigated, the next step was to study the involvement of $^1O_2$. It was evaluated recording its characteristic emission band at 1270 nm upon increasing concentration of the pollutants. The Stern-Volmer fittings allowed determining the kinetic quenching constants for the reaction between singlet oxygen and the drugs, see Figure 42. The values of $k_q$ were in the range of $10^6$ – $10^7$ $M^{-1}s^{-1}$ (Table 11).

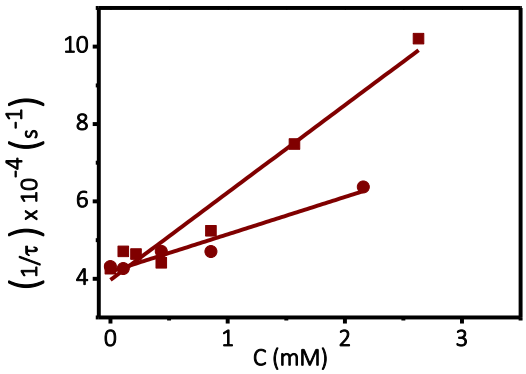


**Figure 42**: Stern-Volmer plots for the quenching of the emission due to $^1O_2$ by DCF (●) and ACF (■).

Thermodynamic estimations using the redox potentials (Table 12) and the photoinduced Gibbs free energy changes (Eq. 2),[7, 172] reveal that photodegradation *via* Type I mechanism is thermodynamically favored for DCF when using both

photocatalysts; whereas, in the case of ACF it is exergonic when using PN, while slightly endergonic for the case of RB, see Table 12.

**Table 12**: Redox potentials for each drug and the corresponding photoinduced Gibbs free energy for the oxidative processes from the triplet excited states of RB and PN.

| | DCF | ACF |
|---|---|---|
| $E_{red}$ ($Q^{\cdot+}/Q$) *vs* SCE (V) | 0.7[173, 174] | 0.9 |
| $\Delta G_{RB\_TRIPLET}$ (kcal·mol$^{-1}$) | -3.5 | +1.2 |
| $\Delta G_{PN\_TRIPLET}$ (kcal·mol$^{-1}$) | -13.4 | -8.8 |

The kinetic analysis points out that the photodegradation of the pollutants conducted by RB or PN can happen through both pathways, *via* Type I (electron transfer) or Type II (reaction with $^1O_2$), see Scheme 5. In fact, the triplet excited states of both photocatalysts are quenched by the pollutants ($k_q$ *ca*. $10^7$ -$10^8$ $M^{-1}s^{-1}$) and by $O_2$ to generate $^1O_2$ ($k_q$ *ca.* $10^9$ $M^{-1}s^{-1}$). The $^1O_2$ formed is also subsequently quenched by the pollutants ($k_q$ *ca*. $10^6$ - $10^7$ $M^{-1}s^{-1}$).

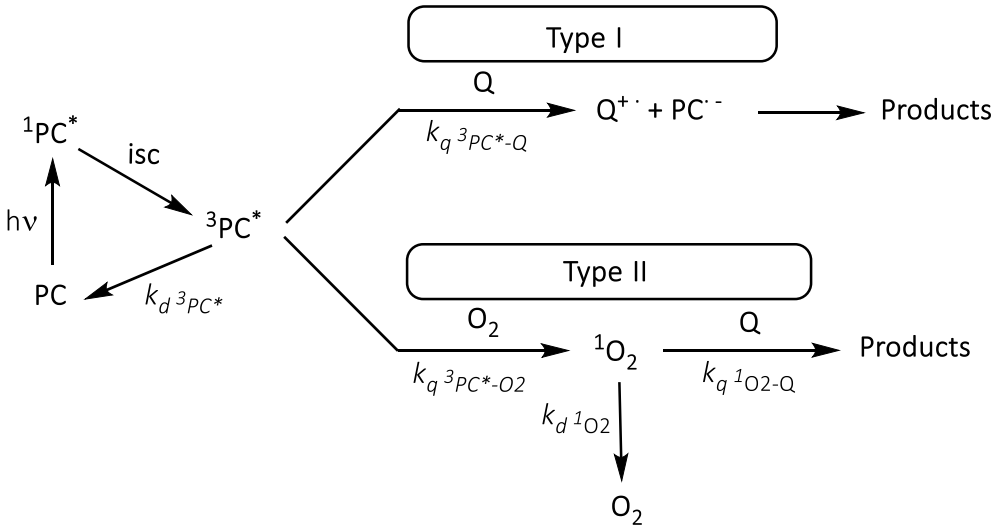


**Scheme 5**: Overall mechanistic pathways potentially operating in the degradation of the pollutants photocatalyzed by RB or PN (PC = RB or PN; Q = DCF or ACF).

As in Chapter 4, a mathematical analysis will determine the real contribution of each pathway. Taking into account the triplet lifetimes of each photocatalyst, (2.4 and 7.0 μs, for RB and PN, respectively), the contribution of the three different pathways can be calculated from Eq. 22, Eq. 23 and Eq. 24.

Eq. 22:

$$\%\ Intrinsic\ triplet\ decay\ (k_{d\ ^3PC^*}) = \frac{\frac{1}{\tau_{^3PC^*}}}{k_{q\ ^3PC^*-O_2}\cdot[O_2]+k_{q\ ^3PC^*-Q}\cdot[Q]+\frac{1}{\tau_{^3PC^*}}} x100$$

Eq. 23:

$$\%\ Quenching\ of\ the\ triplet\ by\ Q\ \left(k_{q\ ^3PC^*-Q}\right) = \frac{k_{q\ ^3PC^*-Q}\cdot[Q]}{k_{q\ ^3PC^*-O_2}\cdot[O_2]+k_{q\ ^3PC^*-Q}\cdot[Q]+\frac{1}{\tau_{^3PC^*}}} x100$$

Eq. 24:

$$\%\ {}^1O_2\ Formation\ (k_{q\ ^3PC^*-O_2}) = \frac{k_{q\ ^3PC^*-O_2}\cdot[O_2]}{k_{q\ ^3PC^*-O_2}\cdot[O_2]+k_{q\ ^3PC^*-Q}\cdot[Q]+\frac{1}{\tau_{^3PC^*}}} x100$$

In the best scenario for the $^1O_2$ formation, the quenching of $^3PC^*$ by $O_2$ will only result in $^1O_2$ formation, Eq. 24; once it has been formed, $^1O_2$ could follow two subsequent pathways, reaction with the pollutant, Eq. 25, or intrinsic deactivation, Eq. 26:

Eq. 25:

$$\%\ Quenching\ of\ {}^1O_2\ by\ Q\ (k_{\ ^1O_2Q}) = \frac{k_{q\ ^3PC^*-O_2}\cdot[O_2]}{k_{q\ ^3PC^*-O_2}\cdot[O_2]+k_{q\ ^3PC^*-Q}\cdot[Q]+\frac{1}{\tau_{^3PC}}} x \frac{k_{\ ^1O_2\ Q}\cdot[Q]}{k_{\ ^1O_2\ Q}\cdot[Q]+\frac{1}{\tau_{\ ^1O_2}}} x100$$

Eq. 26:

$$\%\ {}^1O_2\ Intrinsic\ decay\ (k_{d\ ^1O_2}) = \frac{k_{q\ ^3PC^*-O_2}\cdot[O_2]}{k_{q\ ^3PC^*-O_2}\cdot[O_2]+k_{q\ ^3PC^*-Q}\cdot[Q]+\frac{1}{\tau_{^3PC}}} x \frac{\frac{1}{\tau_{\ ^1O_2}}}{k_{\ ^1O_2\ Q}\cdot[Q]+\frac{1}{\tau_{\ ^1O_2}}} x100$$

To evaluate the individual contribution of Type I and Type II mechanisms in the photodegradation of the pollutants conducted by both photocatalysts, the situation at a typical concentration of emerging pollutants, $10^{-5}$ M, has been simulated. The results are summarized on Table 13.

Table 13: Estimated reactivity for the different pathways in the photodegradation of DCF and ACF as shown in Scheme 5, obtained upon applying Eq. 22- 26 and the experimentally obtained data stated in Table 11.

| PC | Q (0.01 mM) | $^3$PC* intrinsic decay (%) Eq. 22 | *Type I* Quenching of $^3$PC* by Q (%) Eq. 23 | Quenching of $^3$PC* by $O_2$ (%) Eq. 24 | *Type II* Quenching of $^1O_2$ by Q (%) Eq. 25 | $^1O_2$ intrinsic decay (%) Eq. 26 |
|---|---|---|---|---|---|---|
| RB | DCF | 1.5 | 0.3 | 98.2 | 0.1 | 98.1 |
| | ACF | 1.5 | 0.8 | 97.7 | 0.2 | 97.5 |
| PN | DCF | 18.7 | 1.5 | 79.8 | 0.1 | 79.7 |
| | ACF | 18.3 | 3.7 | 77.9 | 0.2 | 77.7 |

Under standard circumstances, the water remediation will take place in the presence of oxygen (aerobic conditions); therefore, a competition between oxygen and the pollutants for the triplets ($^3$RB* or $^3$PN*) will take place. Attending to the typical concentrations ([$O_2$]= 2.9 x $10^{-4}$ M in aqueous aerobic media),[135] and the experimentally determined rate constants (Table 11), formation of $^1O_2$ accounts in both cases for the major quenching pathway (> 97% for RB and >77% for PN, Table 13). However, subsequent quenching of $^1O_2$ by the pollutants, is in the range of $10^6$ – $10^7$ $M^{-1}s^{-1}$ (Table 11); therefore, at the typical contaminant concentration almost all the $^1O_2$ formed decays without reacting, Table 13. Thus, photodegradation of the pollutants still happens mainly through Type I mechanism.

## 6.3. Conclusions

Type I mechanism has demonstrated to be a more effective pathway than Type II when RB is used as photocatalyst for water remediation. This statement is supported by the obtained fast kinetic data and is also true for PN, a photocatalyst with even higher singlet oxygen quantum yield formation.

## 6.4. Experimental

Photodegradations were carried out according to the general methodology explained in section 9.3.1. In this case, photodegradation mixtures were prepared in aqueous solutions (16 mL) containing a mixture of the two pollutants (0.05 mM each or

0.1 mM in global) and either RB or PN (10 mg $L^{-1}$, 0.01 mM and 0.06 mM for RB and PN, respectively) under air or $N_2$. Emission sources were centred at 530 and 420 nm for the oxidations photocatalyzed by RB and PN, respectively.

The extent of the photodegradation was monitored by HPLC. Aliquots of 90 μL at different irradiation times were analyzed using 4-nitrobenzoic acid (10 μL of a 1 x $10^{-4}$ M solution) as internal standard. Mobile phase was a gradient mixture of $H_2O$(pH 3):ACN (70:30-30:70) at a flow rate of 1.5 mL $min^{-1}$; the detection wavelength was fixed at 250 nm.

The photophysical measurements were performed according to the general procedure explained in section 9.3.4.

For the laser flash photolysis experiments, increasing amounts of pollutants (up to 3 mM) were added to ACN:$H_2O$ (4:1) solutions of RB or PN (absorbance *ca*. 0.3 at 532 or 355 nm for RB or PN, respectively), under $N_2$ atmosphere. Lifetime of singlet oxygen was determined from the phosphorescence decay curves at 1270 nm upon increasing amounts of pollutant (up to 3 mM) in aerobic ACN:$H_2O$ (4:1) solutions.

# 7. A Mechanistic Study on the Potential of Quinolinium Salts as Photocatalysts for the Abatement of Chlorinated Pollutants

## 7.1. Introduction

*N*-Methylquinolinium ($NMQ^+$) tetrafluoroborate (Figure 43) is an interesting cationic photocatalyst due to its singular photophysical properties. Its singlet excited state is long-lived (20 ns), quite energetic ($E_S$ = 341 kJ $mol^{-1}$) and its emission is centered at 402 nm with a high fluorescence quantum yield ($\Phi_F$ = 0.85).[70] Moreover, the energy gap between its singlet and its triplet excited states ($\Delta_E \approx$ 86 kJ $mol^{-1}$) allows the generation of singlet oxygen from the excited singlet with an overall yield of $\Phi_\Delta$ = 0.85.[70]. In addition, the reported redox potential for $NMQ^+$ is $E_{red}$ = -0.85 V *vs* SCE.[175] The fact of being a cationic photocatalyst usually increases the efficiency of the photoinduced electron transfer (PET) because the most common side process, back-electron transfer (BET), tends to be unlikely due to the lack of Coulombic attraction between the formed species. Based on these features, several examples of oxidation of aromatic sulfides and sulfoxides using $NMQ^+$ as photocatalyst have been described.[176-181]

However, a couple of drawbacks could be associated to $NMQ^+$: it is not commercially available, and its UV absorption only reaches up to 380 nm. Nevertheless, it can be synthesized through methylation of quinoline,[175, 182] and $NMQ^+$ derivatives with extended absorption bands in the visible range have also been reported.[183]

All these characteristics make $NMQ^+$ an interesting species that could, in principle, act as a photocatalyst able to promote photodegradation of contaminants through Type I and/or Type II mechanisms.

Under this scenario, the main goal of the present chapter is to investigate the capability of $NMQ^+$ as a singular photocatalyst since from its singlet excited state it could produce photodegradation of pollutants through electron transfer or generate $^1O_2$ that could eventually oxidize the pollutants. For this purpose, three chlorinated pollutants namely 2,4,6-trichlorophenol (TCP), 2,4,6-trichloroanisole (TCA) and 5-chloro-2-(2,4-

dichlorophenoxy)phenol (triclosan, TCS) (Figure 43) have been selected. TCP is one of the chlorophenols included as a Priority Substance at the Water Frame Directive, see section 1.5.1; TCA is usually present at the dark complex liquor generated in the wastewaters of cork industry;[140] and TCS is a typical antibacterial substance present in personal care products which is not fully removed from conventional wastewater treatment plants, therefore concentrations of 0.24-37.8 μg/L of TCS have been detected in treated effluents.[184] These three compounds are difficult to oxidize, therefore $NMQ^+$, a photocatalyst with such a great redox potential from its singlet excited state and also, able to generate singlet oxygen, seems to be the ideal candidate for this purpose.

First, photodegradation of these three contaminants under selective irradiation and in the presence of $NMQ^+$ will be evaluated. Afterwards, time-resolved photophysical techniques will help to elucidate the involved mechanism.

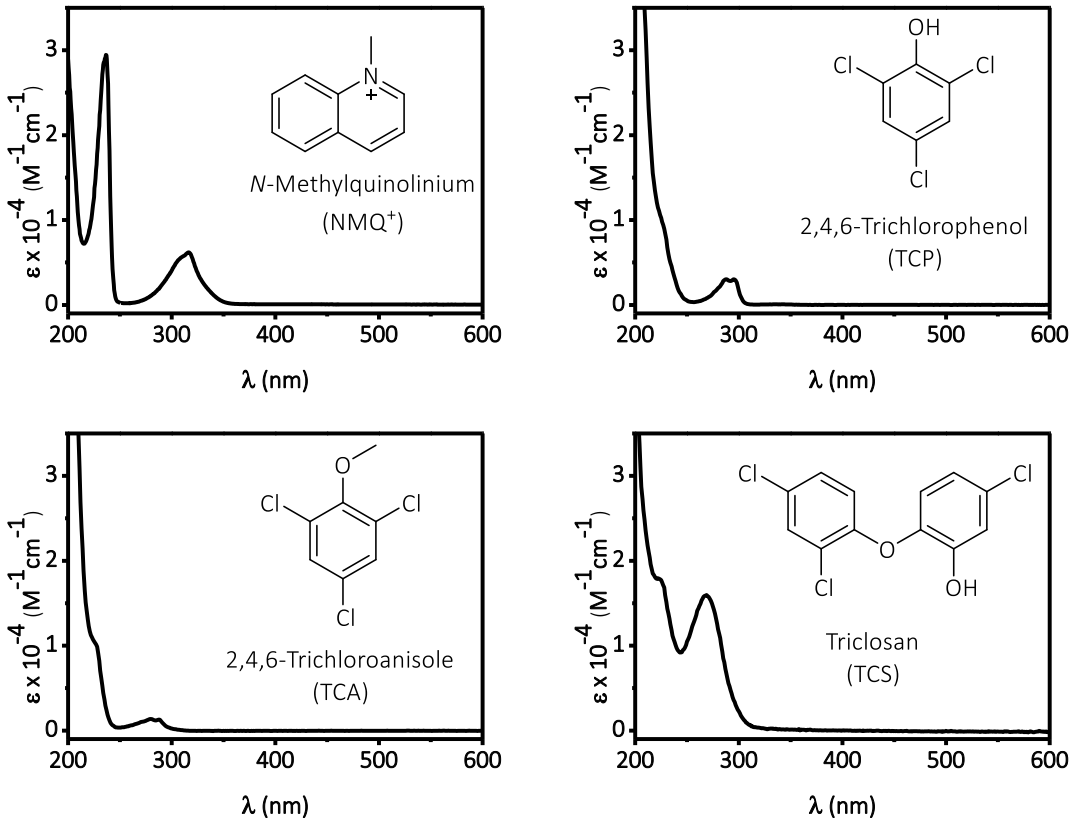


Figure 43: UV spectra in $CH_3CN$ of the selected photocatalyst and contaminants together with their corresponding chemical structures.

## 7.2. Results and discussion

First, mixtures containing one of the pollutants and $NMQ^+$ (1% mol) in aqueous solutions were irradiated with 350 nm centered light under aerated atmosphere. The removal of the pollutants was monitored by HPLC at different irradiation times. The evolution of the removal is shown in Figure 44.

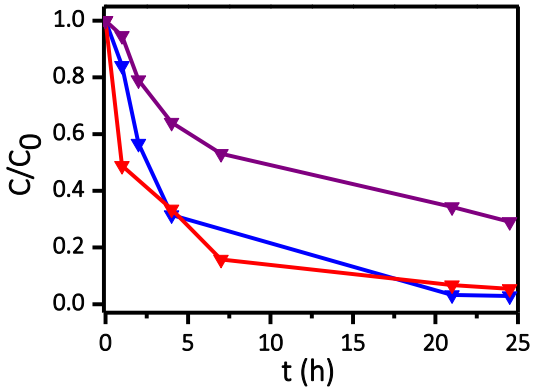


**Figure 44**: Plot of the relative concentration of TCP (▼), TCA (▼) and TCS (▼) versus irradiation (350 nm) time, $C_0$ = 3 x $10^{-5}$ M in the presence of $NMQ^+$ (1% mol, 3 x $10^{-7}$ M) under aerated atmosphere in aqueous media.

Figure 44 shows that photodegradation of TCA and TCP was fully completed after 25 hours, while, in the same period, only 70 % of TCS degradation was achieved. HPLC chromatograms did not reveal any clear peaks that could correspond to the formation of photoproducts. They seem to disappear fast without accumulating sufficient amount to be detected under the employed conditions. To investigate if mineralization was achieved, an aqueous mixture of the three pollutants and $NMQ^+$ was irradiated with the solar simulator during 48 hours under a continuous flow of oxygen, which was bubbled over a saturated solution of $Ba(OH)_2$ to *in situ* trap the potentially formed $CO_2$ as $BaCO_3$. The resulting precipitate was filtered and subjected to elemental analysis, which unequivocally confirmed the formation of $BaCO_3$.

Moreover, additional experiments were carried out in order to assess the involvement of oxygen in the photodegradation. Then, two parallel irradiations containing TCP, TCA or TCS and $NMQ^+$ were carried out at 350 nm under aerated/deaerated atmosphere, see Figure 45. Higher amounts of $NMQ^+$ (10 mg $L^{-1}$ or

0.04 mM) compared to the concentration used in the previous experiments were employed in order to reduce irradiation times; nevertheless, photodegradation was essentially independent on the atmosphere.

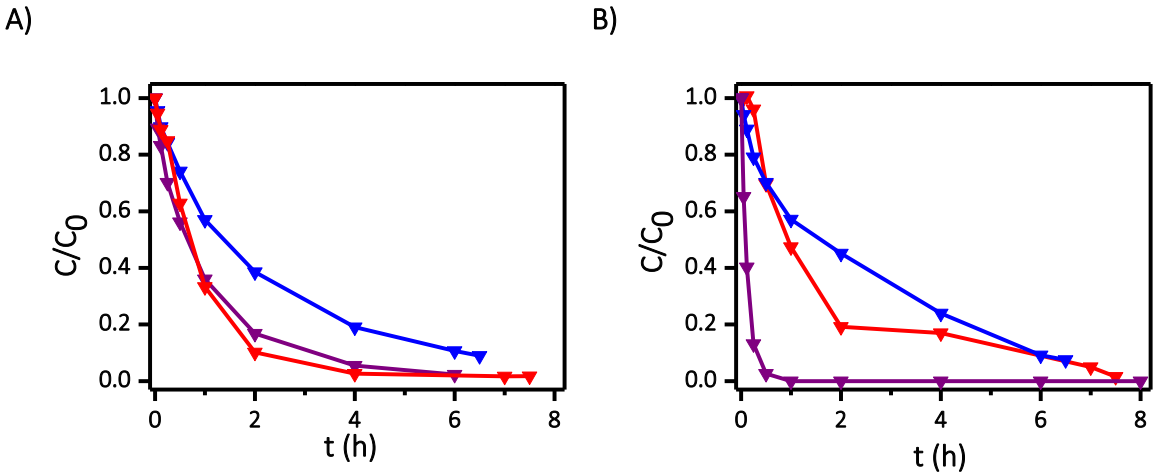


**Figure 45**: Plot of the relative concentration of TCP (▼), TCA (▼) and TCS (▼) at $C_0$ = 0.03 mM in aqueous media *vs* 350 nm irradiation time in the presence of $NMQ^+$ (10 mg $L^{-1}$, 0.04 mM) under **A)** deaerated and **B)** aerated atmosphere.

Attending to UV-visible spectra of the pollutants compared to that of the photocatalyst (see Figure 43), only $NMQ^+$ is able to absorb at that wavelength. Nevertheless, control experiments were carried out in the absence of light and also in the absence of photocatalyst, but in every case, pollutants remained unchanged, see Figure 46.

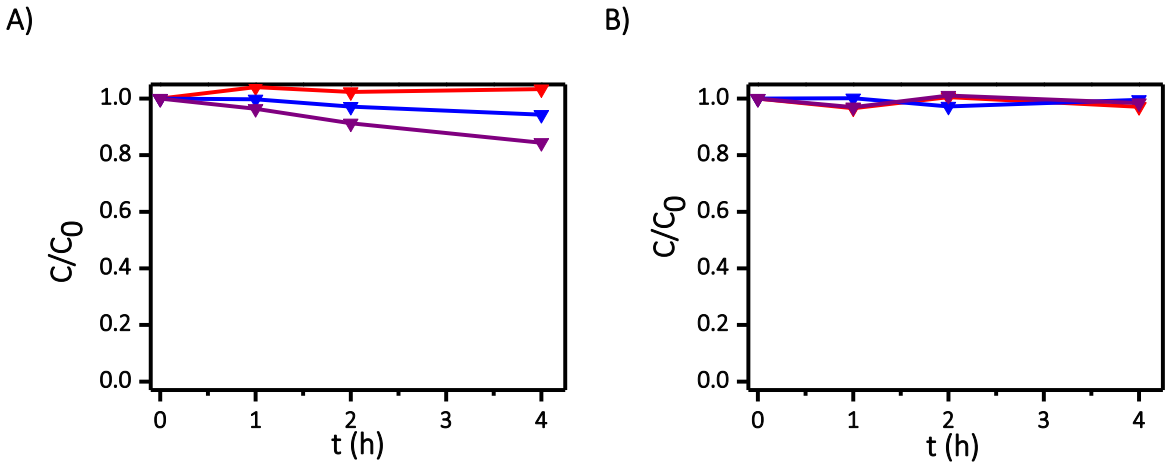


**Figure 46:** Plot of the relative concentration of TCP (▼), TCA (▼) and TCS (▼) at $C_0$ = 0.07 mM in aerobic aqueous media *vs* 350 nm irradiation time in the absence of $NMQ^+$ (**A**) and under dark conditions in the presence of $NMQ^+$ at 10 mg $L^{-1}$ (0.04 mM) (**B**).

Once the ability of $NMQ^+$ as homogeneous photocatalyst had been demonstrated, the heterogenization of the system was evaluated. For this purpose, an inert inorganic support (Zeolite Y 100) was used in order to incorporate the $NMQ^+$. Elemental analysis was used to evaluate the loading of $NMQ^+$ in the heterogeneous photocatalyst Zeolite Y-$NMQ^+$, revealing a *ca.* 13% weight. Moreover, diffuse reflectance and emission measurements, see Figure 47, demonstrated the presence of the unaltered photocatalyst within the zeolite.

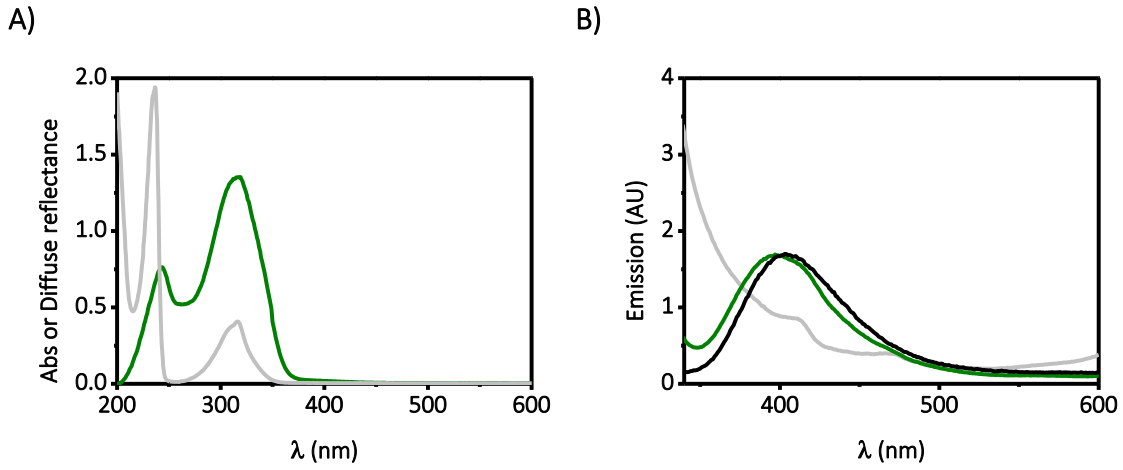


**Figure 47**: **A**) Diffuse reflectance of Zeolite Y-$NMQ^+$ (green) and absorbance of $NMQ^+$ at 66 μM (grey); **B**) Emission of $NMQ^+$ (black), Zeolite Y-$NMQ^+$ (green) and Zeolite Y (grey) upon excitation at $\lambda_{exc}$ = 317 nm.

Then, aqueous mixtures of each contaminant (3 x $10^{-4}$ M) in the presence of supported Zeolite Y-$NMQ^+$ (70 mg $L^{-1}$) were irradiated with light centered at 350 nm, under aerated atmosphere. Figure 48 shows how the supported photocatalyst was also able to produce photodegradation of the three pollutants, although longer times were needed, also due to the higher concentration of pollutants employed. A control experiment was carried out in order to check adsorption of pollutants into the zeolite. First, a sample of the mixture containing all the pollutants (at $10^{-4}$ M each) without Zeolite Y-$NMQ^+$ was taken and injected in the HPLC, then the specific quantity of Zeolite Y-$NMQ^+$ needed was added and the mixture was stirred under dark for an hour. Then, an aliquot was taken, filtered and injected in the HPLC revealing that adsorption into the zeolite was lower than 10%; therefore, removal of the contaminants could safely be attributed to the heterogeneous photodegradation. Besides, chromatograms obtained from the filtered samples revealed no significant presence of $NMQ^+$ in the media, therefore leaching from the zeolite was discarded.

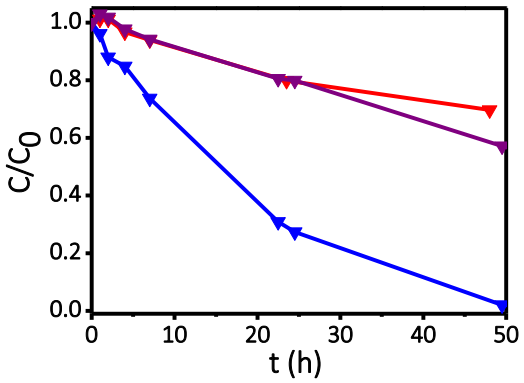


**Figure 48**: Plot of the relative concentration of TCP (▼), TCA (▼) and TCS (▼) at total $C_0$ = 3 x $10^{-4}$ M *vs* irradiation (350 nm) time in the presence of Zeolite Y-$NMQ^+$ (70 mg x $L^{-1}$) in aqueous media under aerated atmosphere.

Next, detoxification of the samples was also studied to evaluate the potential of a photocatalyst such as $NMQ^+$, to be eventually applied to real wastewaters. The toxicity assays were performed in collaboration with the Ecotoxicology Group from the Department of Biotechnology of the Universitat Politècnica de València. For this purpose, photomixtures A and B, containing the three pollutants and $NMQ^+$ or the three pollutants and the benchmark photocatalyst P25-$TiO_2$, were irradiated in parallel. Evaluation of the

toxicity was made for A and B at different irradiation times: at the beginning (initial time), after 23 hours irradiation (intermediate time) and after 70 hours irradiation (final time). In all cases, several aqueous dilutions were made, 1:1, 1:2, 1:4 and 1:8 prior to the toxicity assays. Model systems based on *Daphnia magna* were used for the toxicity assays,[185, 186] and the inhibition of the mobility of *D. magna* was interpreted as a toxic effect, see section 7.4 for details.

The results of the initial toxicity of each individual component, expressed as $EC_{50}$ values (concentration required to produce 50% of the toxic effect) with their 95% confidence intervals, are listed on Table 14.

**Table 14**: $EC_{50}$ values (95% confidence interval) determined for the assayed compounds. [DMSO] = 0.06 M = 4.4 g $L^{-1}$, [$NMQ^+$] = 10 mg $L^{-1}$ (0.04 mM), [$TiO_2$] = 200 mg $L^{-1}$ (2.5 mM) and [TCA] = [TCP] = [TCS] = $3x10^{-5}$ M.

| Sample | *$EC_{50}$ (Daphnia magna)* |
|---|---|
| DMSO[a] | [5.3 (4.2–7.8)] $x10^{-2}$ M |
| $NMQ^+$ | [2.0 (1.4–3.1)] $x10^{-5}$ M |
| $TiO_2$ | maximum toxicity sample < 40%. |
| TCP | [0.9 (0.6–1.4)] $x10^{-5}$ M |
| TCA | [1.7 (1.5–1.9)] x $10^{-5}$ M |
| TCS | [0.5 (0.4–0.6)]$x10^{-5}$ M |

[a]solvent used to predissolve the pollutants.

Table 14 indicates that the sample containing only $NMQ^+$ exhibits a similar level of toxicity than that of the pollutants; while the sample containing only $TiO_2$ (after filtration) resulted non-toxic. In addition, DMSO used to pre-dissolve the samples, was also evaluated, resulting non-toxic. Next, photomixtures A and B were irradiated for 70 hours and the toxicity results are summarized on Figure 49 top and bottom, respectively.

Non-irradiated (dark bars) and irradiated (light bars) samples are shown together for a better comparison in Figure 49. Each bar represents % of daphnids immobilization at serial dilutions of aqueous solutions. The toxicity of both photomixtures decreases upon irradiation being more effective in the case of $NMQ^+$ (photomixture A, Figure 49 top) than in the case of the $TiO_2$ samples (photomixture B, Figure 49 bottom).

Before irradiation (dark bars), samples exhibit a high toxicity, 100% immobilization, at 1:1 dilution and even at 1:2. After 70 hours of irradiation, the photomixture A shows an effective decrease of the toxicity even without diluting the sample (see light bars compared to dark ones in Figure 49 top). After diluting the irradiated sample, the toxicity decreases for both photomixtures, but only after 1:8 dilution, photomixture B results non-toxic (compare light bars in Figure 49, top and bottom).

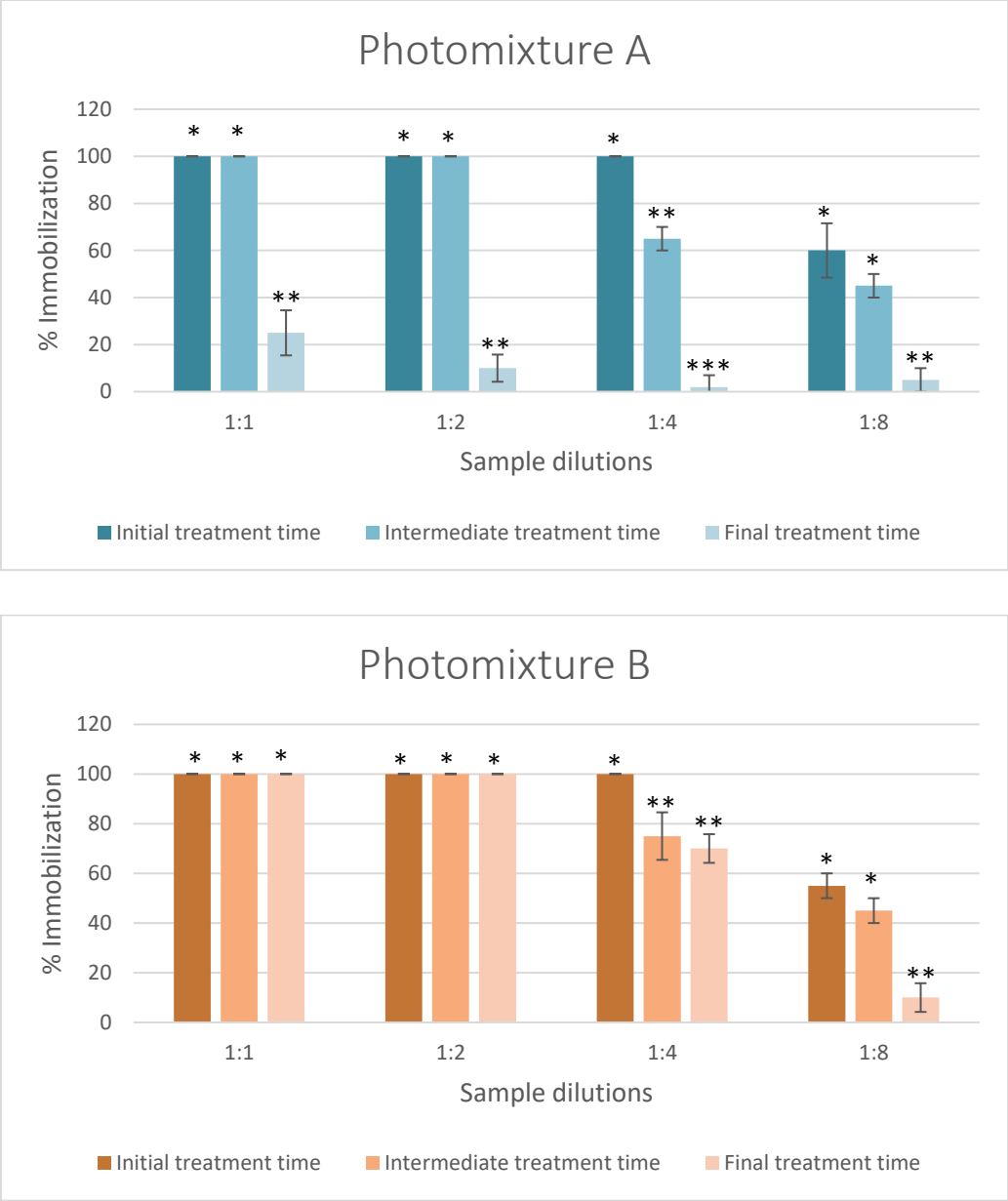


**Figure 49**: Evolution of % immobilization of *D. magna* bioassays conducted during the treatment of samples at several dilutions upon 70 hours irradiation (light bars), 23

hours irradiation (medium bars) or non-irradiated (dark bars). Top: photomixture A ($NMQ^+$); Bottom: photomixture B ($TiO_2$). *Significant differences respect to treatment time ($p< 0.05$).

The latter test claims that the use of an organic photocatalyst such as $NMQ^+$ could produce detoxification of the wastewaters. Results from the toxicity experiments have demonstrated that the use of organic photocatalysts to produce removal of contaminants could be as efficient or even more than the use of inorganic photocatalysts as $TiO_2$ to produce detoxification and should be considered as an alternative.

As it has been mentioned in the introduction of the chapter, singlet excited state redox potential of $NMQ^+$ is extremely high (*ca.* 2.7 V). Accordingly, Table 15 reveals that photodegradation via Type I mechanism is thermodynamically favored in every case.

**Table 15**: Redox potentials for each pollutant and the corresponding photoinduced Gibbs free energy (Eq. 2) changes of the oxidation processes from the singlet excited state of $NMQ^+$.

| | TCP | TCA | TCS |
|---|---|---|---|
| $E_{red}$ ($Q^{\cdot+}/Q$) *vs* SCE (V) * | 1.3 | 1.9 | 1.2 |
| $\Delta G_{NMQ+\_SINGLET}$ (kcal·mol$^{-1}$) | -32.2 | -18.4 | -34.5 |

* Experimentally measured, see Figure 19 and Figure 53

First, the electron transfer from the pollutants to the singlet excited state was evaluated by steady-state and time-resolved fluorescence experiments. In fact, the fluorescence emission intensity and the singlet excited state lifetime of $NMQ^+$ decreased upon addition of every pollutant as it also does upon increasing oxygen concentration, see Figure 50, confirming the dynamic nature of the electron transfer process. The corresponding kinetic constants were also determined by means of the Stern-Volmer equation plotting $I_0/I$ or $\tau_0/\tau$ *vs* quencher concentration. In every case, the values are close to the diffusion limit in $CH_3CN$ ($k_{diff}$ = 1.9 x $10^{10}$ $M^{-1}s^{-1}$, see Figure 50 right and Table 16).[135]

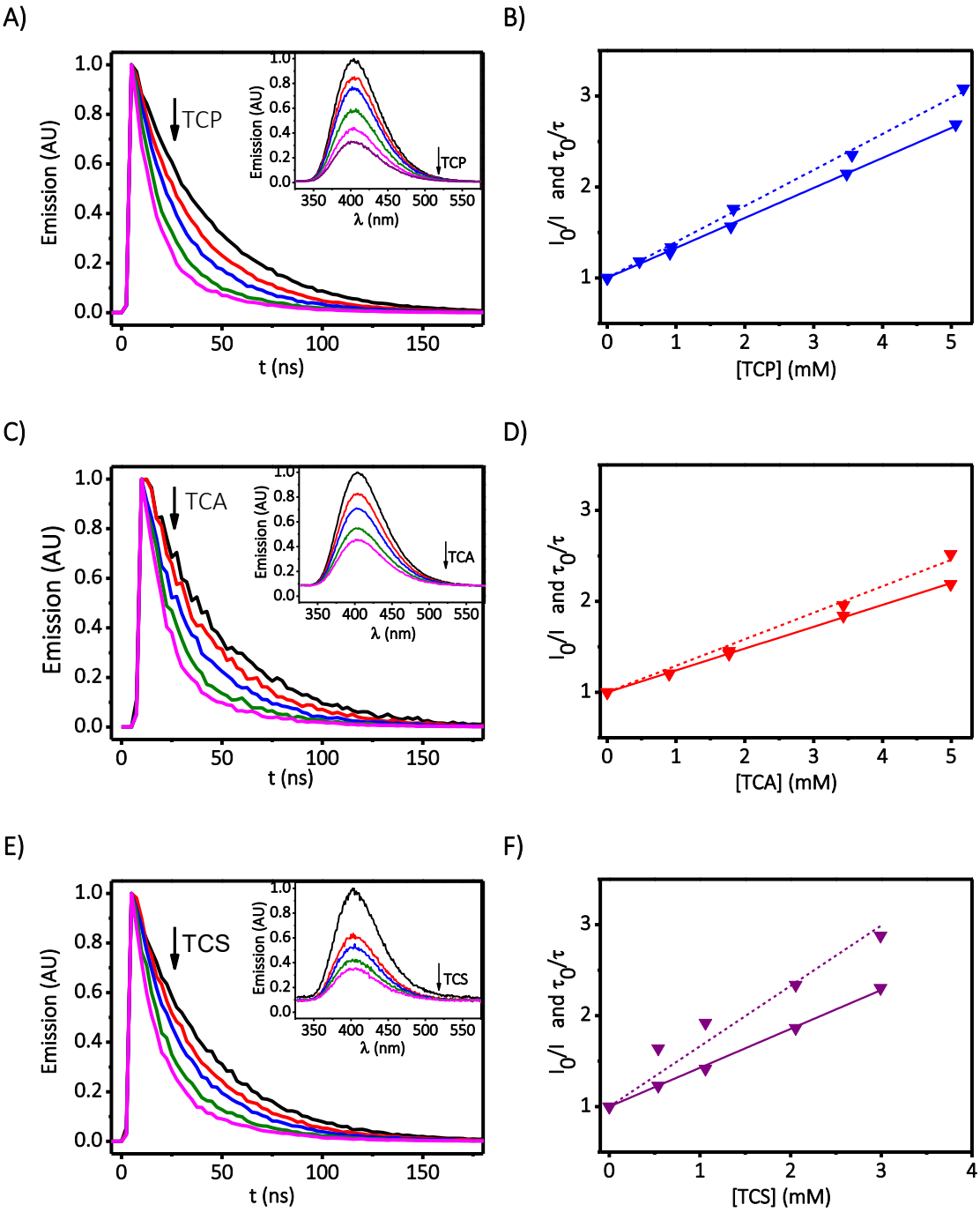
A)
B)
C)
D)
E)
F)
TCP
TCA
TCS
Emission (AU)
t (ns)
λ (nm)
$I_0/I$ and $\tau_0/\tau$
[TCP] (mM)
[TCA] (mM)
[TCS] (mM)

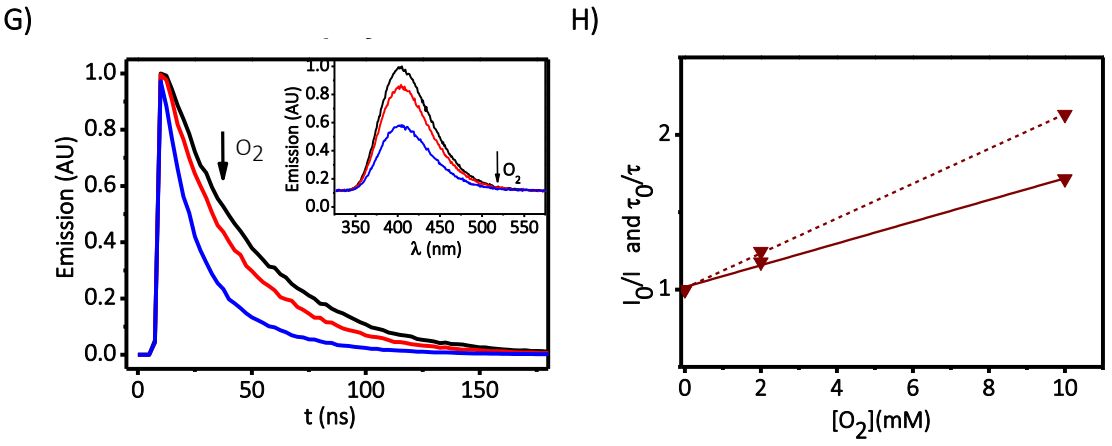


**Figure 50**: Left column: Time-resolved and steady-state (inset) $^{1}(NMQ^{+})^{*}$ fluorescence quenching upon addition of increasing concentrations of TCP, TCA and TCS and $O_2$ ($Abs_{NMQ+}$ = 0.15 at 317 nm, $[TCP]_{FINAL} = [TCA]_{FINAL} = 5 \times 10^{-3}$ M, $[TCS]_{FINAL} = 3 \times 10^{-3}$ M, $[O_2]_{FINAL} = 1 \times 10^{-2}$ M in $CH_3CN$ under $N_2$; $\lambda_{exc}$ = 317 nm. Right column: Stern-Volmer plots obtained from the steady-state (dash) and time-resolved (solid) fluorescence quenching experiments.

The next step was the evaluation of the potential involvement of $^{1}O_2$ in the oxidation of pollutants. For this purpose, PN was employed as singlet oxygen generator and its characteristic emission band at 1270 nm was recorded upon increasing amounts of every pollutant, see the corresponding Stern-Volmer plots in Figure 51.

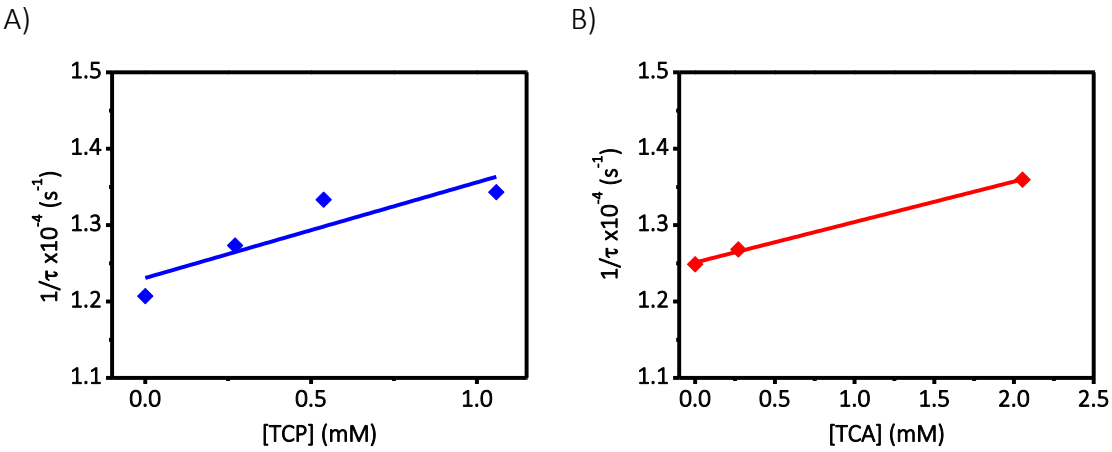

C)

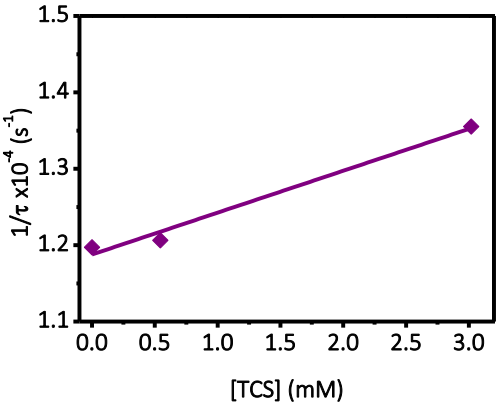


**Figure 51**: Stern Volmer plots for singlet oxygen quenching by TCP (A), TCA (B) and TCS (C). LFP excitation (355 nm) of aerated acetonitrile solutions of PN ($A_{PN}$ = 0.5 at 355 nm) were used as $^1O_2$ generator.

Quenching of $^1O_2$ by the pollutants (Table 16) was very poor with rate constants between 5.3 x $10^5$ $M^{-1}s^{-1}$ and 1.3 x $10^6$ $M^{-1}s^{-1}$; although in agreement with reported values for the quenching of $^1O_2$ by organic compounds.[187]

**Table 16**: Rate constant values for the reaction between the pollutants and $^1(NMQ^+)$* obtained from the steady-state and time-resolved experiments ($k_{qS}$, $M^{-1}s^{-1}$), and for the reaction between $^1O_2$ and the pollutants ($k_{q1_{O_2}}$, $M^{-1}s^{-1}$).

| Quencher | $k_{qS}$ x $10^{-9}$, $M^{-1}s^{-1}$ (from steady-state experiments) | $k_{qS}$ x $10^{-9}$, $M^{-1}s^{-1}$ (from time-resolved experiments) | $k_{q1_{O_2}}$ x $10^{-5}$, $M^{-1}s^{-1}$ |
|---|---|---|---|
| TCP | 10.2 | 8.5 | 13 |
| TCA | 6.3 | 7.6 | 5.3 |
| TCS | 17.5 | 11.3 | 5.5 |
| $O_2$ | 4.5 | 6.9 | - |

To get further evidence of the redox reactions, laser flash photolysis experiments were carried out in order to identify the corresponding reduced species of the photocatalyst ($NMQ^{\cdot}$) and/or the radical cations resulting from the pollutants. To unequivocally identify the photocatalyst reduced species ($NMQ^{\cdot}$), it was obtained upon laser flash excitation (355 nm) of $NMQ^+$ in the presence of a good electron donor, such as DABCO ($E_{DABCO^{+\cdot}/DABCO}$ = + 0.56 V *vs* SCE).[135] In good agreement with the expected redox process, [179] a weak broad signal attributed to $NMQ^{\cdot}$ and centered at 400 nm was

obtained, see Figure 52A. Then, the same experiment was carried out using the pollutants as reducing agents, see Figure 52B-D. In every case, the expected band centered at 400 nm, due to the reduced photocatalyst, was observed. No extra signals due to the radical cations were identified in the spectra obtained for the cases of TCP, see Figure 52 B, and TCS, see Figure 52D, in the recorded spectral window (370 – 650 nm); while in the case of TCA, see Figure 52C, a new strong band centred at 500 nm is observed. This band could be assigned to the corresponding oxidized species of TCA ($TCA^{\cdot+}$) by comparison to the signal reported for the related thioanisole radical cation, centred at 520 nm.[176]

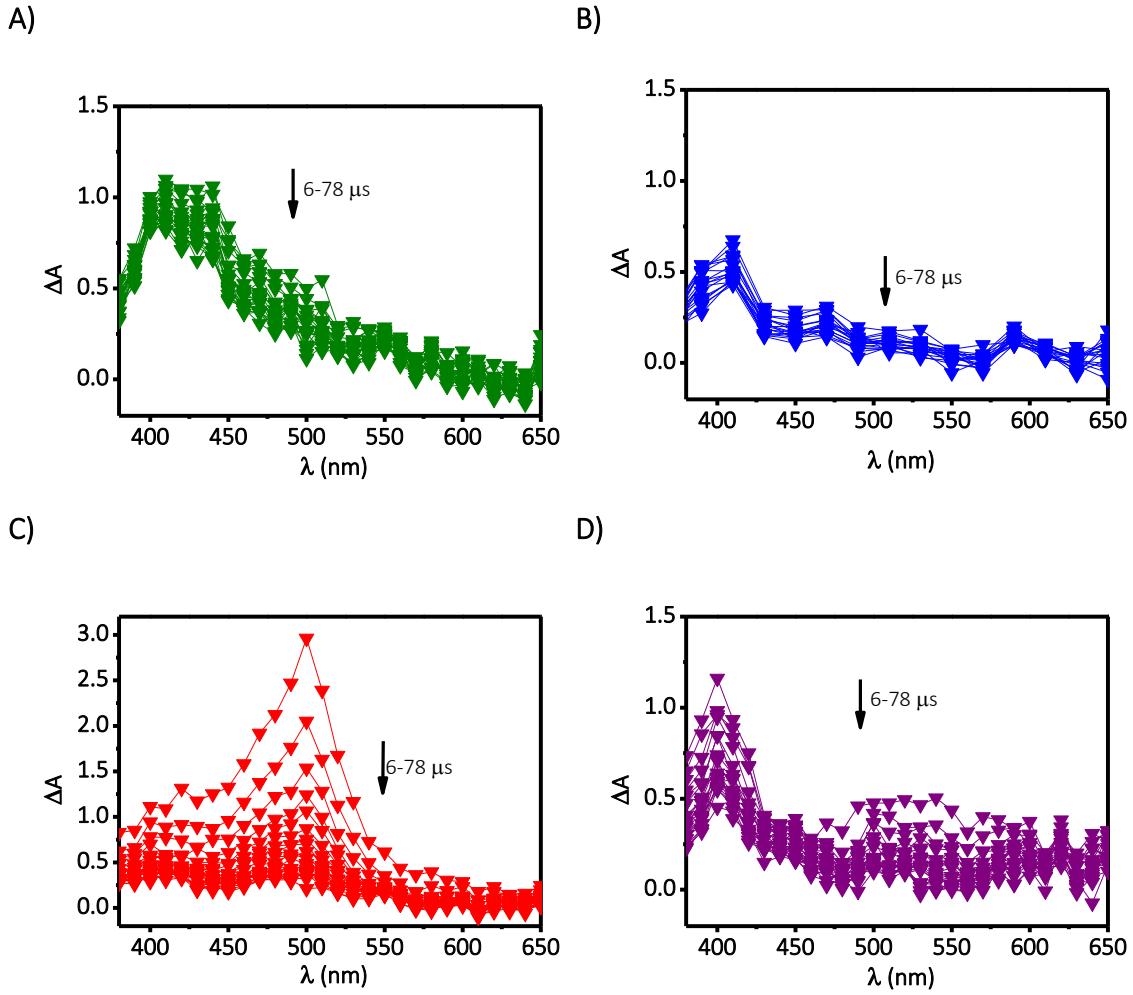


**Figure 52**: Transient absorption spectra obtained upon laser flash excitation of $NMQ^+$ in deareated $CH_3CN$ (absorbance *ca.* 0.3 at 355 nm) recorded at different times after the laser pulse (6 – 78 μs) in the presence of (A) DABCO ($5 \times 10^{-2}$ M); (B) TCP ($3 \times 10^{-3}$ M); (C) TCA ($3 \times 10^{-3}$ M) and (D) TCS ($3 \times 10^{-3}$ M).

In agreement with the long singlet lifetime and the high redox potential of $^1(NMQ^+)^*$, quenching by the pollutants ($k_{qs}$) and also by oxygen ($k_{Qo2}$) is very efficient, with diffusion-controlled quenching constants (Scheme 6). Attending to the equations described in Chapter 6, in air-equilibrated water at room temperature, in which the concentration of $O_2$ is *ca*. 2.9 x $10^{-4}$ M,[135] and with pollutant concentrations of *ca*. $10^{-6}$-$10^{-5}$ M, more than 90% of $^1(NMQ^+)^*$ is quenched by oxygen, while less than 10% is due to electron transfer from the pollutants. However, the contaminants quench quite inefficiently the $^1O_2$ ($kq_{1O2}$ *ca*. $10^5$-$10^6$ $M^{-1}s^{-1}$). Therefore, for concentrations of pollutants in the range of $10^{-6}$ - $10^{-5}$ M, quenching of singlet oxygen by the pollutants cannot compete with its intrinsic deactivation ($k_q = 1/\tau$ *ca*. $10^6$ $s^{-1}$). Thus, Type I (electron transfer) is actually the main pathway involved in the photodegradation of the pollutants when their concentrations are in the micromolar range, in good agreement with the observed photodegradation, independent from the presence of air.

In this sense, the only variable agent would be the contaminants concentration, as the $O_2$ concentration in air-equilibrated water only depends on the temperature and the quenching constants of $^1O_2$ and $^1(NMQ^+)^*$ are inherent to their nature. Therefore, if the contaminants concentration is reduced to *ca.* $10^{-8}$ M, almost all the $^1(NMQ^+)^*$ will be quenched by $O_2$, and subsequent quenching of $^1O_2$ by the pollutants at that low concentration will be negligible compared to its intrinsic deactivation.[104] Thus, at such low concentrations, photodegradation is expected to be almost null. If the concentration is increased to the milimolar range, the electron transfer pathway would be responsible for the quenching of more than 80% of $^1(NMQ^+)^*$, being again Type I the main photodegradation pathway.

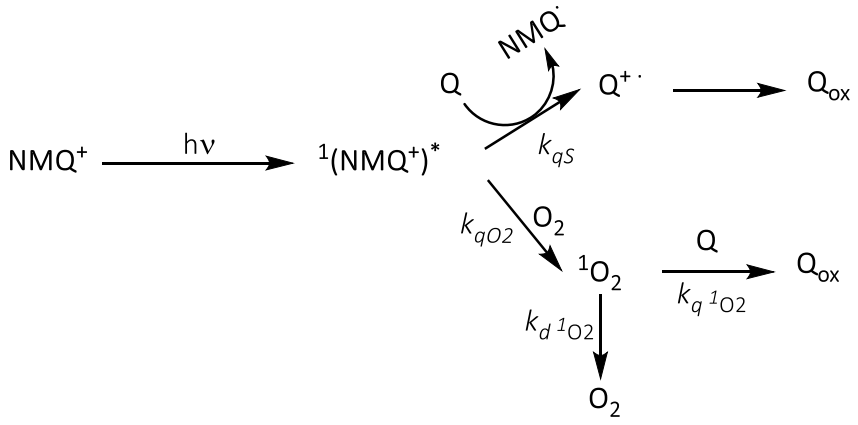


**Scheme 6:** Potential mechanistic pathways to explain photodegradation of the pollutants in the presence of $NMQ^+$.

## 7.3. Conclusions

In agreement with the long singlet lifetime and the high redox potential of $^1(NMQ^+)^*$, singlet excited state of $NMQ^+$ is efficiently quenched by TCP, TCA and TCS and also by oxygen. However, the contaminants quench inefficiently the $^1O_2$ ($kq_{1O2}$ *ca*. $10^5$-$10^6$ $M^{-1}s^{-1}$). Therefore, for concentrations of pollutants, in the range of $10^{-6}$ - $10^{-5}$ M quenching of singlet oxygen by the pollutants cannot compete with its intrinsic deactivation ($k_q = 1/\tau$ *ca*. $10^6$ $s^{-1}$). Thus, Type I (electron transfer) is actually the main pathway involved in the photodegradation of the pollutants in the micromolar range, what is in good agreement with the observed photodegradation independent from the presence of air.

## 7.4. Experimental

Photodegradations were carried out according to the general methodology explained in section 9.3.1. Aqueous solutions (10 mL) containing one of the pollutants (3 x $10^{-5}$ M each) and $NMQ^+$ (3 x $10^{-7}$ M) were irradiated with 350 nm centered light (Luzchem photoreactor) under air or $N_2$ atmosphere.

The evolution of the photodegradation was monitored by HPLC. Thus, aliquots of 75 μL were injected together with 5 μL of 2-nitrobenzoic acid (8.8 x $10^{-4}$ M) used as internal standard. The mobile phase was an isocratic mixture of water pH 3 (80%) and acetonitrile (20%) with a flux fixed at 1.5 mL x $min^{-1}$, and the detection wavelength was fixed at 215 nm for TCP and TCS, and 228 nm for TCA.

For the heterogeneous photoreactions, aqueous solutions of 10 mL containing a mixture of one of the pollutants ($3\times10^{-4}$ M) and Zeolite Y-$NMQ^+$ (70 mg $L^{-1}$) were irradiated with light centered at 350 nm under air, using the Luzchem photoreactor. The removal of the pollutants was monitored by HPLC at different irradiation times using the same conditions than for the homogeneous analysis.

The mineralization was studied following the general procedure explained in 9.3.2: an aqueous solution (40 mL) containing a mixture of the three pollutants (2 g $L^{-1}$ each, 30 mM global concentration) and $NMQ^+$ (30 mg $L^{-1}$, 0.13 mM) was irradiated using the solar simulator described in 9.2 for 48 hours.

The photophysical measurements were performed according to the general procedure 9.3.4.

Steady-state and time-resolved fluorescence experiments were performed under $N_2$ and the final quencher concentration was up to 5 x $10^{-3}$ M for each pollutant. The excitation wavelength was fixed at 317 nm in the case of steady-state experiments, while a pulsed LED ($\lambda_{exc}$ = 310 nm) excitation source with a cut-off filter (50% transmission at 320 nm) to remove residual excitation signal in emission was used in the case of the time-resolved fluorescence measurements. In the case of the quenching with oxygen, traces, were recorded under different atmospheres: $N_2$, air and saturated $O_2$, the concentration of $O_2$ was obtained from the literature.[135].

For the laser flash photolysis experiments, the final concentration of each pollutant was up to 3 x $10^{-3}$ M and the solution of the photocatalyst was prepared with an absorbance at the excitation wavelength (355 nm) of 0.3 in deaerated $CH_3CN$.

Solid emission fluorescence of supported Zeolite Y-$NMQ^+$ was recorded upon excitation at 317 nm and collected at 90° to minimize the scattered light.

Redox potentials measurements were carried out according to 9.3.3

A)

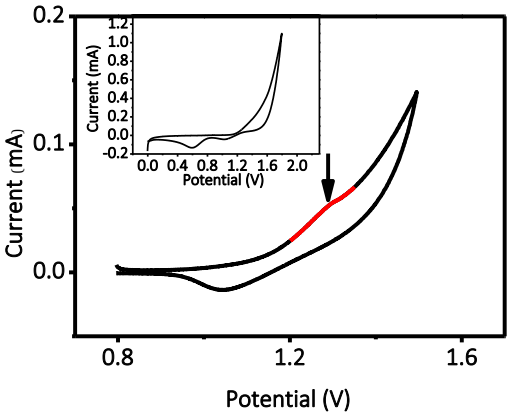


| ELECTRODE | E ($TCP^{\cdot+}$/TCP) |
|---|---|
| AgCl/Ag (3M NaCl) | 1.30 V |
| SCE* | 1.25 |

B)

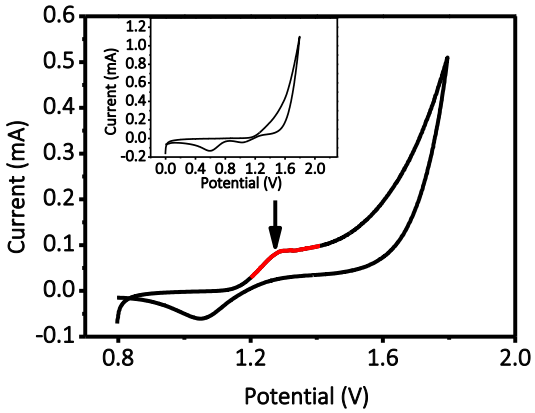


| ELECTRODE | E ($TCS^{\cdot+}$/TCS) |
|---|---|
| Ag/AgCl (3M NaCl) | 1.28 V |
| SCE* | 1.23 V |

**Figure 53**: Cyclic voltammetry of TCP and TCS (30 μM) measured in tetrabutyl ammonium perchlorate (TBA) solution (0.1 M) as electrolyte at 0.05 V $s^{-1}$. Inset: Cyclic voltammetry of the electrolyte TBA, blank measurement. *The obtained data from the AgCl/Ag (3 M NaCl) were converted into redox potential values *vs* SCE as E (*vs* SCE, in V) = E (*vs* AgCl/Ag, in V) -0.047.

For the toxicity assays, mixtures (250 mL) of the three pollutants (3 x $10^{-5}$ M each) and $NMQ^+$ (10 mg $L^{-1}$, 0.04 mM) or $TiO_2$ (200 mg $L^{-1}$) were irradiated using the Luzchem photoreactor (λ = 350 nm) under aerobic atmosphere, up to 70 hours, in order to evaluate the toxicity of the samples. The standard ISO 6341:1996 procedure,[188] was followed to perform bioassays based on the inhibition of the mobility of *D. magna*, using 24-h old organisms hatched from the ephippia. Five neonates were located at appropriate containers with test dilution (10 mL). Constant temperature of 21 ± 1 ºC and dark conditions were used to conduct the assays. After 24 h (end of the test period)

mobile *D. magna* were counted in each container, considering immobile those unable to swim in the 15 s after agitation. Then, controls and sample dilutions were prepared with the standard freshwater and all of them were tested in quadruplicate. Standard freshwater was also used as hatching medium. The recorded assay data, whenever possible, was used to calculate the $EC_{50}$ (concentration required to produce 50% of effect) by Probit analysis, using the Statistical Analysis System SPSS (version 16.0). Besides, toxicity data were statistically analysed to determine the effect of irradiation procedure on toxicity. A $p < 0.05$ was taken to indicate statistical significance (STATGRAPHICS PLUS version 5.1).

*PART III:*

*REDUCTIVE ELECTRON TRANSFER PROCESSES*

# Preamble

In the recent years, photoredox catalysis mediated by UV-vis light has received increasing attention as a powerful synthetic tool, mainly due to its ability to generate radicals that initiate the pursued reactions.

In order to initiate the reaction, light of the adequate wavelength is used to excite the photocatalyst. Then, the photocatalyst from its singlet or/and from its triplet excited state, reacts with a first substrate. Depending on the redox potentials of the excited photocatalyst and of this first substrate, the electron transfer happens in one or the other direction. For example, Scheme 7, shows a photocatalytic cycle in which, after excitation of the photocatalyst, a first substrate is acting as a donor (D), therefore, the donor is oxidized ($D^{\cdot+}$) and the photocatalyst is reduced ($PC^{\cdot-}$). The excited photocatalyst and the formed radicals are the key species involved in the photocatalytic step and their detection could be crucial to understand the process. Next step is a thermal process governed by radical chemistry. In the example shown in Scheme 7, the radical anion of the photocatalyst reduces a second substrate, which acts as an acceptor (A). As a consequence, the photocatalyst returns to its ground state and the acceptor is reduced to its radical anion ($A^{\cdot-}$). Further reactions of the radicals with other species in the media end into the desired final products. Alternatively, as a result of the photochemical step, the radical anion of the first substrate (acting now as an acceptor, $A^{\cdot-}$) and the corresponding radical cation of the photocatalyst ($PC^{\cdot+}$) could be formed. Then, the subsequent thermal step involves oxidation of the second substrate (acting now as a donor, D) and the recovery of the photocatalyst.

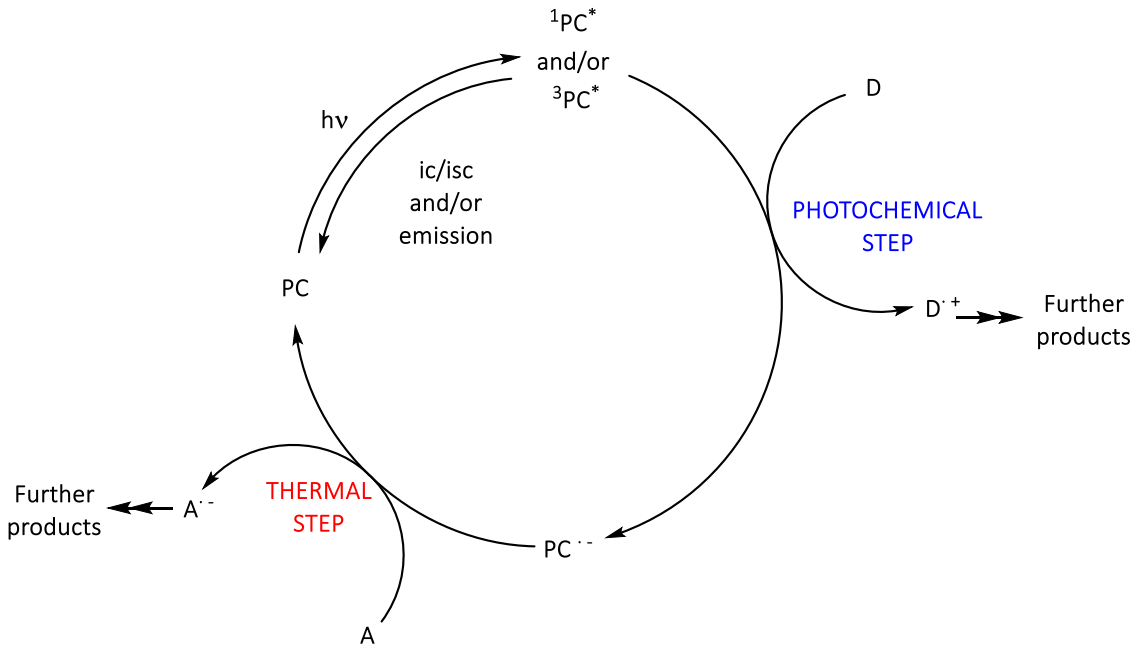


**Scheme 7:** General photocatalytic cycle in a photoredox system in which the photochemical step involves the oxidation of a first substrate, D, and the thermal step represents the reduction of a second substrate, A.

Among the typical visible-light photocatalysts, transition-metal mainly based on Ru or Ir have been the most commonly employed in the last decade, although organic dyes have also been used.[6, 11, 38, 189-195] Metallic ones offer higher stability and activity; however, they are also scarce and expensive, what hinders its large-scale applicability in industry. Maybe that is why photocatalysis, despite demonstrating of being a potential tool, it is still regarded as a process confined to the laboratory.

Nevertheless, the development of new routes, based on common metals or, even more desirable, metal-free ones and visible light, is actually a hot topic for the development of sustainable organic processes. Deeper understanding of the involved mechanisms should also be desirable

Under this context, Part III of the present thesis contains a chapter in which reduction of halides has been studied. As a photocatalyst, a non-metallic organic dye has been employed, riboflavin. In addition, careful attention has been paid to the detection of the intermediate species, as well as to the thermodynamics of each step of the catalytic cycle.

# 8. Metal-Free Photocatalytic Reductive Dehalogenation Using Visible-Light. A Time-Resolved Mechanistic Study

## 8.1. Introduction

During the past years, photoredox catalysis mediated by solar light has received increasing attention in myriads of different applications. As a result, transition-metal based and alternative metal-free photocatalysts, typically organic dyes, have been developed. [6, 11, 38, 189-195] One of these organic dyes is riboflavin (RF), which is present in waters of seas, rivers and lakes, and it is also responsible for the redox activity of flavin adenine dinucleotide (FAD) and cofactor flavin mononucleotide (FMN). Its chemical structure is composed of a tricyclic system with a 7, 8-dimethyl substitution and a ribotyl chain at the *N*-10 position (Figure 54). Its UV-vis absorption spectrum exhibits two defined bands peaking *ca.* 450 and 350.

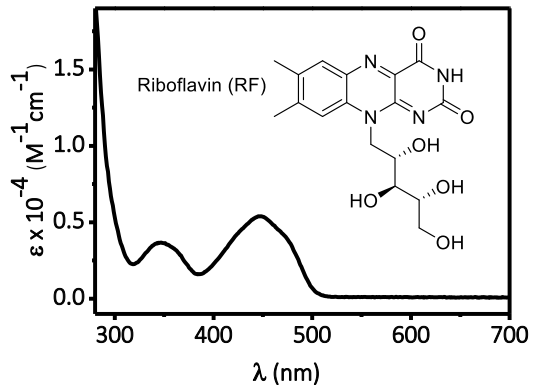


| PARAMETER | RF |
|---|---|
| $\Phi_F$ (water)<br>$\Phi_F$ (ACN) | 0.26<br>0.47 |
| $\Phi_{ISC}$ | 0.70 |
| $\Phi_\Delta$ | 0.47 |
| $E_S$ | 2.48 eV |
| $E_T$ | 2.17 eV |
| $E^0_{red}$ (RF/RF$^{\cdot-}$) | -0.80 to -0.45 V (solvent dependent) |

**Figure 54:** Chemical structure and absorption spectrum of Riboflavin (RF) in dimethylformamide (left). Photophysical properties [196] and redox potential [197-201] of RF (right).

Therefore, RF has been suggested as one of the substances present in water responsible for the "natural" photodegradation of pollutants in the environment and its photophysical properties have been deeply studied, see Figure 54 for details.[196] More specifically, it has been employed to promote photooxidation of phenolic or *N*-heteroaromatic pollutants upon solar irradiation.[70, 84, 142, 202-207] The mechanistic

studies, based on time-resolved techniques, beyond these reactions have demonstrated that the excited states (singlet and/or triplet) of RF are quenched by the pollutants. Then, the pollutants are oxidized, and RF is reduced, giving rise to the corresponding pollutant radical cations and $RF^{\bullet-}$. Subsequent oxidation of the pollutants has been mainly attributed to the reactivity between the radical cations and superoxide anion ($O_2^{\bullet-}$), which is expected to be formed from $RF^{\bullet-}$ by a thermodynamically favored electron transfer process to $O_2$.

Furthermore, RF or flavin derivatives have recently been employed as visible-light redox photocatalysts with synthetic purposes, *e.g.* oxidative chlorination of arenes,[208] selective removal of benzylic protecting groups,[209] or aerobic photooxidation of sulfides,[210] among others. All these examples deal with the oxidation of the substrates, but little attention has been paid to the potential of RF as a reductant in either water remediation or organic synthesis.

It is worth mentioning that reductive dehalogenation methods are used in a wide variety of synthetic contexts and these procedures have already been optimized using visible-light photocatalysts such as $Ru(bpy)_3Cl_2$.[211-222] However, many of the recent publications lack a kinetic study of the involved excited states; therefore, a deeper mechanistic understanding of the processes based on time-resolved techniques could help to broaden the substrate scope of the photocatalyzed organic reactions.[70, 103, 104, 111, 140, 167]

Under this context, the objective of the present chapter is to perform reductive dehalogenation of different bromo-derivatives using RF as a metal-free photocatalyst upon visible light irradiation (460 nm), in the presence of amines and isopropanol as $e^-$ and H-donors, respectively. The selected halogenated compounds are: bromobenzene (**1**), benzyl bromide (**2**) and α-bromoacetophenone (**3**) (Figure 55). The reactions will be followed by HPLC analysis, and commercial reagents benzene (**1'**), toluene (**2'**) and acetophenone (**3'**) will be used as standards to assess the concentration of the corresponding reaction products. Besides, an analysis of the thermodynamics and the kinetics of all the competing pathways involved in the photocatalyzed redox processes will provide a deep understanding of the overall reaction mechanisms.

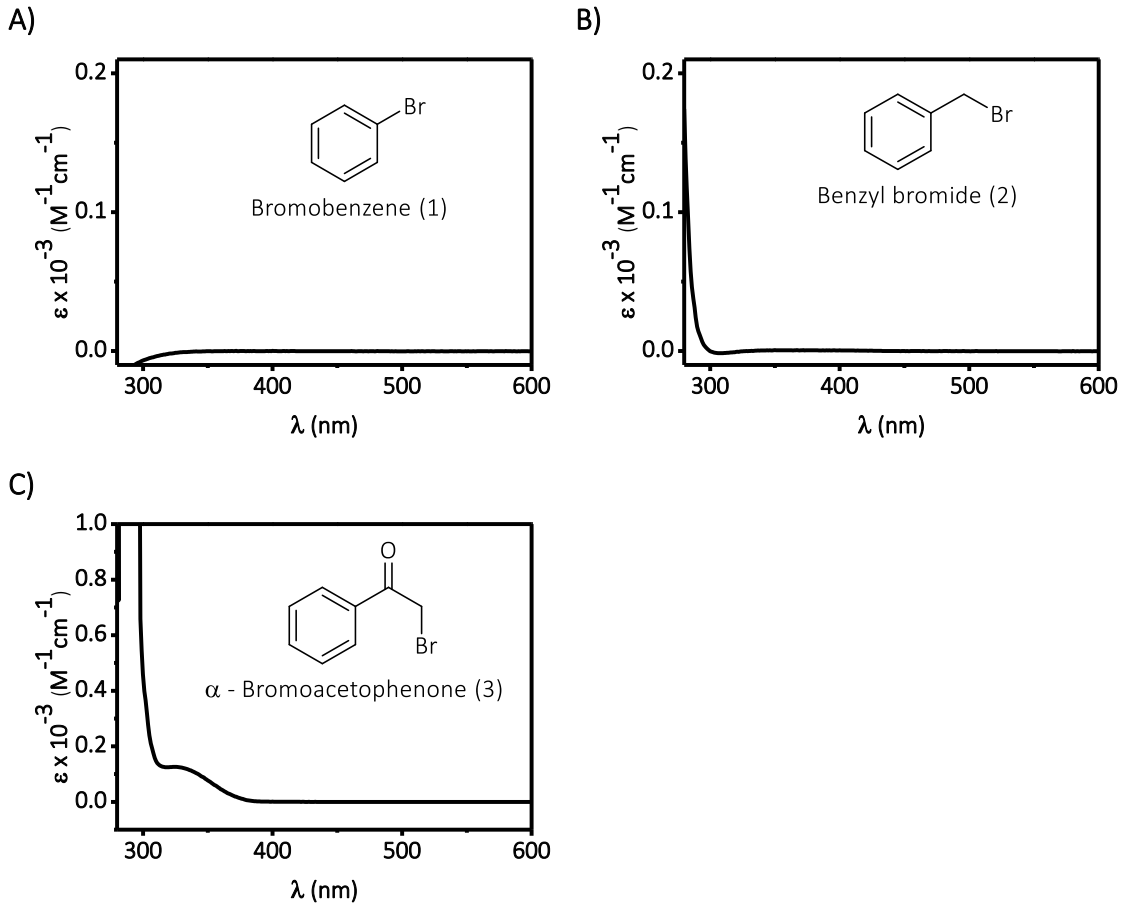


**Figure 55**: Chemical structures of selected organic bromides and their corresponding UV-vis absorption spectra recorded in $CH_3CN$.

## 8.2. Results and discussion

Initially, reaction conditions were optimized using **3** as substrate. First, 1,4-diazabicyclo[2.2.2]octane (DABCO, 2 eq), acting as the $e^-$ donor, and *i*-PrOH (2 eq), acting as the H-donor, were tested in different media, anhydrous or aqueous DMF, DMSO and $CH_3CN$, and in the presence of RF (2.5 mol %, relative to **3**) under inert atmosphere. The mixture was irradiated using two LEDs ($\lambda_{em}$ = 460 nm, 20 W each); however, conversion after 18 hours of irradiation was low, particularly when aqueous mixtures were employed, mainly due to solubility problems. Nevertheless, using anhydrous DMSO as a solvent and diisopropyl amine (DIPA) at higher amounts (up to 5 eq) as donor, reaction resulted in 100% conversion after 12 hours of irradiation. Lower concentrations of amine or *i*-PrOH (1 eq each) decreased the rate of conversion, but still 100% was obtained upon 18 h. Reactions carried out in the presence of air, gave low conversion and the HPLC analysis revealed the presence of other side-products, maybe due to the formation of $O_2^{\cdot}$,

that caused photodegradation of RF among other side processes. Control experiments were also carried out, in the absence of light and in the absence of RF, and conversions resulted only in 10%. From all these experimental results, the final optimized reaction conditions are shown in Scheme 8.

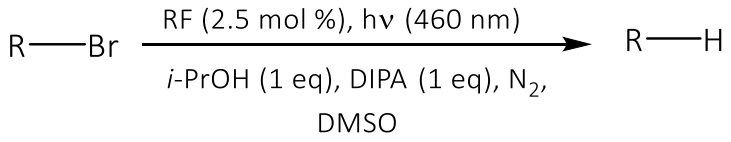


**Scheme 8**: Optimized reaction conditions to perform the reductive dehalogenation of bromides using RF as metal-free photocatalyst and blue LEDs.

Using the optimized conditions, dehalogenation of **2** also resulted in 100% conversion. Dehalogenation of **1** was also carried out under these conditions; however, conversion was low even at long irradiation times.

Next step was the study of the involved mechanism. In principle, quenching of the excited states of the photocatalyst could be due to both, energy transfer or electron transfer (singlet and triplet energies for RF are quite high, 2.48 eV and 2.17 eV, respectively).[198]. Besides, attending to the UV-visible spectrum of the photocatalyst, which absorbs up to 500 nm, Figure 54, compared to those of the bromides, which absorb at much shorter wavelength, below 300 nm for **1** and **2**, and below 400 nm for **3**, Figure 55, much more energetic excited states in the case of the bromides than in the case of RF can be anticipated. Therefore, the energy transfer mechanism can be safely ruled out since it is expected to be thermodynamically disfavored in all cases.

Then, photoinduced electron transfer looks to be the operating pathway. If this is the case, the first step will be the reduction of the singlet and/or the triplet excited state of RF in the presence of $e^-$ donors such as DABCO, DIPA, *N,N'*-dimethylaniline (DMA) or triethylamine (TEA), generating the corresponding reduced species ($RF^{\bullet-}$). The second step will be the reduction of the bromides by the radical anion $RF^{\bullet-}$. With this hypothesis, the photoinduced electron transfer from the different amines to the excited states of RF was evaluated using the photoinduced Gibbs free energy equation adapted for this case, Eq. 27.[7, 223]

$$\text{Eq. 27: } \Delta G^{o}_{et}(eV) = -(E^{o}_{red}(RF/RF^{\cdot -}) - E^{o}_{red}(D^{\cdot +}/D)) - E(RF^{*})$$

Paying attention to the redox potentials (see Figure 54 and Table 17), **Eq. 27** reveals that oxidation of the amines from the singlet or the triplet excited state of RF is exergonic in every case, see Table 17.

**Table 17**: Thermodynamic redox potentials for the amines and the bromide derivatives and $\Delta G^{0}_{et}$ values for the redox processes between amines and RF from its singlet and triplet excited estates.

| COMPOUND | $E(D^{\cdot +}/D)$ (V) | $E(A/A^{\cdot -})$ (V) | $\Delta G^{0}$ from $^{1}RF^{*}$ (eV) | $\Delta G^{0}$ from $^{3}RF^{*}$ ($eV^{1}$) |
|---|---|---|---|---|
| DABCO | +0.56[135] | - | -1.12 | -0.81 |
| DIPA | +1.31[198] | - | -0.37 | -0.06 |
| DMA | +0.81[135] | - | -0.87 | -0.56 |
| TEA | +0.96[135] | - | -0.72 | -0.41 |
| 1 | - | -1.56[224] | | |
| 2 | - | -0.57[224] | | |
| 3 | - | -0.49[225] | | |
| $O_2$ | - | -0.33[226] | | |
| | [a] in V *vs* SCE. | | | |

The subsequent reduction of the bromides was evaluated with the "thermal" Gibbs free energy relationship adapted for this system, Eq. 28:

$$\text{Eq. 28: } \Delta G^{o}(eV) = -(E^{o}_{red}(C-Br/C-Br^{\cdot -}) - E^{o}_{red}(RF/RF^{\cdot -}))$$

Using Eq. 28, the resulting $\Delta G^{0}$ values are +0.76 eV; -0.23 eV and -0.31 eV, for bromides **1**, **2** and **3**, respectively and -0.47 V for the reaction with $O_2$ to give $O_2^{\cdot -}$. Therefore, reduction of bromobenzene (**1**) is not expected from the $RF^{\cdot -}$, however the reduction of **2** and **3** is thermodynamically exergonic, in both cases.

Once the thermodynamics has been estimated, the kinetics of the competing processes in the time scale of the corresponding RF excited states or $RF^{\cdot -}$ had to be experimentally determined. First, steady state and time-resolved fluorescence experiments were performed to investigate the involvement of the singlet excited state of RF. Afterwards, the participation of the triplet excited state of RF and also of RF radical anion was investigated based on laser flash photolysis experiments.

$^1$RF* fluorescence quenching by amines in aerated DMF was very efficient in all cases as it can be observed from steady-state and time-resolved emission experiments, see Figure 56; furthermore, it proceeded in all cases without changes in the spectral shape. The observed emission quenching is in good agreement with the expectations based on the redox potential of RF and those of the employed amines (see Table 17).[198] Then, using the Stern-Volmer fitting (see Figure 56 insets), the corresponding quenching constants were determined (see Table 18). The values are all close to the diffusion limit, [135] confirming the dynamic participation of $^1$RF* in the electron transfer process. Control experiments were also carried out to evaluate the direct reactivity between bromides **1-3** and $^1$RF*. Singlet lifetime of $^1$RF* remained unchanged upon addition of bromides **1-3**, up to 5 x $10^{-2}$ M concentration.

**Table 18**: Determined rate constants for the quenching of excited states of RF by amines and $RF^{\bullet-}$ by the selected bromides.

| | $k_{qS}$ ($M^{-1}s^{-1}$) | $k_{qT}$ ($M^{-1}s^{-1}$) | $k_{qRF^{\bullet-}}$ ($M^{-1}s^{-1}$) |
|---|---|---|---|
| DABCO | 4.5 x$10^9$ | N.D. | - |
| DIPA | 1.6 x$10^9$ | N.D. | - |
| DMA | 5.3 x$10^9$ | N.D. | - |
| TEA | 2.9 x$10^9$ | N.D. | - |
| 1 | - | - | < $10^6$ |
| 2 | - | - | 9.1x$10^7$ |
| 3 | - | - | 1.7x$10^8$ |
| $O_2$ | - | 9.0x$10^8$[202] | 1.4x$10^8$[202] |
| | N.D.: not determined. | | |

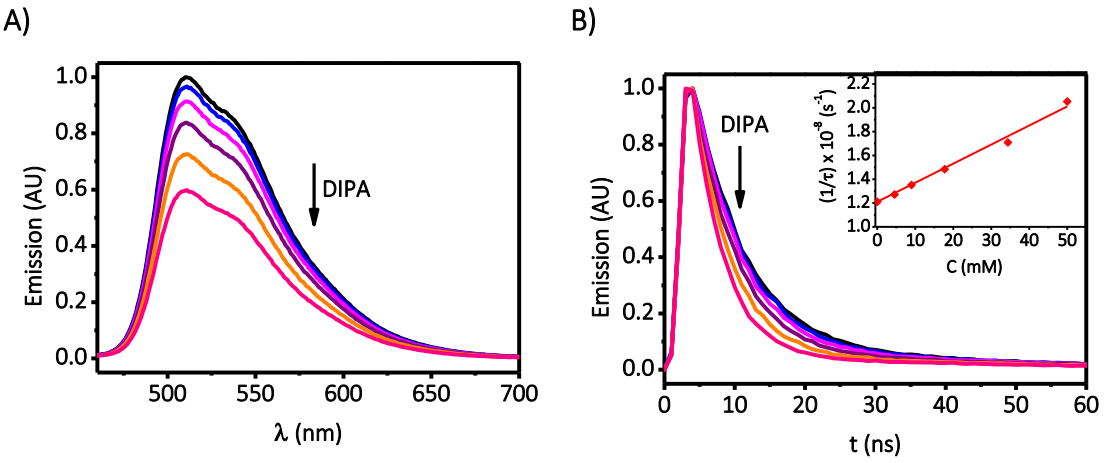

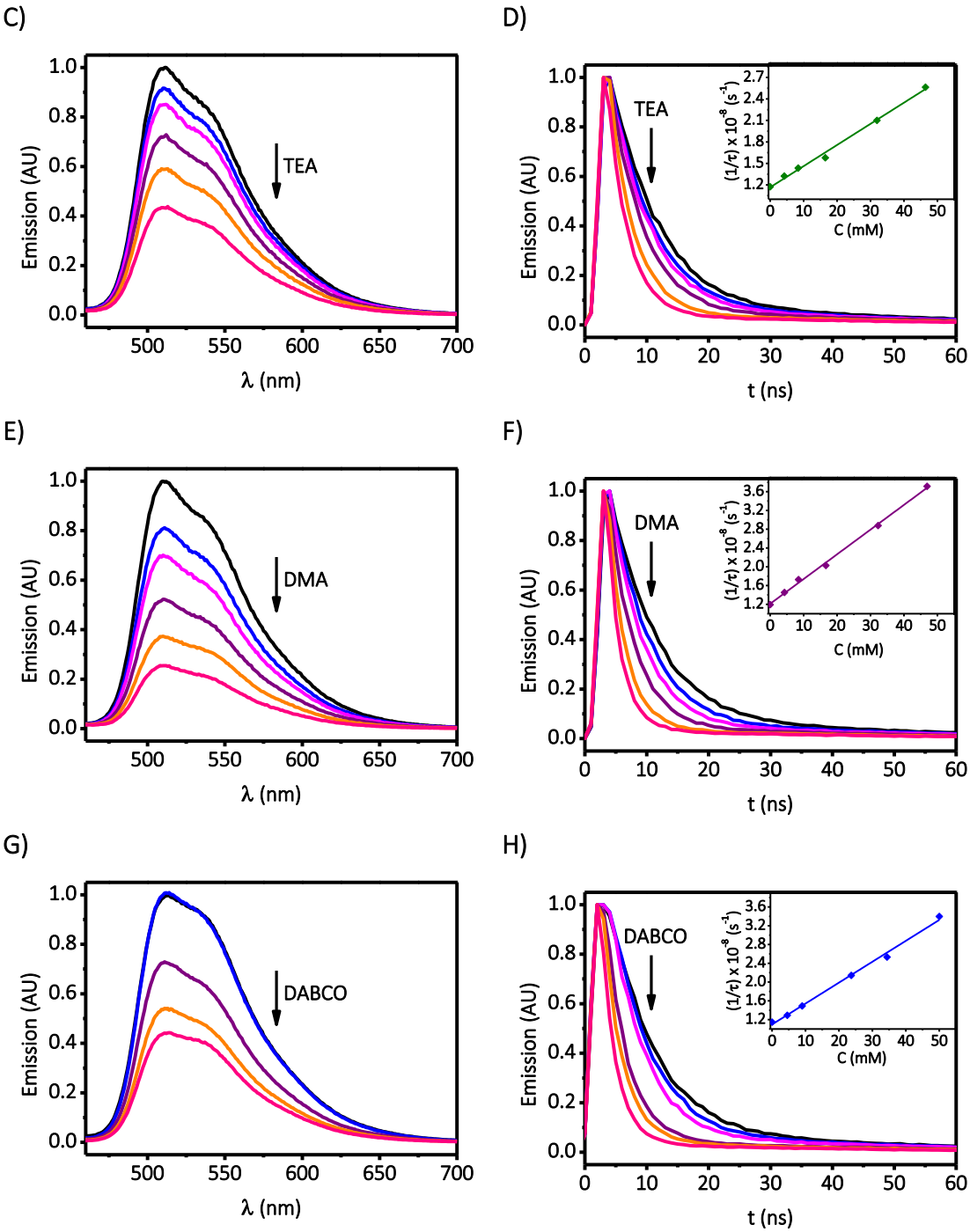


**Figure 56**: Steady-state ($\lambda_{exc}$ = 446 nm) emission behavior of RF (left column) and changes in the singlet lifetime of RF ($\lambda_{exc}$= 460 nm) (right column), upon addition of increasing concentrations of DIPA (♦), TEA (♦), DMA (♦) and DABCO (♦) in aerated DMF. Inset: Stern-Volmer plots obtained from the time-resolved experiments.

Next, $^3$RF* was investigated upon LFP excitation (355 nm) of deaerated solutions of RF (4 x $10^{-5}$ M) in DMF. First, the spectra obtained before and after adding the amines were compared. Before the addition, the already described triplet excited state ($^3$RF*)

spectrum was obtained: a maximum centered at 380 and a huge band between 500 and 700 nm, see Figure 57A orange trace.[70] After the addition, the spectrum showed a much more intense maximum at 380 nm and a less intense wide band between 500 and 650 nm (see Figure 57A for the case of DABCO), that could safely be assigned to $RF^{\cdot-}$, based on literature data.[70, 227] The comparison of these two spectra also acted as an additional confirmation of the efficient redox process between either $^{1}RF^{*}$ or $^{3}RF^{*}$ with the amines.

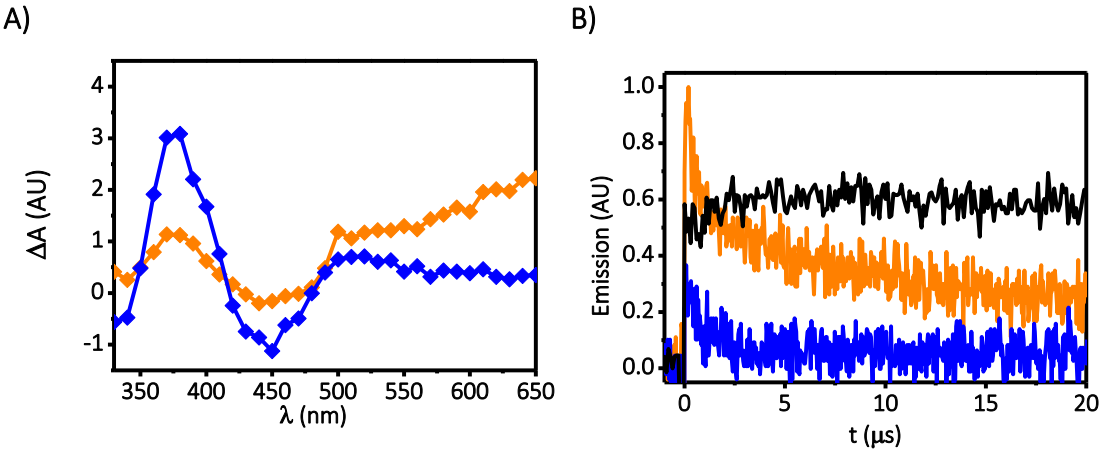


**Figure 57: A**) Transient absorption spectra obtained upon laser flash excitation of RF (4 x $10^{-5}$ M) in deaerated DMF ($\lambda_{exc}$ = 355 nm) recorded 2 μs after the laser pulse in the absence (♦) and in the presence of DABCO 5.4 x $10^{-2}$ M (♦). **B**) $^{3}RF^{*}$ monitored at 620 nm in the absence (orange) or in the presence (blue) of DABCO 5.4 x $10^{-2}$ M; growth of $RF^{\cdot-}$ monitored at 380 nm (black) in the presence of DABCO 5.4 x $10^{-2}$ M.

Further experiments aiming to investigate quenching of the triplet excited state were difficult due to the efficient quenching from the singlet. In fact, when traces at 620 nm ($^{3}RF^{*}$) were recorded without and with the different amines, the transient absorbance immediately decreased after the laser pulse, see Figure 57B traces orange and blue; revealing that a great part of the excited molecules reacted from the singlet excited state, and therefore they could not reach the triplet excited state. Nevertheless, the participation of the triplet excited state is not excluded, monitoring the signal at 380 nm in the presence of amine indicated a significant formation of $RF^{\cdot-}$ from the $^{3}RF^{*}$. Control experiments were also carried out to evaluate direct reaction between $^{3}RF^{*}$ and the bromides and no reaction was observed.

The next step was to evaluate the reactivity between reduced species of RF ($RF^{\bullet-}$) and the bromides **1-3**. Then, deaerated DMF solutions containing both, RF ($4 \times 10^{-5}$ M) and DABCO ($5.4 \times 10^{-2}$ M), were subjected to LFP excitation and the evolution of the radical anion was monitored upon increasing concentrations of the bromides. $RF^{\bullet-}$ exhibits a transient absorption spectrum with an intense band centred at 380 nm and a broad maximum in the 500-600 nm region, therefore $RF^{\bullet-}$ quenching was monitored at 380 nm. Figure 58 shows how the lifetime of $RF^{\bullet-}$ decreased after adding increasing concentrations of bromides **2** and **3**. However, in the case of bromide **1**, the lifetime of $RF^{\bullet-}$ remained unchanged, in agreement with the thermodynamic calculations. Therefore, kinetic results were in good agreement with the thermodynamic studies since bromides **2** and **3** are able to quench the $RF^{\bullet-}$, but bromide **1** did not produce any change, see Figure 58 and Table 18 for the determined kinetic quenching constant values.

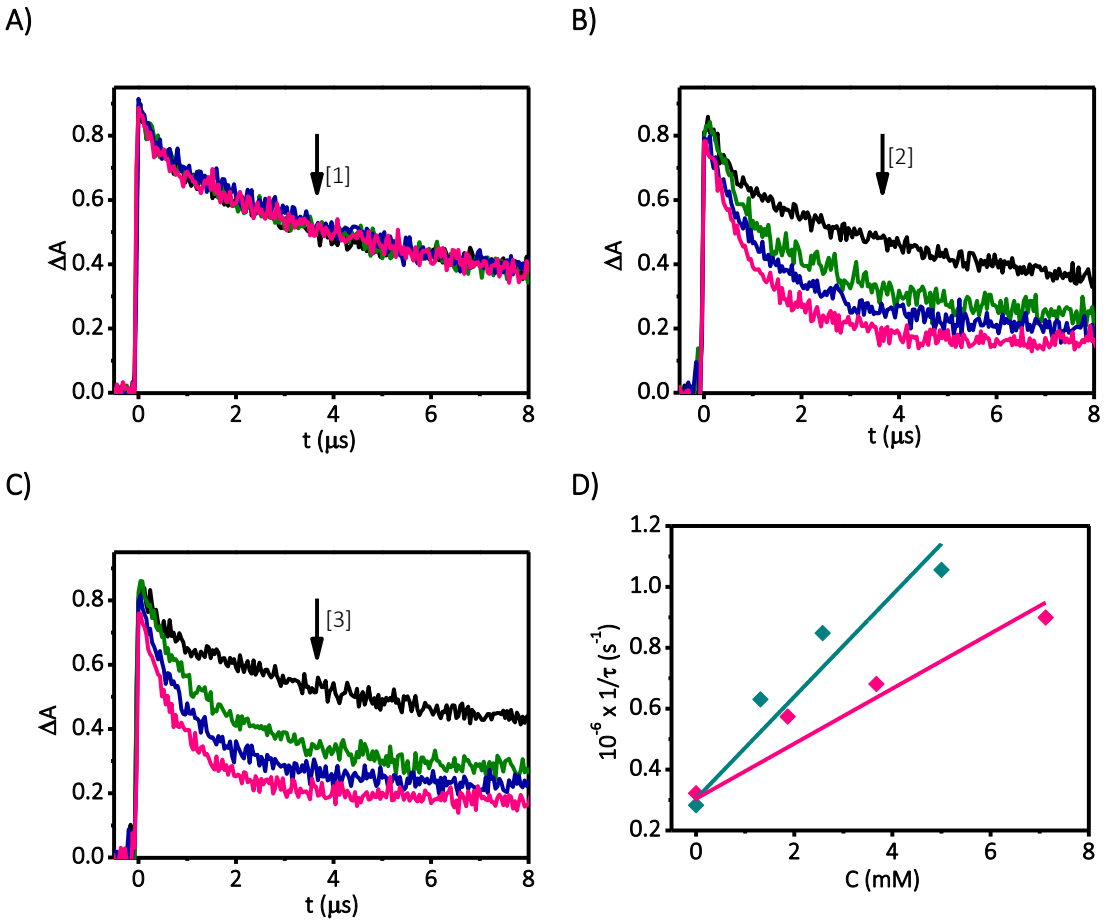


**Figure 58**: Traces corresponding to $RF^{\bullet-}$ monitored at 380 nm upon laser flash photolysis excitation of RF ($4 \times 10^{-5}$ M) in the presence of DABCO (10 mM), in deaerated DMF ($\lambda_{exc}$ = 355 nm), in the presence of increasing concentrations of bromides **1** (A), **2**

(**B**) and **3** (**C**). Stern-Volmer plots corresponding to the quenching of $RF^{\bullet-}$ by bromides **2** (♦) or **3** (♦)(**D**).

All the reported experiments allow us to postulate the mechanism shown in Scheme 9.

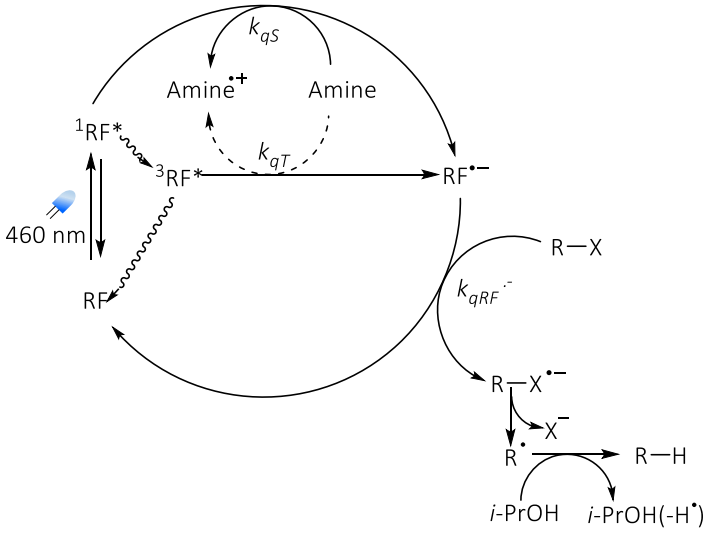


**Scheme 9:** Postulated reaction mechanism.

The formation of $RF^{\bullet-}$ due to the quenching of $^1$RF* or $^3$RF* can be calculated with Eq. 29 and Eq. 30, which correspond to the adaptation of the corresponding Eq. 10 to Eq. 21.

**Eq. 29**: $$\%Quenching\ of\ {}^1RF^* = \frac{k_{qS}[Amine]}{\frac{\Phi_F}{\tau_S}+\frac{\Phi_{ISC}}{\tau_S}+k_{qS}[Amine]}\ x\ 100$$

**Eq. 30**: $$\%Quenching\ of\ {}^3RF^* = \frac{\frac{\Phi_{ISC}}{\tau_S}}{\frac{\Phi_F}{\tau_S}+\frac{\Phi_{ISC}}{\tau_S}+k_{qS}[Amine]}\ x\ \frac{k_{qT}[Amine]}{\frac{1}{\tau_T}+k_{qT}[Amine]}\ x100$$

Taking into account the reported values for $\Phi_F$ = 0.26 and $\Phi_{ISC}$ = 0.70, see Figure 54, the experimental obtained value of $\tau_S$ = 8.3 ns, an averaged experimental value of 3 x $10^9$ $M^{-1}s^{-1}$ for the quenching of the singlet by amines and a concentration of 0.15 M for the amines, the formation of $RF^{\bullet-}$ from $^1$RF* (according to Eq. 29) is *ca.* 0.80. Therefore, the quenching from $^1$RF* is almost quantitative, supporting the postulated mechanism, Scheme 9. According to the thermodynamics, reaction of $RF^{\bullet-}$ with bromides **2** and **3** and also with $O_2$ is exergonic. Therefore, if the reactions are performed under $O_2$, competence

between the bromide and the $O_2$ would be observed, decreasing the efficiency of the reaction.

## 8.3. Conclusions

A detailed mechanistic understanding of the steps involved in the photocatalytic reduction of three bromides in the presence of riboflavin has been achieved based on time-resolved techniques. First, efficient quenching of the singlet excited state of riboflavin ($^1$RF*) by amines with kinetic constant values close to diffusion limit results in the formation of the radical anion ($RF^{\bullet-}$). Second, the rate constant values for the quenching of $RF^{\bullet-}$ by the organic bromides are in good agreement with the thermodynamic estimations for the thermal redox process, what demonstrates the key role of this intermediate.

## 8.4. Experimental

Photocatalytic reactions were performed at 0.5 mmol scale in the case of **3** and at 2 mmol scale for **1** and **2**. General procedure is as follows: 8 mL of DMSO solutions containing a mixture of RF (2.5 mol %), one of the bromides, DIPA (1-5 eq) and *i*-PrOH (1-5 eq) were irradiated using two LEDs centered at 460 nm, see section 9.2 for details, under $N_2$ atmosphere in Pyrex tubes. The real concentrations are summarized in Table 19.

**Table 19:** Experimental conditions for the photocatalytic reactions performed in deaerated DMSO (8 mL).

| Bromide | Amount (mmol) | DIPA (mmol) | / *i*-PrOH |
|---|---|---|---|
| **Br1** | 2 | 2 | 2 |
| | | 10 | 10 |
| **Br2** | 2 | 2 | 2 |
| | | 10 | 10 |
| **Br3** | 0.5 | 0.5 | 0.5 |
| | | 2.5 | 2.5 |

Reactions were monitored by taking aliquots (5 μL) that were injected into the HPLC running with acetonitrile (70%)/water (pH 3) in isocratic mode at a flow rate of 1.5 mL $min^{-1}$ and using 1,3,5-trimethylbenzene (10 μL of a 0.2 M solution) as internal

standard. The chromatograms were analyzed at 250 (bromides **1** and **2**) or 275 nm (bromide **3**). Starting materials and final compounds were identified by comparison to commercial standards.

The photophysical measurements were performed according to the general procedure 9.3.4.

For the steady-state and time-resolved fluorescence experiments, aerated DMF solutions of RF (absorbance lower than 0.15 at $\lambda_{exc}$ = 446 or 460 nm, respectively) were treated with increasing concentrations of amines or bromides (up to 5 x $10^{-2}$ M).

Laser flash photolysis experiments were performed on deaerated solutions of RF (4 x $10^{-5}$ M) and DABCO (1 x $10^{-2}$ M) in DMF, to which increasing concentration of each bromide (up to 7 mM for bromo derivatives **1** and **2** and 5 mM for bromo derivative **3**) were added.

# 9. Experimental

## 9.1. Reagents

Acetaminophen (ACF), acetamiprid (ACP), α-bromoacetophenone, barium hydroxide octahydrate, benzyl bromide, bromobenzene, caffeine (CAF), carbamazepine (CBZ), clofibric acid (CLOF), 1,4-diazabicyclo[2.2.2]octane (DABCO), diclofenac (DCF), diisopropyl amine (DIPA), gallic acid (GA), 2-nitrobenzoic acid, 4-nitrobenzoic acid, *N,N'*-dimethylaniline (DMA), pentadecane, perinaphthenone (PN), riboflavin (RF), rose bengal disodium salt (RB), titanium dioxide as AEROXIDE® P25-$TiO_2$, 2,4,6-trichloroanisole (TCA), 2,4,6-trichlorophenol (TCP), triclosan (TCS), triethylamine (TEA), 1,3,5-trimethylbenzene and 2,4,6-triphenylpyrylium ($TPP^+$) used as hydrogen sulphate or tetrafluoroborate salt were obtained from Aldrich. Ephippia (dormant eggs) of crustacean Daphnia magna were supplied by ECOtest S.L. (Valencia, Spain). Zeolite Y 100 was obtained from Zeolyst International.

Dimethylformamide (DMF) 99% purity was from Accross, $CH_3CN$ was of HPLC quality from Merck or Scharlau and anhydrous dimethyl sulfoxide (DMSO) was from Aldrich. Milli-Q grade water was used for the HPLC analyses and for photochemical experiments.

2,4,6-Triphenylthiapyrylium ($TPTP^+$) perchlorate was obtained from $TPP^+$ as described previously.[228] Briefly, a solution of $TPP^+$ (0.50 g) in acetone (23.6 mL) was treated with aqueous sodium sulfide (10% w/w, 1.97 mL) until the mixture turned red-coloured. Then, perchloric acid (20% w/w, 5.9 mL) and water (23.6 mL) were added to precipitate the $TPTP^+$ salt as a yellow powder. Then, the solid was filtered, washed with water and purified by re-precipitation from acetone-ether. $^1H$ (300 MHz, $CDCl_3$): δ (ppm) 7.67 (m, 9H); 8.04 (m, 6H); 8.75 (s, 2H), Figure 59.

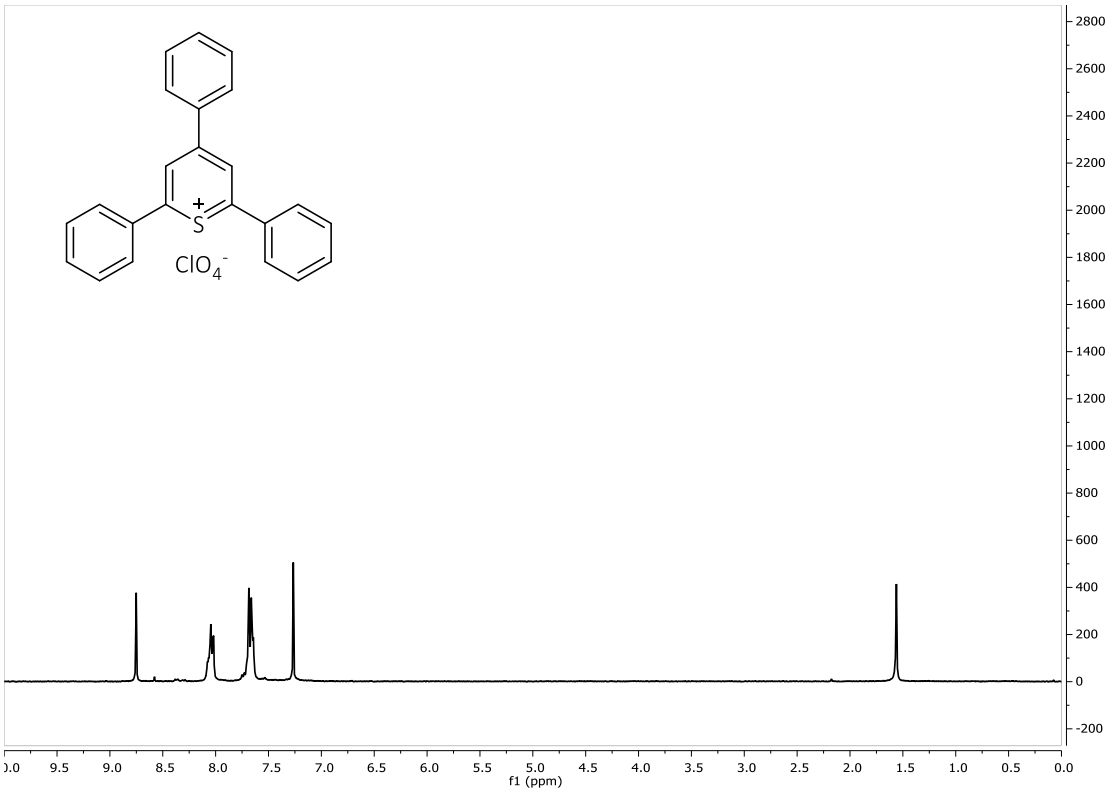


Figure 59: $^{1}H$ NMR of $TPTP^{+}ClO_4^{-}$

*N*-methylquinolinium tetrafluoroborate salt was obtained from quinoline (Aldrich) as described previously.[182, 229, 230] First, quinoline (0.42 mol, 49.6 mL) and methyl iodide (0.64 mol, 1.5 eq, 39.8 mL) were heated in a round bottom flask, at 65 °C, under reflux for 24 h, and the resulting solid (*N*-methylquinolinium iodide) was washed with ether. $^{1}H$ (300 MHz, $CD_3OD$): δ (ppm) 4.72 (s, 3H, $CH_3$); 8.09 (m, 2H); 8.31 (m, 1H); 8.45 (d, *J*=8.3 Hz, 1H); 8.53 (d, *J*=9.1 Hz, 1H); 9.23 (d, *J*=8.4 Hz, 1H); 9.40 (d, *J*=5.9 Hz, 1H), (Figure 60); $^{13}C$ NMR (75 MHz, $CD_3OD$): δ (ppm) 46.3, 119.8, 123.0, 131.3, 131.5, 131.8, 137.2, 140.4, 148.9, 151.1. The crude *N*-methylquinolinium iodide was treated with $BF_3{\cdot}Et_2O$ (2.6 eq) under nitrogen atmosphere. The mixture was stirred and heated at 50 °C under reflux for 2.5 h. An additional amount of $BF_3{\cdot}Et_2O$ was then added and the mixture was stirred for another 2.5 h. The resulting solid was washed with ether and recrystallized from ethanol to yield *N*-methylquinolinium tetrafluoroborate. $^{1}H$ (300 MHz, $CD_3OD$): δ (ppm) 4.70 (s, 3H, $CH_3$); 8.06 (m, 2H); 8.29 (m, 1H); 8.42 (d, *J*=8.2 Hz, 1H); 8.51 (d, *J*=9.0 Hz, 1H); 9.19 (d, *J*=8.5 Hz, 1H); 9.33 (d, J=5.6 Hz, 1H) (Figure 61); $^{13}C$ NMR (75 MHz, $CD_3OD$): δ (ppm) 46.2, 119.8, 122.9, 131.3, 131.4, 131.7, 137.2, 140.3, 148.8, 151.1.

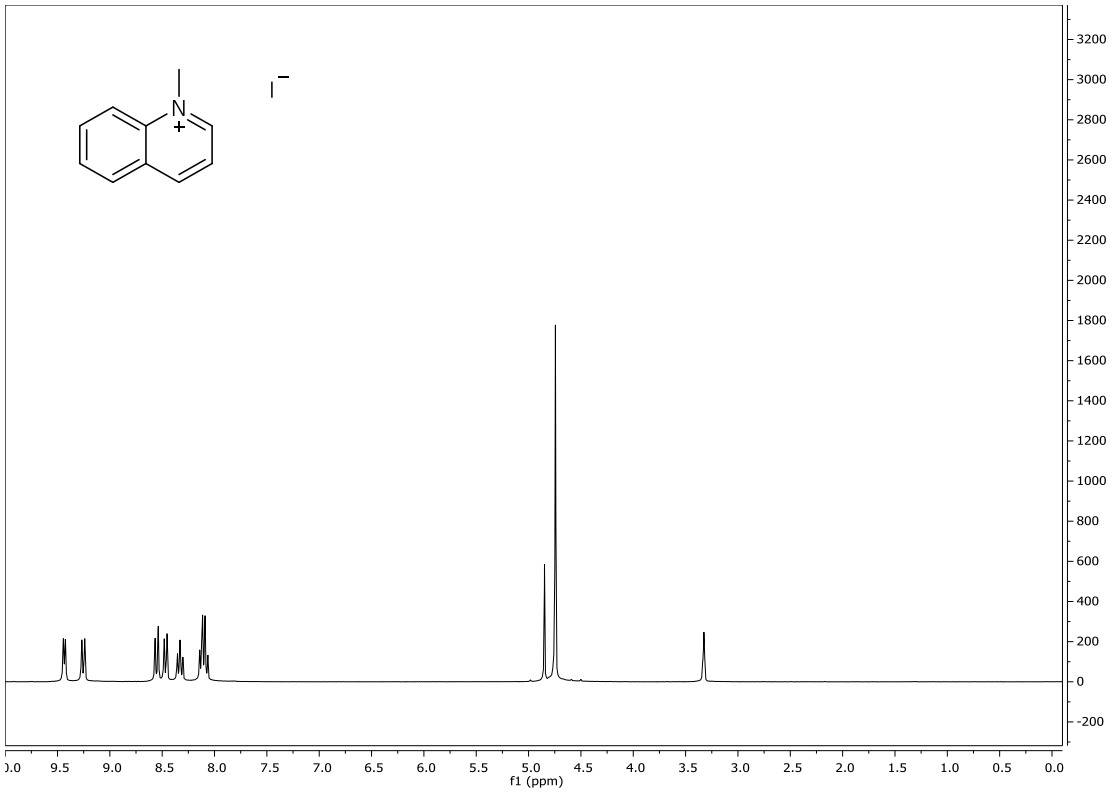


**Figure 60**: $^{1}H$ NMR of $NMQ^{+}\ I^{-}$.

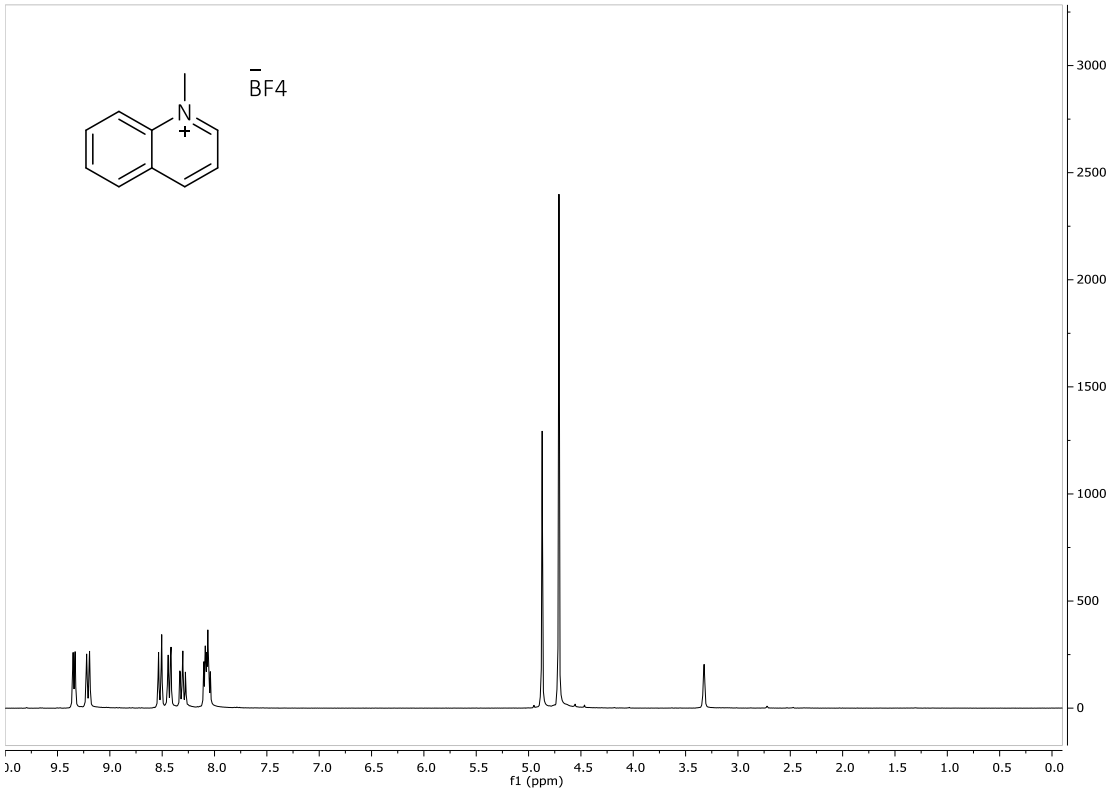


**Figure 61**: $^{1}H$ NMR of $NMQ^{+}\ BF_4^{-}$.

*N*-methylquinolinium tetrafluoroborate was adsorbed onto Y zeolite 100 according to a procedure described previously for other organic photocatalysts.[85] Briefly, Y-zeolite 100 (6.2 g) was suspended in 25 mL of an aqueous solution containing *N*-methylquinolinium tetrafluoroborate (1.0 g). The mixture was heated at 40 °C in the dark and stirred for 24 h. Then, the solid was filtered, washed with water (30 mL) and dried at 100 °C for 72 h. Elemental analysis indicated a loading of $NMQ^+$ on zeolite Y of 13.8% wt.

## 9.2. Equipment

### Solar simulator

A solar simulator from Oriel Instruments, Model 81160, equipped with a 300 W Xenon lamp (Figure 62) was used for the experiments described in chapters 4, 5 and 7.

A) B)

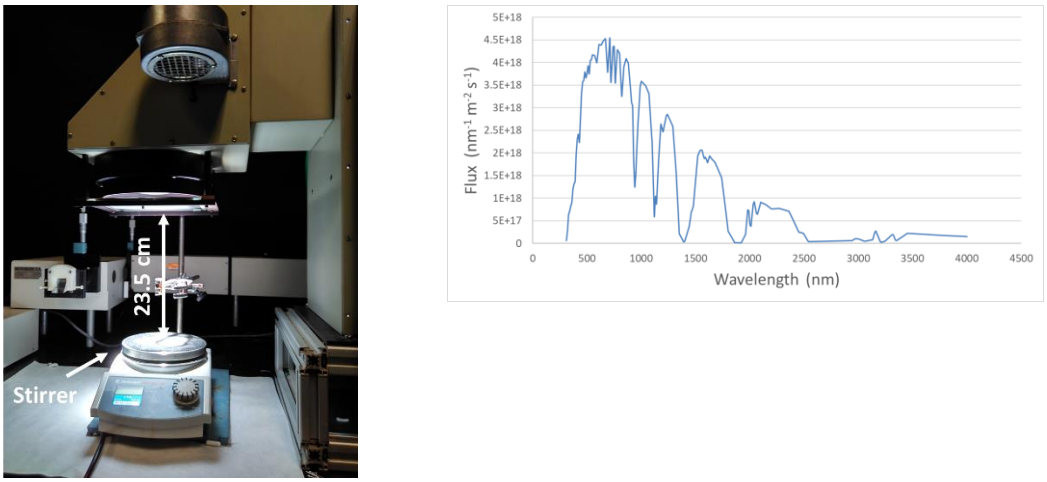


**Figure 62**: **(A)** Solar simulator from Oriel Instruments (Model 81160) equipped with a 300 W Xenon lamp. **(B)** Emission of the 300 W Xenon lamp.

### Photoreactors

Several photoreactors have been used:

- Luzchem photoreactor, model LZC-4V equipped with 12 lamps emitting at 350 nm in Chapter 7 and with 14 lamps emitting at 420 nm in Chapters 3 and 6, see Figure 63.

A)

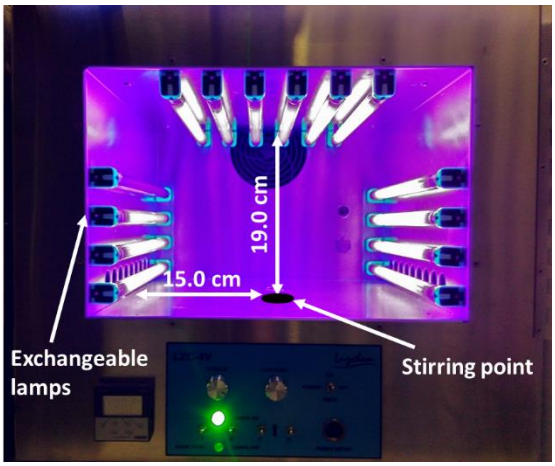


B)

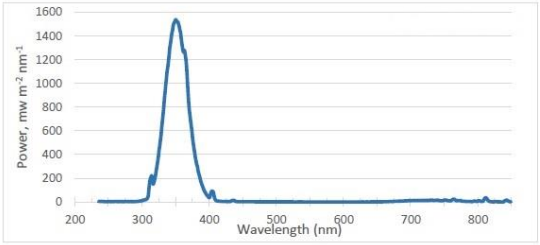


C)

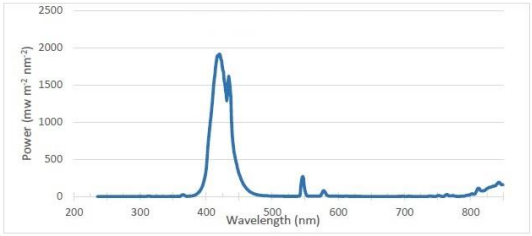


Figure 63: (A) Luzchem photoreactor, model LZC-4V equipped with 16 lamps positions and a stirring centered point. Emission spectrum of the 350 nm (B) and 420 nm (C) lamps.

- Home-made photoreactor built with a spiral set-up of 2.5 m strip green LEDs ($\lambda_{em}$ centered at 530 nm) Samsung SMD5630IP20 (40 W) in Chapter 6, see Figure 64.

A)

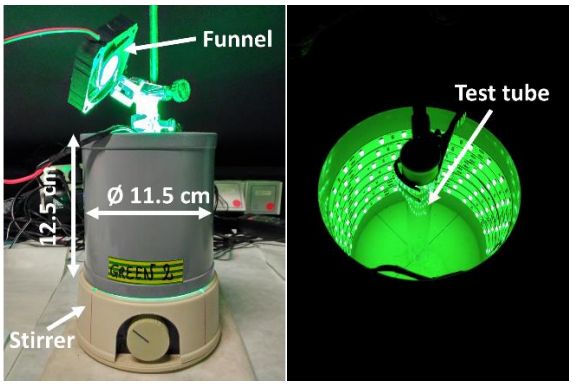


B)

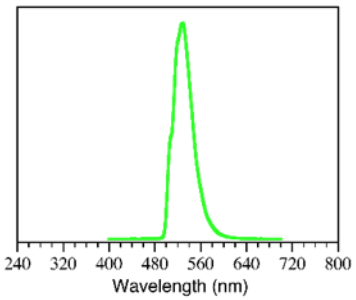


Figure 64: (A) Home-made 530 nm LED photoreactor, equipped with 2.5 m strip green LEDs (40 W Samsung SMD5630IP20). (B) Emission spectrum of the 530 nm LED.

- Home-made photoreactor built with two blue light emitting LEDs ($\lambda_{em}$ centered at 460 nm) centered at 460 nm in Chapter 8.

A)

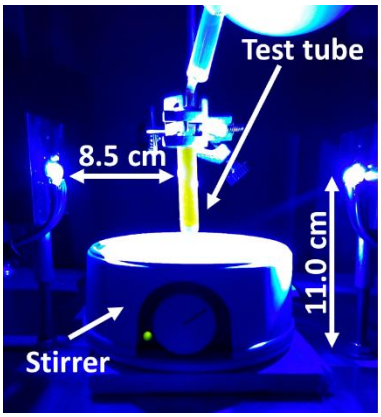


B)

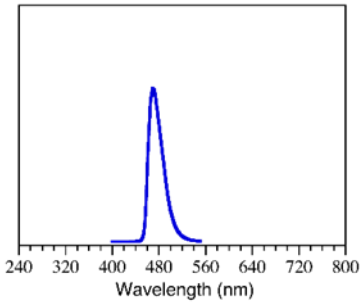


**Figure 65: (A)** Home-made 460 nm LED photoreactor, equipped with 2 blue LEDs. **(B)** Emission spectrum of the 460 nm LED.

<u>High pressure liquid chromatograph</u>

Several HPLC equipment have been used:

- Varian 240 model with quaternary pump 9012Q, photodiode detector DAD 9065 and wavelength detection from 200 to 360 nm was employed in Chapter 3.
- Agilent 1220 Infinity LC model with a quaternary pump G4290B, photodiode detector G4290B and wavelength detection from 200 to 360 nm was employed in Chapter 6.
- Agilent 1100 Series model with quaternary pump G1311A, photodiode detector DAD G1315B, standard liquid autosampler G1313A and degasser G1322A was employed in Chapter 7.
- Waters 600 C Chromatograph equipped with a Waters 600 Pump and Controller, a Waters in-Line degasser AF and a Waters 996 Photodiode Array Detector) was used in Chapter 8.

For all the above HPLC equipment a Teknokroma C18 Mediterranea Sea (25 × 0.46 cm and 5 μm particle size) analytical column was used as stationary phase

An UPLC equipment was used:

- Perkin Elmer model Flexar UPLC FX-10 equipped with a UV-Vis detector equipped with a Brownlee DB-C18 (100 x 4.6 mm and 3 μm particle size) analytical column as stationary phase was employed in Chapters 4 and 5.

### Gas chromatography

In Chapter 3, the GC equipment used was a Bruker instrument 430–GC equipped with a ZB50 (30 m × 0.25 mm × 0.5 μm) column with stationary phase of 5% of alternated phenylmethyl silicone.

### Elemental analysis

In Chapters 4 and 7 a EuroEA Elemental Analyser from EuroVector Instruments and Software was used.

### Cyclic voltammetry

Electrochemical measurements were carried out using a cylindrical three-electrode quartz cell on a VersaSTAT 3 (Princeton Applied Research) electrochemical workstation with a Pt wire counter electrode, a glassy carbon (GCE) working electrode, and a AgCl/Ag (sat KCl) or a AgCl/Ag (3 M NaCl) as the reference electrode for organic and aqueous measurements, respectively, in a one compartment electrochemical cell.

### Absorption measurements (UV/Vis)

Several UV/Vis spectrophotometers have been used:

- A Shimadzu UV-2101PC spectrophotometer was employed in Chapters 3, 4, 5, 7 and 8.
- A Cary 50 (Varian) spectrophotometer was employed in Chapter 6.
- A Cary 5000 from Agilent Technologies was used for the diffuse reflectance measurements of Chapter 7.

### Steady-state fluorescence

Several steady state fluorescence equipments were used:

- A FS900 fluorometer from Edinburgh Instruments was used in Chapters 3, 4 and 5.
- A Photon Technology International (PTI) LPS-220B spectrofluorometer was used in Chapters 7 and 8.

Time-resolved fluorescence

Several time-resolved fluorescence equipments were used:

- A FL900 setup from Edinburgh Instruments was used in Chapters 3, 4 and 5. Lifetime measurements were based on single-photon-counting using a 1.5 ns pulse width hydrogen flash-lamp as excitation source with light centred at 420 nm. The kinetic traces were fitted by monoexponential decay functions using a deconvolution procedure to separate them from the lamp pulse profile.
- A EasyLife V spectrofluorometer from OBB was used in Chapters 7 and 8. The apparatus was equipped with a diode LED excitation source ($\lambda_{exc}$ = 310 nm and 460 nm for chapters 7 and 8, respectively); residual excitation signal was filtered in emission by using a cut-off filter (50% transmission at 320 nm and 475 nm for chapters 7 and 8, respectively). The kinetic traces were fitted by monoexponential decay functions using a deconvolution procedure to separate them from the lamp pulse profile.

Laser flash photolysis (LFP)

Experiments were carried out with a pulsed Nd: YAG SL404G-10 Spectron Laser Systems at the excitation wavelength of 355 (Chapters 3 - 8) or 532 nm (Chapter 6). The energy of the single pulses (~10 ns duration) was lower than 15 mJ $pulse^{-1}$. The laser flash photolysis system consisted of the pulsed laser, a pulsed Lo255 Oriel Xenon lamp, a 77200 Oriel monochromator, an Oriel photomultiplier tube (PMT) housing, a 70705 PMT power supply and a TDS-640A Tektronix oscilloscope. The output signal from the oscilloscope was transferred to a personal computer.

Lifetime of singlet oxygen was recorded at 1270 nm with a Hamamatsu NIR emission detector upon excitation of the appropriate precursor with a 355 nm Nd:YAG laser.

## 9.3. Methods

### 9.3.1. General procedure for photodegradations

Photodegradation reactions were performed in Pyrex glass vessels with magnetic stirring using a solar simulator, a Luzchem photoreactor or with individual LED's as stated in each chapter, see section 9.2 for the equipment description.

Aliquots were taken at different irradiation times, then an internal standard was added, and the removal of the pollutants was monitored by HPLC or GC. For the HPLC analysis, mobile phase was a mixture of water pH 3 and acetonitrile at the ratio described in each chapter.

### 9.3.2. General procedure for $CO_2$ trapping

The mineralization was checked upon trapping the formed carbon dioxide as $BaCO_3$. For that purpose, an aqueous solution of the pollutant/s and the photocatalyst was irradiated using the solar simulator with stirring, with a continuous flow of oxygen. The evolved $CO_2$ was *in situ* trapped by bubbling it through a saturated solution of $Ba(OH)_2$, see Figure 66. The formed precipitate was submitted to elemental analysis.

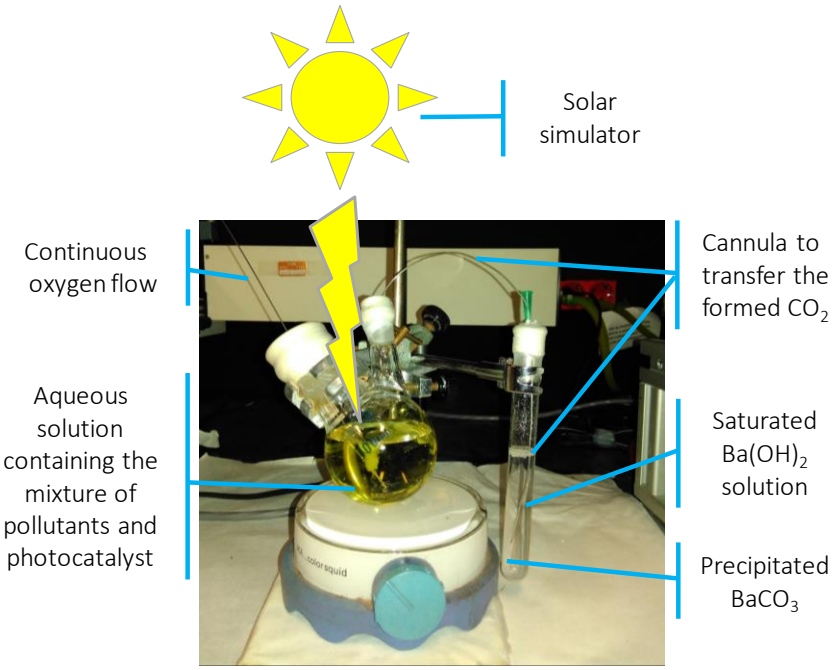


**Figure 66**: Set-up used to trap the evolved $CO_2$ from the reaction mixture as $BaCO_3$ upon bubbling through a saturated $Ba(OH)_2$ solution.

### 9.3.3. Redox potential measurements

Stock solutions (1 mM) of each compound were prepared in ACN. The cyclic voltammetries were carried out at room temperature, under a constant flux of $N_2$. The glassy carbon electrode, GCE, and the Pt electrodes were polished using diamond spray (particle size 0.05 μm) before each experiment. Measurements were carried out using solutions of 30 μM of each pollutant in 0.1 M aqueous phosphate buffer pH 7 for ACF, TCP and TCS or in 0.1 M tetrabutyl ammonium perchlorate (TBA) in ACN for TCA, ACP, CAF and CLOF. The speed for the measurements was fixed at 0.05 or 0.1 $V \cdot s^{-1}$. The obtained data from the AgCl/Ag (sat KCl) were converted into redox potential values *vs* SCE as follows: E (*vs* SCE, in V) = E (*vs* AgCl/Ag, in V) -0.045, while the obtained data from the AgCl/Ag (3 M NaCl) were converted into redox potential values *vs* SCE as E (*vs* SCE, in V) = E (*vs* AgCl/Ag, in V) -0.047.

### 9.3.4. Photophysical experiments

Quartz cells of 1 cm optical path length were employed for all photophysical measurements, which were run at room temperature.

For the steady-state and time-resolved fluorescence experiments, increasing volumes of quencher solution (up to 300 μL) were added to solutions of the photocatalyst (3 mL) prepared with absorbance 0.1-0.15 at the indicated irradiation wavelength. Subsequent mono-exponential fitting was applied to obtain the lifetime.

For the Job's plot experiments, a set of diluted mixtures (3mL) containing the photocatalyst (PC) and the quencher (Q) were prepared with total concentration of $10^{-5}$ M ([PC] + [Q] = $10^{-5}$ M). The first sample contained [PC] = $10^{-5}$ and [Q] = 0 M, then, several samples were prepared with different $X_Q$, up to reach a final sample with [PC] = 0 M and [Q] = $10^{-5}$ M. Next, absorbance spectra were recorded, and the measurement at an specific wavelength was multiplied by the specific concentration of Q from each sample. Finally, this value was represented *versus* the molar fraction of quencher, see Figure 14D.

For the laser flash photolysis experiments, increasing volumes (up to 300 μL) of quencher (at the concentration specified at each chapter), were added to 3 mL solutions of the photocatalyst (prepared at the concentration/absorbance specified at each

chapter) under $N_2$ atmosphere. The decays were recorded after each addition. Subsequent mono-exponential fitting was applied to obtain the lifetime.

### 9.3.5. Quantification of $^3(TPP^+)^*/TPP^\cdot$ procedure

Species quantification was carried out from the exponential decay fitting (EDF) of the traces recorded at 550 nm upon LFP excitation of $TPP^+$. In the absence of quencher, a monoexponential decay fitting was applied, see Eq. 31, while in the presence of quencher, two monoexponential terms were necessary to accurately fit the decay trace, Eq. 32.[231]

$$\text{Eq. 31: EDF 1: } \Delta A = A_T \cdot e^{-t/\tau_T} + \Delta A_0$$

$$\text{Eq. 32: EDF 2: } \Delta A = A_T \cdot e^{-t/\tau_T} + A_R \cdot e^{-t/\tau_R} + \Delta A_0$$

Where, mathematically, $\Delta A_0$ is the offset, $\tau$ is the time constant and $\Delta A$ is the amplitude. When analysing transient absorption spectra, $\tau_T$ corresponds to the lifetime of the triplet excited state and $\tau_R$ to that of the radical; $A_T$ represents the population of excited states decaying with a specific lifetime ($\tau_T$) and $A_R$ represents the population of radicals decaying with a specific lifetime ($\tau_R$).

Calculation of $A_T$ and $A_R$ values procedure was as follows:

- The trace recorded at 550 nm with [Q] = 0 M corresponds to the triplet excited state, therefore it was fitted according to an EDF 1, obtaining the corresponding amplitude ($A_{T\,0M}$) and the lifetime of $^3(TPP^+)^*$ ($\tau_{T\,0mM}$, this value must be around 5.5 μs, see Table 1 at Preamble of Part I), see Figure 67.

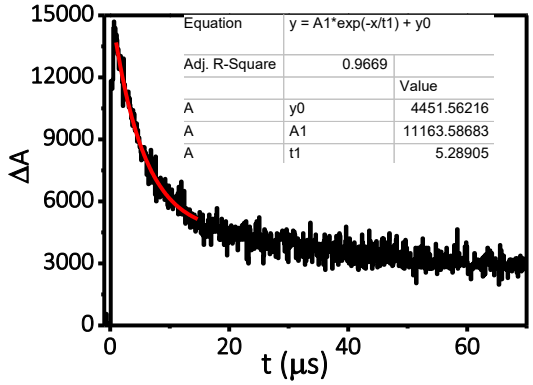


**Figure 67**: Kinetic trace recorded at 550 nm, obtained upon LFP excitation ($\lambda_{exc}$ = 355 nm) of deaerated acetonitrile solutions of $TPP^+$ (7 x $10^{-5}$ M) and its corresponding fitting according to EDF 1.

- The traces recorded at 550 nm with [Q] = 7 x $10^{-5}$ M (maximum concentration used), where both remaining species (triplet and radical) may be present, were fitted according to EDF 2, obtaining the corresponding amplitudes ($A_{T\ 0.07mM}$ and $A_{R\ 0.07mM}$) and the lifetimes of $^3(TPP^+)^*$ and $TPP^{\cdot}$ ($\tau_{T\ 0.07M}$ and $\tau_R$). The values of $\tau_R$ were 35 – 35.9 μs in all cases and these values were fixed for the rest of the intermediate concentration fittings. See Figure 68 as an example with CAF.

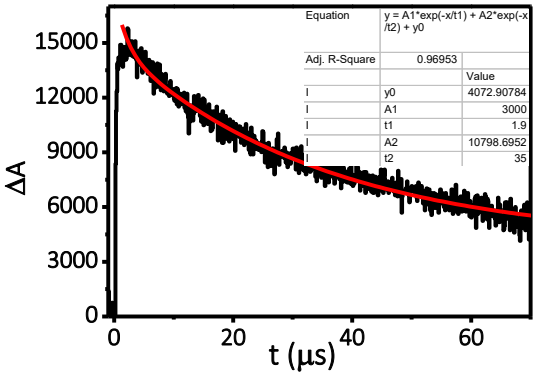


**Figure 68**: Kinetic trace recorded at 550 nm, obtained upon LFP excitation ($\lambda_{exc}$ = 355 nm) of deaerated acetonitrile solutions of $TPP^+$ (7 x $10^{-5}$ M) in the presence of CAF (7 x $10^{-5}$ M) and its corresponding fitting according to EDF 2.

- The decay traces recorded at 550 nm with the intermediate concentrations of quencher were then fitted according to EDF 2, obtaining the corresponding

amplitudes ($A_{T\ xM}$ and $A_{R\ xM}$). The radical lifetime value ($\tau_R$) was manually fixed in the fitting, using the same value than in the previous step, see Figure 69 as an example with CAF.

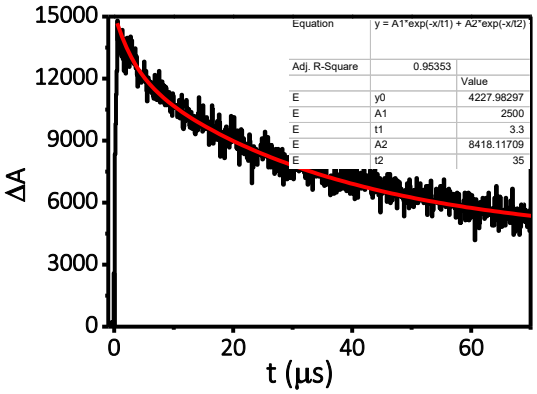


**Figure 69**: Kinetic trace recorded at 550 nm, obtained upon LFP excitation ($\lambda_{exc}$ = 355 nm) of deaerated acetonitrile solutions of $TPP^+$ ($7.0 \times 10^{-5}$ M) in the presence of CAF ($2.5 \times 10^{-5}$ M) and its corresponding EDF 2.

- An extra support for the $\tau_T$ values found at each intermediate concentration was obtained from the corresponding Stern-Volmer fittings. With all the found lifetimes values of the triplet excited state ($\tau_T$) at each concentration, a Stern – Volmer adjustment was plotted. When these fittings exhibited a $R^2 > 0.92$, the values were considered confident enough, and the corresponding amplitude values ($A_T$ and $A_R$) were used. In case that the $R^2 < 0.92$, the lifetimes ($\tau_T$) in the EDF 2 were manually re-adjusted, obtaining new amplitude values. As criteria, the EDF 2 was also considered only if its $R^2 > 0.92$. This readjustment was made as many times as necessary until reaching the desired $R^2$ minimum in both, the EDF 2 and Stern – Volmer fittings. In the case of ACP, in which quenching is inefficient, an $R^2 = 0.87$ was accepted in the Stern Volmer fitting, see Figure 70 as an example of the Stern – Volmer fitting obtained with the EDF values for the case of CAF.

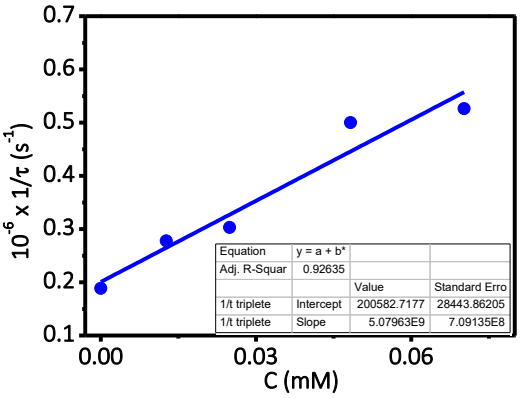


**Figure 70**: Stern – Volmer adjustment obtained with the lifetimes obtained with EDF 1 and EDF 2 of the traces of CAF.

Once the $A_T$ and $A_R$ were obtained, relative contribution of each species was calculated as indicated at Eq. 33 and Eq. 34 and plotted in Figure 25 at Chapter 3.

**Eq. 33**: $$RELATIVE\ TRIPLET\ POPULATION = \frac{A_T}{A_T + A_R}$$

**Eq. 34**: $$RELATIVE\ RADICAL\ POPULATION = \frac{A_R}{A_T + A_R}$$

# 10. Conclusions

This Doctoral Thesis explores several photocatalytic processes which look forward to both environmental and chemical applications. The final conclusions of each part can be summarized as follows:

## Part I: Oxidative Electron Transfer Processes:

1. $TPP^+$ and $TPTP^+$ are efficient photocatalysts in the treatment of two real pollutants resulting from to the cork industry:
   - In fact, removal of GA photocatalyzed by $TP(T)P^+$ is fast, while TCA is more reluctant, in good agreement with the thermodynamic calculations.
   - For the case of GA, electron transfer to the triplet excited state of the photocatalysts has been demonstrated by photophysical experiments.
   - In the case of TCA, formation of a ground state complex is the only operating mechanism.
2. Organic photocatalysts such as $TPP^+$ allow monitoring all the short-lived intermediates in a photoredox process providing valuable mechanistic data.
   - Time-resolved fluorescence measurements demonstrate the participation of $^1(TPP^+)^*$; besides, laser flash photolysis experiments give parallel information on $^3(TPP^+)^*$. Those experiments reveal that the oxidation of the selected pollutants (ACF, ACP, CAF and CBZ) is concomitant with the $TPP^+$ reduction, therefore with the formation of pyranyl radical ($TPP^{\cdot}$).
   - The detection of the reduced photocatalyst ($TPP^{\cdot}$) by laser flash photolysis is a fingerprint of the redox nature of the photodegradation process.
3. From the results obtained using $TPTP^+$ as photocatalyst in the abatement of ACF, ACP, CAF, CBZ and CLOF, general conclusions on the features that an ideal photocatalyst should fulfill could be stated:
   - It should absorb in the visible region.
   - It should have appropriate redox potential from its excited states.
   - Its intersystem crossing quantum yield should be high.
   - The lifetime of its triplet excited state should be long.

4. From the results obtained using $TPTP^+$ as photocatalyst in the abatement of ACF, ACP, CAF, CBZ and CLOF, two different scenarios to treat an industrial effluent can be found:

- In the source of the production of the waste, when the concentration of the pollutants is the highest, because the efficiency of a photocatalytic treatment is the best.
- Once the effluent reaches an open area, and the concentration of the pollutants has decreased, because although the efficiency of the triplets is low, natural sunlight becomes an inexpensive illumination source.

### Part II: Type I *vs* Type II processes:

1. Experimental results highlight the importance of performing a careful mechanistic study to clarify the role of each potential pathway when more than one is, in principle, possible.
2. Triplet excited states of RB and PN, are efficiently quenched by DCF and ACF and also by oxygen with diffusion-controlled constants.
3. $^1O_2$ is inefficiently quenched by selected drugs as expected from typical reactivity of $^1O_2$ with organic substances.
4. The same is true for $NMQ^+$, an example of photocatalyst with high redox potential and also able to produce $^1O_2$, from the singlet excited state.
5. Therefore, photocatalysts capable of forming singlet oxygen even with a low oxidation potential are in general acting as efficient Type I oxidants from their excited states, contributing eventually this pathway more than Type II in the photodegradation.

### Part III: Reductive Electron Transfer Processes:

1. Time-resolved techniques provide useful data to analyse the kinetic feasibility of the thermodynamically allowed pathways in the photocatalytic reduction of several halides mediated by RF.
2. Kinetics of the $RF^{\bullet-}$ in the presence of the bromides are in agreement with the thermodynamic calculations and demonstrate the key role of this intermediate.
3. Therefore, the employed methodology provides a deep understanding of the overall mechanism for the photocatalytic reduction of halides.

# 11. Bibliography

[1] G. Ciamician, The photochemistry of the future, Science, 36 (1912) 385-394.

[2] J. Bourdelande, S. Nonell, A. Acuña, R. Sastre, J. Verhoeven, Glosario de términos usados en fotoquímica, Pure & Appl. Chem, 68 (1996) 2223-2286.

[3] N.J. Turro, V. Ramamurthy, J.C. Scaiano, Modern molecular photochemistry of organic molecules, Wiley Online Library, 2012.

[4] I. Tinoco, Jr., K. Sauer, J.C. Wang, Physical Chemistry : Principles and Applications in Biological Sciences, 3rd Edition, Prentice Hall1995.

[5] D.L. Dexter, A theory of sensitized luminescence in solids, J. Chem. Phys., 21 (1953) 836-850.

[6] S.P. Pitre, C.D. McTiernan, J.C. Scaiano, Understanding the Kinetics and Spectroscopy of Photoredox Catalysis and Transition-Metal-Free Alternatives, Acc. Chem. Res., 49 (2016) 1320-1330.

[7] D. Rehm, A. Weller, Kinetics of fluorescence quenching by electron and H-atom transfer, Isr. J. Chem., 8 (1970) 259-271.

[8] H.A. Benesi, J.H. Hildebrand, A spectrophotometric investigation of the interaction of iodine with aromatic hydrocarbons, J. Am. Chem. Soc., 71 (1949) 2703-2707.

[9] S. Nigam, G. Durocher, Spectral and photophysical studies of inclusion complexes of some neutral 3H-indoles and their cations and anions with beta-cyclodextrin, J. Phys. Chem., 100 (1996) 7135-7142.

[10] S.P. Pitre, C.D. McTiernan, J.C. Scaiano, Library of Cationic Organic Dyes for Visible-Light-Driven Photoredox Transformations, ACS Omega, 1 (2016) 66-76.

[11] N.A. Romero, D.A. Nicewicz, Organic Photoredox Catalysis, Chem. Rev., 116 (2016) 10075-10166.

[12] D. Ravelli, D. Dondi, M. Fagnoni, A. Albini, Photocatalysis. A multi-faceted concept for green chemistry, Chem. Soc. Rev., 38 (2009) 1999-2011.

[13] A. Fenwick, Waterborne infectious diseases—could they be consigned to history?, Science, 313 (2006) 1077-1081.

[14] M.J. Gil, A.M. Soto, J.I. Usma, O.D. Gutiérrez, Contaminantes emergentes en aguas, efectos y posibles tratamientos, Producción+ limpia, 7 (2013).

[15] C.G. Daughton, Non-regulated water contaminants: emerging research, Environmental Impact Assessment Review, 24 (2004) 711-732.

[16] D. Barceló, M.J. López, Contaminación y calidad química del agua: el problema de los contaminantes emergentes, Jornadas de presentación de resultados: el estado ecológico de las masas de agua. Panel científico-técnico de seguimiento de la política de aguas, Sevilla, (2008).

[17] M. Stuart, D. Lapworth, E. Crane, A. Hart, Review of risk from potential emerging contaminants in UK groundwater, Sci. Total Environ., 416 (2012) 1-21.

[18] K. Fent, A.A. Weston, D. Caminada, Ecotoxicology of human pharmaceuticals, Aquat. Toxicol., 76 (2006) 122-159.

[19] K. Kümmerer, Drugs in the environment: emission of drugs, diagnostic aids and disinfectants into wastewater by hospitals in relation to other sources–a review, Chemosphere, 45 (2001) 957-969.

[20] N. Watanabe, B.A. Bergamaschi, K.A. Loftin, M.T. Meyer, T. Harter, Use and environmental occurrence of antibiotics in freestall dairy farms with manured forage fields, Environ. Sci. Technol., 44 (2010) 6591-6600.

[21] C.G. Daughton, Non-regulated water contaminants: emerging research, Environmental Impact Assessment Review, 24 (2004) 711-732.

[22] C.G. Daughton, T.A. Ternes, Pharmaceuticals and personal care products in the environment: agents of subtle change?, Environ. Health Perspect., 107 (1999) 907.

[23] M. Trojanowicz, A. Bojanowska-Czajka, A.G. Capodaglio, Can radiation chemistry supply a highly efficient AO(R)P process for organics removal from drinking and waste water? A review, Environ. Sci. Poll. Res., 24 (2017) 20187-20208.

[24] S. Malato, P. Fernandez-Ibanez, M.I. Maldonado, J. Blanco, W. Gernjak, Decontamination and disinfection of water by solar photocatalysis: Recent overview and trends, Catal. Today, 147 (2009) 1-59.

[25] M. Petrović, S. Gonzalez, D. Barceló, Analysis and removal of emerging contaminants in wastewater and drinking water, TrAC, 22 (2003) 685-696.

[26] W.H. Glaze, J.W. Kang, D.H. Chapin, The chemistry of water treatment processes involving ozone, hydrogen peroxide and ultraviolet radiation, Ozone: Sci. Eng., 9 (1987) 335-352.

[27] Y. Deng, R. Zhao, Advanced Oxidation Processes (AOPs) in Wastewater Treatment, Curr. Pollution Rep., 1 (2015) 167-176.

[28] F.J. Beltran, M. Gonzalez, J.F. Gonzalez, Industrial wastewater advanced oxidation .1. UV radiation in the presence and absence of hydrogen peroxide, Water Research, 31 (1997) 2405-2414.

[29] C.L.J.A.S.A. Gottschalk, Ozonation of water and wastewater, Weinheim, 2000.

[30] S.J. Masten, S.H.R. Davies, The Use of Ozonation to Degrade Organic Contaminants in Wastewaters, Environ. Sci. Technol., 28 (1994) A180-A185.

[31] S. Imamura, Catalytic and noncatalytic wet oxidation, Ind. Eng. Chem. Res., 38 (1999) 1743-1753.

[32] K.E. O'Shea, D.D. Dionysiou, Advanced Oxidation Processes for Water Treatment, J. Phys. Chem. Lett., 3 (2012) 2112-2113.

[33] H.K. Shon, S. Vigneswaran, S.A. Snyder, Effluent organic matter (EfOM) in wastewater: Constituents, effects, and treatment, Crit. Rev. Env. Sci. Technol., 36 (2006) 327-374.

[34] C. Comninellis, A. Kapalka, S. Malato, S.A. Parsons, L. Poulios, D. Mantzavinos, Advanced oxidation processes for water treatment: advances and trends for R&D, J. Chem. Technol. Biotechnol., 83 (2008) 769-776.

[35] P.R. Gogate, A.B. Pandit, A review of imperative technologies for wastewater treatment I: oxidation technologies at ambient conditions, Adv. Environ. Res., 8 (2004) 501-551.

[36] O. Legrini, E. Oliveros, A.M. Braun, Photochemical Processes for Water-Treatment, Chem. Rev., 93 (1993) 671-698.

[37] T. Openländer, Photochemical purification of water and air. Advanced oxidation processes: Principles, Reaction Mechanisms, Reactor concepts, Wiley, V. C. H., Weinheim, 2003.

[38] M. Fagnoni, D. Dondi, D. Ravelli, A. Albini, Photocatalysis for the formation of the C-C bond, Chem. Rev., 107 (2007) 2725-2756.

[39] G. Palmisano, V. Augugliaro, M. Pagliaro, L. Palmisano, Photocatalysis: a promising route for 21st century organic chemistry, Chem. Commun., (2007) 3425-3437.

[40] H.D. Burrows, M. Canle L, J.A. Santaballa, S. Steenken, Reaction pathways and mechanisms of photodegradation of pesticides, J. Photoch. Photobio. B, 67 (2002) 71-108.

[41] R. Munter, Advanced oxidation processes–current status and prospects, Proc. Estonian Acad. Sci. Chem, 50 (2001) 59-80.

[42] I.K. Konstantinou, T.A. Albanis, TiO2-assisted photocatalytic degradation of azo dyes in aqueous solution: kinetic and mechanistic investigations: A review, Appl. Catal. B, 49 (2004) 1-14.

[43] H.M.K.K. Pathirana, R.A. Maithreepala, Photodegradation of 3,4-dichloropropionamide in aqueous TiO2 suspensions, J. Photochem. Photobiol., A, 102 (1997) 273-277.

[44] E. Moctezuma, E. Leyva, E. Monreal, N. Villegas, D. Infante, Photocatalytic degradation of the herbicide “Paraquat”, Chemosphere, 39 (1999) 511-517.

[45] J.P. Percherancier, R. Chapelon, B. Pouyet, Semiconductor-sensitized photodegradation of pesticides in water: the case of carbetamide, J. Photochem. Photobiol., A, 87 (1995) 261-266.

[46] A.B. Prevot, E. Pramauro, M. de la Guardian, Photocatalytic degradation of carbaryl in aqueous TiO2 suspensions containing surfactants, Chemosphere, 39 (1999) 493-502.

[47] K. Tanaka, S.M. Robledo, T. Hisanaga, R. Ali, Z. Ramli, W.A. Bakar, Photocatalytic degradation of 3,4-xylyl N-methylcarbamate (MPMC) and other carbamate pesticides in aqueous TiO2 suspensions, J. Mol. Catal. A: Chem., 144 (1999) 425-430.

[48] M. Sturini, E. Fasani, C. Prandi, A. Casaschi, A. Albini, Titanium dioxide-photocatalysed decomposition of some thiocarbamates in water, J. Photochem. Photobiol., A, 101 (1996) 251-255.

[49] R.-S. Juang, C.-H. Chen, Comparative study on photocatalytic degradation of methomyl and parathion over UV-irradiated TiO2 particles in aqueous solutions, J. Taiwan Inst. Chem. Eng., 45 (2014) 989-995.

[50] H. Wamhoff, V. Schneider, Photodegradation of imidacloprid, J. Agric. Food Chem., 47 (1999) 1730-1734.

[51] R. Žabar, T. Komel, J. Fabjan, M.B. Kralj, P. Trebše, Photocatalytic degradation with immobilised TiO2 of three selected neonicotinoid insecticides: Imidacloprid, thiamethoxam and clothianidin, Chemosphere, 89 (2012) 293-301.

[52] R. Hazime, C. Ferronato, L. Fine, A. Salvador, F. Jaber, J.-M. Chovelon, Photocatalytic degradation of imazalil in an aqueous suspension of TiO2 and influence of alcohols on the degradation, Appl. Catal. B, 126 (2012) 90-99.

[53] J. Tseng, C. Huang, Removal of chlorophenols from water by photocatalytic oxidation, Wat. Sci. Tech., 23 (1991) 377-387.

[54] C. Guillard, J. Disdier, J.-M. Herrmann, C. Lehaut, T. Chopin, S. Malato, J. Blanco, Comparison of various titania samples of industrial origin in the solar photocatalytic detoxification of water containing 4-chlorophenol, Catal. Today, 54 (1999) 217-228.

[55] A. Topalov, D. Molnar-Gabor, M. Kosanić, B. Abramović, Photomineralization of the herbicide mecoprop dissolved in water sensitized by TiO2, Water research, 34 (2000) 1473-1478.

[56] E. Diaz, M. Cebrian, A. Bahamonde, M. Faraldos, A.F. Mohedano, J.A. Casas, J.J. Rodriguez, Degradation of organochlorinated pollutants in water by catalytic hydrodechlorination and photocatalysis, Catal. Today, 266 (2016) 168-174.

[57] D. Chen, A.K. Ray, Photodegradation kinetics of 4-nitrophenol in TiO2 suspension, Water Research, 32 (1998) 3223-3234.

[58] A. Vidal, Developments in solar photocatalysis for water purification, Chemosphere, 36 (1998) 2593-2606.

[59] A. Zaleska, J. Hupka, M. Wiergowski, M. Biziuk, Photocatalytic degradation of lindane, p, p'-DDT and methoxychlor in an aqueous environment, J. Photochem. Photobiol., A, 135 (2000) 213-220.

[60] I.K. Konstantinou, T.M. Sakellarides, V.A. Sakkas, T.A. Albanis, Photocatalytic degradation of selected s-triazine herbicides and organophosphorus insecticides over aqueous TiO2 suspensions, Environ. Sci. Technol., 35 (2001) 398-405.

[61] A. Sanjuan, G. Aguirre, M. Alvaro, H. Garcia, J.C. Scaiano, Degradation of propoxur in water using 2,4,6-triphenylpyrylium-Zeolite Y as photocatalyst - Product study and laser flash photolysis, Appl. Catal. B, 25 (2000) 257-265.

[62] L. Muszkat, L. Bir, L. Feigelson, Solar photocatalytic mineralization of pesticides in polluted waters, J. Photochem. Photobiol., A, 87 (1995) 85-88.

[63] M. Kerzhentsev, C. Guillard, J.-M. Herrmann, P. Pichat, Photocatalytic pollutant removal in water at room temperature: case study of the total degradation of the insecticide fenitrothion (phosphorothioic acid O, O-dimethyl-O-(3-methyl-4-nitro-phenyl) ester), Catal. Today, 27 (1996) 215-220.

[64] R.-a. Doong, W.-h. Chang, Photoassisted titanium dioxide mediated degradation of organophosphorus pesticides by hydrogen peroxide, J. Photochem. Photobiol., A, 107 (1997) 239-244.

[65] Y. Ku, I.-L. Jung, Decomposition of monocrotophos in aqueous solution by UV irradiation in the presence of titanium dioxide, Chemosphere, 37 (1998) 2589-2597.

[66] V.G.G. Kanmoni, S. Daniel, G.A.G. Raj, Photocatalytic degradation of chlorpyrifos in aqueous suspensions using nanocrystals of ZnO and TiO2, React. Kinet. Mech. Cat., 106 (2012) 325-339.

[67] A. Aguera, E. Almansa, A. Tejedor, A.R. Fernandez-Alba, S. Malato, M.I. Maldonado, Photocatalytic pilot scale degradation study of pyrimethanil and of its main degradation products in waters by means of solid-phase extraction followed by gas and liquid chromatography with mass spectrometry detection, Environ. Sci. Technol., 34 (2000) 1563-1571.

[68] J. Fenoll, P. Sabater, G. Navarro, G. Pérez-Lucas, S. Navarro, Photocatalytic transformation of sixteen substituted phenylurea herbicides in aqueous semiconductor suspensions: intermediates and degradation pathways, J. Hazard. Mater., 244 (2013) 370-379.

[69] P.A.K. Reddy, B. Srinivas, V. Durgakumari, M. Subrahmanyam, Solar photocatalytic degradation of the herbicide isoproturon on a Bi–TiO2/zeolite photocatalyst, Toxicol. Environ. Chem., 94 (2012) 512-524.

[70] M.L. Marin, L. Santos-Juanes, A. Arques, A.M. Amat, M.A. Miranda, Organic photocatalysts for the oxidation of pollutants and model compounds, Chem. Rev., 112 (2012) 1710-1750.

[71] A. Galadi, M. Julliard, Photosensitized oxidative degradation of pesticides, Chemosphere, 33 (1996) 1-15.

[72] A. Galadi, H. Bitar, M. Chanon, M. Julliard, Photosensitized reductive dechlorination of chloroaromatic pesticides, Chemosphere, 30 (1995) 1655-1669.

[73] G. Durand, D. Barceló, J. Albaigés, M. Mansour, Utilisation of liquid chromatography in aquatic photodegradation studies of pesticides: A comparison between distilled water and seawater, Chromatographia, 29 (1990) 120-124.

[74] D. Barcelo, G. Durand, N. De Bertrand, Photodegradation of the organophosphorus pesticides chlorpyrifos, fenamiphos and vamidothion in water, Toxicol. Environ. Chem., 38 (1993) 183-199.

[75] M. Kamiya, K. Kameyama, Photochemical effects of humic substances on the degradation of organophosphorus pesticides, Chemosphere, 36 (1998) 2337-2344.

[76] K. Hustert, P. Moza, A. Kettrup, Photochemical degradation of carboxin and oxycarboxin in the presence of humic substances and soil, Chemosphere, 38 (1999) 3423-3429.

[77] C. Rering, K. Williams, M. Hengel, R. Tjeerdema, Comparison of direct and indirect photolysis in imazosulfuron photodegradation, J. Agric. Food Chem., 65 (2017) 3103-3108.

[78] A. Amarathunga, F. Kazama, Photodegradation of chlorpyrifos with humic acid-bound suspended matter, J. Hazard. Mater., 280 (2014) 671-677.

[79] M.D. Dave, U. Pande, Photoinduced electron transfer reaction of 2-mercaptobenzothiazole and methylene blue: Mechanism and kinetics, J. Indian Chem. Soc., 91 (2014) 2217-2226.

[80] F. Cermola, M. DellaGreca, M.R. Iesce, S. Montella, A. Pollio, F. Temussi, A mild photochemical approach to the degradation of phenols from olive oil mill wastewater, Chemosphere, 55 (2004) 1035-1041.

[81] E. Marais, R. Klein, E. Antunes, T. Nyokong, Photocatalysis of 4-nitrophenol using zinc phthalocyanine complexes, J. Mol. Catal. A, 261 (2007) 36-42.

[82] M.A. Miranda, F. Galindo, A.M. Amat, A. Arques, Pyrylium salt-photosensitized degradation of phenolic contaminants derived from cinnamic acid with solar light: Correlation of the observed reactivities with fluorescence quenching, Appl. Catal. B, 28 (2000) 127-133.

[83] M. Nowakowska, M. Sterzel, S. Zapotoczny, E. Kot, Photosensitized degradation of ethyl parathion pesticide in aqueous solution of anthracene modified photoactive dextran, Appl. Catal. B, 57 (2005) 1-8.

[84] J.P. Escalada, A. Pajares, J. Gianotti, W.A. Massad, S. Bertolotti, F. Amat-Guerri, N.A. Garcia, Dye-sensitized photodegradation of the fungicide carbendazim and related benzimidazoles, Chemosphere, 65 (2006) 237-244.

[85] A. Arques, A.M. Amat, L. Santos-Juanes, R.F. Vercher, M.L. Marin, M.A. Miranda, Abatement of methidathion and carbaryl from aqueous solutions using organic photocatalysts, Catal. Today, 144 (2009) 106-111.

[86] M.A. Miranda, H. Garcia, 2,4,6-Triphenylpyrylium tetrafluoroborate as an electron-transfer photosensitizer, Chem. Rev., 94 (1994) 1063-1089.

[87] M.C. DeRosa, R.J. Crutchley, Photosensitized singlet oxygen and its applications, Coordin. Chem. Rev., 233 (2002) 351-371.

[88] M.S. Baptista, J. Cadet, P. Di Mascio, A.A. Ghogare, A. Greer, M.R. Hamblin, C. Lorente, S.C. Nunez, M.S. Ribeiro, A.H. Thomas, M. Vignoni, T.M. Yoshimura, Type I and Type II Photosensitized Oxidation Reactions: Guidelines and Mechanistic Pathways, Photochem. Photobiol., 93 (2017) 912-919.

[89] C.S. Foote, Definition of Type I and Type II photosensitized oxidation, Photochem. Photobiol., 54 (1991) 659-659.

[90] T. Vidòczy, Type I and type II photosensitized reactions: reasons for dispute, J. Photochem. Photobio. B, 14 (1992) 139-142.

[91] B.P. Vellanki, B. Batchelor, A. Abdel-Wahab, Advanced reduction processes: a new class of treatment processes, Environ. Eng. Sci., 30 (2013) 264-271.

[92] S.V. Makarov, Recent trends in the chemistry of sulfur-containing reducing agents, Russ. Chem. Rev., 70 (2001) 885-895.

[93] O.P. Chawla, N.L. Arthur, R.W. Fessenden, Electron spin resonance study of the photolysis of aqueous sulfite solutions, J. Phys. Chem. B, 77 (1973) 772-776.

[94] R. Devonshire, J.J. Weiss, Nature of the transient species in the photochemistry of negative ions in aqueous solution, J. Phys. Chem. B, 72 (1968) 3815-3820.

[95] L. Dogliotti, E. Hayon, Flash photolysis study of sulfite, thiocyanate, and thiosulfate ions in solution, J. Phys. Chem. B, 72 (1968) 1800-1807.

[96] Y.-H. Kim, E.R. Carraway, Dechlorination of Pentachlorophenol by Zero Valent Iron and Modified Zero Valent Irons, Environ. Sci. Technol., 34 (2000) 2014-2017.

[97] F. Fu, D.D. Dionysiou, H. Liu, The use of zero-valent iron for groundwater remediation and wastewater treatment: A review, J. Hazard. Mater., 267 (2014) 194-205.

[98] M. Trojanowicz, A. Bojanowska-Czajka, I. Bartosiewicz, K. Kulisa, Advanced Oxidation/Reduction Processes treatment for aqueous perfluorooctanoate (PFOA) and perfluorooctanesulfonate (PFOS) – A review of recent advances, Chem. Eng. J., 336 (2018) 170-199.

[99] H. Yu, E. Nie, J. Xu, S. Yan, W.J. Cooper, W. Song, Degradation of Diclofenac by Advanced Oxidation and Reduction Processes: Kinetic Studies, Degradation Pathways and Toxicity Assessments, Water Research, 47 (2013) 1909-1918.

[100] G.V. Buxton, C.L. Greenstock, W.P. Helman, A.B. Ross, Critical review of rate constants for reactions of hydrated electrons, hydrogen atoms and hydroxyl radicals (· OH/· O− in aqueous solution, J. Phys. Chem. Ref. Data, 17 (1988) 513-886.

[101] G. Moussavi, M. Mahdavianpour, The selective direct oxidation of ammonium in the contaminated water to nitrogen gas using the chemical-less VUV photochemical continuous-flow reactor, Chem. Eng. J., 295 (2016) 57-63.

[102] G. Moussavi, M. Rezaei, Exploring the advanced oxidation/reduction processes in the VUV photoreactor for dechlorination and mineralization of trichloroacetic acid: Parametric experiments, degradation pathway and bioassessment, Chem. Eng. J., 328 (2017) 331-342.

[103] M.L. Marin, V. Lhiaubet-Vallet, L. Santos-Juanes, J. Soler, J. Gomis, A. Argues, A.M. Amat, M.A. Miranda, A photophysical approach to investigate the photooxidation mechanism of pesticides: Hydroxyl radical versus electron transfer, Appl. Catal. B, 103 (2011) 48-53.

[104] G.M. Rodriguez-Muñiz, J. Gomis, A. Arques, A.M. Amat, M.L. Marin, M.A. Miranda, Hydroxyl radical as an unlikely key intermediate in the photodegradation of emerging pollutants, Photochem. Photobiol., 90 (2014) 1467-1469.

[105] S. Malato, J. Blanco, A. Vidal, D. Alarcon, M.I. Maldonado, J. Caceres, W. Gernjak, Applied studies in solar photocatalytic detoxification: an overview, Sol. Energy, 75 (2003) 329-336.

[106] I. Oller, S. Malato, J.A. Sánchez-Pérez, Combination of Advanced Oxidation Processes and biological treatments for wastewater decontamination—A review, Sci. Total Environ., 409 (2011) 4141-4166.

[107] S.K. Khetan, T.J. Collins, Human pharmaceuticals in the aquatic environment: A challenge to green chemistry, Chem. Rev., 107 (2007) 2319-2364.

[108] C. Tixier, H.P. Singer, S. Oellers, S.R. Müller, Occurrence and fate of carbamazepine, clofibric acid, diclofenac, ibuprofen, ketoprofen, and naproxen in surface waters, Environ. Sci. Technol., 37 (2003) 1061-1068.

[109] A. Bernabeu, R.F. Vercher, L. Santos-Juanes, P.J. Simon, C. Lardin, M.A. Martinez, J.A. Vicente, R. Gonzalez, C. Llosa, A. Arques, A.M. Amat, Solar photocatalysis

as a tertiary treatment to remove emerging pollutants from wastewater treatment plant effluents, Catal. Today, 161 (2011) 235-240.

[110] N. Klamerth, N. Miranda, S. Malato, A. Aguera, A.R. Fernandez-Alba, M.I. Maldonado, J.M. Coronado, Degradation of emerging contaminants at low concentrations in MWTPs effluents with mild solar photo-Fenton and TiO2, Catal. Today, 144 (2009) 124-130.

[111] P. Miro, A. Arques, A.M. Amat, M.L. Marin, M.A. Miranda, A mechanistic study on the oxidative photodegradation of 2,6-dichlorodiphenylamine-derived drugs: Photo-Fenton versus photocatalysis with a triphenylpyrylium salt, Appl. Catal. B, 140 (2013) 412-418.

[112] S. Canonica, Oxidation of aquatic organic contaminants induced by excited triplet states, Chimia, 61 (2007) 641-644.

[113] A. Arques, A.M. Amat, L. Santos-Juanes, R.F. Vercher, M.L. Marin, M.A. Miranda, 2,4,6-triphenylthiapyrylium cation as homogeneous solar photocatalyst, Catal. Today, 129 (2007) 37-42.

[114] M.A. Miranda, M.a.L. Marín, A.M. Amat, A. Arques, S. Seguí, Pyrylium salt-photosensitized degradation of phenolic contaminants present in olive oil wastewater with solar light: Part III. Tyrosol and p-hydroxyphenylacetic acid, Appl. Catal. B, 35 (2002) 167-174.

[115] M.A. Miranda, F. Galindo, A.M. Amat, A. Arques, Pyrylium salt-photosensitised degradation of phenolic contaminants present in olive oil wastewaters with solar light: Part II. Benzoic acid derivatives, Appl. Catal. B, 30 (2001) 437-444.

[116] M.L. Marin, A. Miguel, L. Santos-Juanes, A. Arques, A.M. Amat, M.A. Miranda, Involvement of triplet excited states in the electron transfer photodegradation of cinnamic acids using pyrylium and thiapyrylium salts as photocatalysts, Photochem. Photobiol. Sci., 6 (2007) 848-852.

[117] J. Gomis, A. Arques, A.M. Amat, M.L. Marin, M.A. Miranda, A mechanistic study on photocatalysis by thiapyrylium salts. Photodegradation of dimethoate, alachlor and pyrimethanil under simulated sunlight, Appl. Catal. B, 123 (2012) 208-213.

[118] A.M.F.M. Guedes, L.M.P. Madeira, R.A.R. Boaventura, C.A.V. Costa, Fenton oxidation of cork cooking wastewater—overall kinetic analysis, Water Research, 37 (2003) 3061-3069.

[119] V.J.P. Vilar, M.I. Maldonado, I. Oller, S. Malato, R.A.R. Boaventura, Solar treatment of cork boiling and bleaching wastewaters in a pilot plant, Water Research, 43 (2009) 4050-4062.

[120] M. Dias-Machado, L.M. Madeira, B. Nogales, O.C. Nunes, C.M. Manaia, Treatment of cork boiling wastewater using chemical oxidation and biodegradation, Chemosphere, 64 (2006) 455-461.

[121] E. Mendonca, P. Pereira, A. Martins, A.M. Anselmo, Fungal biodegradation and detoxification of cork boiling wastewaters, Eng. Life Sci., 4 (2004) 144-149.

[122] D. Mantzavinos, E. Psillakis, Enhancement of biodegradability of industrial wastewaters by chemical oxidation pre-treatment, J. Chem. Technol. Biotechnol., 79 (2004) 431-454.

[123] M. Bernardo, A. Santos, P. Cantinho, M. Minhalma, Biodegradation rate constants in different NF/UF fractions of cork processing wastewaters, Desalin. Water Treat., 29 (2011) 264-270.

[124] A. Santos, M. Bernardo, C. Vespeira, P. Cantinho, M. Minhalma, Cork industry wastewater characterization: assessment of the biodegradability, reuse and of the relationship between BOD, COD and tannins with TOC, J. Water Reuse Desalin., 2 (2012) 33-39.

[125] M.A. Miranda, H. Garcia, 2,4,6-Triphenylpyrylium Tetrafluoroborate As An Electron-Transfer Photosensitizer, Chemical Reviews, 94 (1994) 1063-1089.

[126] F. Morlet-Savary, S. Parret, J.P. Fouassier, K. Inomata, T. Matsumoto, Excited state interactions of thiopyrylium salts, J. Chem. Soc.-Faraday Trans., 94 (1998) 745-752.

[127] C.Y. Huang, [27] Determination of binding stoichiometry by the continuous variation method: The job plot, in: L.P. Daniel (Ed.) Methods in Enzymology, Academic Press1982, pp. 509-525.

[128] P. Maccarthy, Simplified experimental route for obtaining jobs curves, Anal. Chem., 50 (1978) 2165-2165.

[129] M. Martiny, E. Steckhan, T. Esch, Cycloaddition reactions initiated by photochemically excited pyrylium salts, Chem. Ber. Recl., 126 (1993) 1671-1682.

[130] S.L.C. Murov, I.; Hug, G. L., Handbook of Photochemistry, 2nd ed., Marcel Dekker, New York, 1993.

[131] D. Barcelo, Emerging pollutants in water analysis, TRAC Trends in Analytical Chemistry, 22 (2003) xiv-xvi.

[132] D. Barceló, M. Petrovic, EU aims for comprehensive analysis of emerging pollutants: Report on Chemical Analysis of Emerging Pollutants, 1st Thematic Workshop of EU Project NORMAN, held 27-28 November 2006 at Maó, Menorca, Spain, TRAC Trends in Analytical Chemistry, 26 (2007) 85-87.

[133] S.S. Kalanur, J. Seetharamappa, Electrochemical Oxidation of Bioactive Carbamazepine and Its Interaction with DNA, Anal. Lett., 43 (2010) 618-630.

[134] M.A. Miranda, A.M. Amat, A. Arques, Stability and performance of silica gel-supported triphenylpyrylium cation as heterogeneous photocatalyst, Catal. Today, 76 (2002) 113-119.

[135] S.L. Murov, I. Carmichael, G.L. Hug, Handbook of Photochemistry, 2nd ed., Marcel Dekker, New York, 2009.

[136] J.V. Goldstone, B.M. Voelker, Chemistry of Superoxide Radical in Seawater: CDOM Associated Sink of Superoxide in Coastal Waters, Environ. Sci. Technol., 34 (2000) 1043-1048.

[137] A. Paul, S. Hackbarth, R.D. Vogt, B. Roder, B.K. Burnison, C.E.W. Steinberg, Photogeneration of singlet oxygen by humic substances: comparison of humic substances of aquatic and terrestrial origin, Photochem. Photobiol. Sci., 3 (2004) 273-280.

[138] P.P. Vaughan, N.V. Blough, Photochemical formation of hydroxyl radical by constituents of natural waters, Environ. Sci. Technol., 32 (1998) 2947-2953.

[139] J.L. Packer, J.J. Werner, D.E. Latch, K. McNeill, W.A. Arnold, Photochemical fate of pharmaceuticals in the environment: Naproxen, diclofenac, clofibric acid, and ibuprofen, Aquatic Sciences, 65 (2003) 342-351.

[140] R. Martinez-Haya, M.H. Barecka, P. Miro, M.L. Marin, M.A. Miranda, Photocatalytic treatment of cork wastewater pollutants. Degradation of gallic acid and trichloroanisole using triphenyl(thia)pyrylium salts, Appl. Catal. B, 179 (2015) 433-438.

[141] C.Y. Huang, Determination of Binding Stoichiometry by the Continuous Variation Method - the Job Plot, Methods in Enzymology, 87 (1982) 509-525.

[142] N.A. García, F. Amat-Guerri, Photodegradation of hydroxylated N-heteroaromatic derivatives in natural-like aquatic environments: A review of kinetic data of pesticide model compounds, Chemosphere, 59 (2005) 1067-1082.

[143] A. Pajares, J. Gianotti, E. Haggi, G. Stettler, F. Amat-Guerri, S. Criado, S. Miskoski, N.A. Garcia, Kinetic study of the singlet molecular oxygen-mediated photodegradation of monohydroxylated N-heteroaromatic compounds, J. Photochem. Photobiol., A, 119 (1998) 9-14.

[144] A. Pajares, J. Gianotti, G. Stettler, J.P. Escalada, S. Bertolotti, S. Miskoski, F. Amat-Guerri, N.A. García, Ionization effects on the sensitized photooxidation of 2, 3-dihydroxypyridine and 2, 4-dihydroxypyridine: a kinetic study, J. Photochem. Photobiol., A, 153 (2002) 101-107.

[145] E. Amat-Guerri, A. Pajares, J. Gianotti, E. Haggi, G. Stettler, S. Bertolotti, S. Miskoski, N.A. Garcia, Singlet molecular oxygen-mediated photooxidation of 2-substituted 3-hydroxypyridines, J. Photochem. Photobiol., A, 126 (1999) 59-64.

[146] A. Pajares, J. Gianotti, G. Stettler, E. Haggi, S. Miskoski, S. Criado, F. Amat-Guerri, N.A. Garcia, Kinetics of the dye sensitized photooxidation of 2-amino-4-hydroxy-6-methylpyrimidine, a model compound for some fungicides, J. Photochem. Photobiol., A, 135 (2000) 207-212.

[147] J.S. Miller, Rose bengal-sensitized photooxidation of 2-chlorophenol in water using solar simulated light, Water Research, 39 (2005) 412-422.

[148] K. Ozoemena, N. Kuznetsova, T. Nyokong, Photosensitized transformation of 4-chlorophenol in the presence of aggregated and non-aggregated metallophthalocyanines, J. Photochem. Photobiol., A, 139 (2001) 217-224.

[149] R. Gerdes, D. Wöhrle, W. Spiller, G. Schneider, G. Schnurpfeil, G. Schulz-Ekloff, Photo-oxidation of phenol and monochlorophenols in oxygen-saturated aqueous solutions by different photosensitizers, J. Photochem. Photobiol., A, 111 (1997) 65-74.

[150] P.G. Tratnyek, J. Holgne, Oxidation of Substituted Phenols in the Environment - A Qsar Analysis of Rate Constants for Reaction with Singlet Oxygen, Environ. Sci. Technol., 25 (1991) 1596-1604.

[151] D. Gryglik, M. Lach, J.S. Miller, The aqueous photosensitized degradation of butylparaben, Photochem. Photobiol. Sci., 8 (2009) 549-555.

[152] V.V. De Rosso, F.E. Morán Vieyra, A.Z. Mercadante, C.D. Borsarelli, Singlet oxygen quenching by anthocyanin's flavylium cations, Free Radic. Res., 42 (2008) 885-891.

[153] S. Criado, A. Pajares, J. Gianotti, G. Stettler, J.P. Escalada, S. Bertolotti, F. Amat-Guerri, Garcı, x, N.A. a, Kinetic study of the riboflavin-sensitised photooxygenation of two hydroxyquinolines of biological interest, J. Photoch. Photobio. B, 71 (2003) 19-25.

[154] R. Andreozzi, M. Raffaele, P. Nicklas, Pharmaceuticals in STP effluents and their solar photodegradation in aquatic environment, Chemosphere, 50 (2003) 1319-1330.

[155] X. Sun, H. Liu, Y. Zhang, Y. Zhao, X. Quan, Effects of Cu(II) and humic acid on atrazine photodegradation, J. Environ. Sci., 23 (2011) 773-777.

[156] H. Horiuchi, S. Ishibashi, S. Tobita, M. Uchida, M. Sato, K.-i. Toriba, K. Otaguro, H. Hiratsuka, Photodegradation Processes of Cyanine Dyes in the Film State Induced by Singlet Molecular Oxygen, J. Phys. Chem. B, 107 (2003) 7739-7746.

[157] Y. Usui, H. Koike, Y. Kurimura, An efficient regeneration of singlet oxygen from 2,5-diphenylfuran endoperoxide produced by a dye- sensitized oxygenation, Bull. Chem. Soc. Jpn., 60 (1987) 3373-3378.

[158] F. Wilkinson, W.P. Helman, A.B. Ross, Rate constants for the decay and reactions of the lowest electronically excited singlet-state of molecular-oxygen in solution - an expanden and revised compilation, J. Phys. Chem. Ref. Data, 24 (1995) 663-1021.

[159] D.C. Neckers, Rose Bengal, J. Photochem. Photobiol., A, 47 (1989) 1-29.

[160] Y.I. Skurlatov, L.S. Ernestova, E.V. Vichutinskaya, D.P. Samsonov, I.V. Semenova, I.Y. Rod'ko, V.O. Shvidky, R.I. Pervunina, T.J. Kemp, Photochemical transformation of polychlorinated phenols, Journal of Photochemistry and Photobiology A: Chemistry, 107 (1997) 207-213.

[161] D. Gryglik, J.S. Miller, S. Ledakowicz, Singlet molecular oxygen application for 2-chlorophenol removal, J. Hazard. Mater., 146 (2007) 502-507.

[162] D.A. Nicewicz, D.W. MacMillan, Merging photoredox catalysis with organocatalysis: the direct asymmetric alkylation of aldehydes, Science, 322 (2008) 77-80.

[163] C. Lambert, T. Sarna, T.G. Truscott, Rose bengal radicals and their reactivity, J. Chem. Soc., Faraday Trans., 86 (1990) 3879-3882.

[164] C.R. Lambert, I.E. Kochevar, Electron Transfer Quenching of the Rose Bengal Triplet State, Photochem. Photobiol., 66 (1997) 15-25.

[165] P.B. Merkel, D.R. Kearns, Radiationless decay of singlet molecular oxygen in solution. Experimental and theoretical study of electronic-to-vibrational energy transfer, J. Am. Chem. Soc., 94 (1972) 7244-7253.

[166] J.R. Hurst, J.D. McDonald, G.B. Schuster, Lifetime of singlet oxygen in solution directly determined by laser spectroscopy, J. Am. Chem. Soc., 104 (1982) 2065-2067.

[167] R. Martinez-Haya, J. Gomis, A. Arques, M.L. Marin, A.M. Amat, M.A. Miranda, Time-resolved kinetic assessment of the role of singlet and triplet excited states in the photocatalytic treatment of pollutants at different concentrations, Appl. Catal. B, 203 (2017) 381-388.

[168] R. Schmidt, C. Tanielian, R. Dunsbach, C. Wolff, Phenalenone, a universal reference compound for the determination of quantum yields of singlet oxygen O2(1Δg) sensitization, J. Photochem. Photobiol., A, 79 (1994) 11-17.

[169] C. Lorente, E. Arzoumanian, C. Castano, E. Oliveros, A.H. Thomas, A non-singlet oxygen mediated reaction photoinduced by phenalenone, a universal reference for singlet oxygen sensitization, RSC Advances, 4 (2014) 10718-10727.

[170] L.E. Manring, J. Eriksen, C.S. Foote, Electron-transfer photooxygenation. 4. Photooxygenation of trans-stilbene sensitized by methylene blue, J. Am. Chem. Soc., 102 (1980) 4275-4277.

[171] C. Flors, S. Nonell, Radical species derived from phenalenone: characterization and role of upper excited states, J. Photochem. Photobiol., A, 163 (2004) 9-12.

[172] S.E. Braslavsky, A.U. Acuna, W. Adam, F. Amat, D. Armesto, T.D.Z. Atvars, A. Bard, E. Bill, L.O. Bjoern, C. Bohne, J. Bolton, R. Bonneau, H. Bouas-Laurent, A.M. Braun, R. Dale, K. Dill, D. Doepp, H. Duerr, M.A. Fox, T. Gandolfi, Z.R. Grabowski, A. Griesbeck, A. Kutateladze, M. Litter, J. Lorimer, J. Mattay, J. Michl, R.J.D. Miller, L. Moggi, S. Monti, S. Nonell, P. Ogilby, G. Olbrich, E. Oliveros, M. Olivucci, G. Orellana, V. Prokorenko, K.R. Naqvi, W. Rettig, A. Rizzi, R.A. Rossi, R.E. San, F. Scandola, S. Schneider, E.W. Thulstrup, B. Valeur, J. Verhoeven, J. Warman, R. Weiss, J. Wirz, K. Zachariasse, Glossary of Terms Used in Photochemistry, 3rd edition (IUPAC recommendations 2006), Pure Appl. Chem., 79 (2007) 293-465.

[173] W. Jin, J. Zhang, Determination of diclofenac sodium by capillary zone electrophoresis with electrochemical detection, J. Chromatogr. A, 868 (2000) 101-107.

[174] A.A. Ensafi, M. Izadi, H. Karimi-Maleh, Sensitive voltammetric determination of diclofenac using room-temperature ionic liquid-modified carbon nanotubes paste electrode, Ionics, 19 (2013) 137-144.

[175] U.C. Yoon, S.L. Quillen, P.S. Mariano, R. Swanson, J.L. Stavinoha, E. Bay, Exploratory and Mechanistic Aspects of the Electron-Transfer Photochemistry of Olefin-N-Heteroaromatic Cation Systems, J. Am. Chem. Soc., 105 (1983) 1204-1218.

[176] H. Yokoi, A. Hatta, K. Ishiguro, Y. Sawaki, Formation of sigma- and pi-type dimer radical cations by the photochemical one-electron oxidation of aromatic sulfides, J. Am. Chem. Soc., 120 (1998) 12728-12733.

[177] E. Baciocchi, T.D. Giacco, F. Elisei, M.F. Gerini, M. Guerra, A. Lapi, P. Liberali, Electron Transfer and Singlet Oxygen Mechanisms in the Photooxygenation of Dibutyl Sulfide and Thioanisole in MeCN Sensitized by N-Methylquinolinium Tetrafluoborate and 9,10-Dicyanoanthracene. The Probable Involvement of a Thiadioxirane Intermediate in Electron Transfer Photooxygenations, J. Am. Chem. Soc., 125 (2003) 16444-16454.

[178] Y.K. Che, W.H. Ma, Y.J. Ren, C.C. Chen, X.Z. Zhang, J.C. Zhao, L. Zang, Photooxidation of dibenzothiophene and 4,6-dimethyldibenzothiophene sensitized by N-methylquinolinium tetrafluoborate: Mechanism and intermediates investigation, J. Phys. Chem. B, 109 (2005) 8270-8276.

[179] E. Baciocchi, T. Del Giacco, M.F. Gerini, O. Lanzalunga, Aryl sulfoxide radical cations. Generation, spectral properties, and theoretical calculations, J. Phys. Chem. A, 110 (2006) 9940-9948.

[180] E. Baciocchi, T. Del Giacco, O. Lanzalunga, P. Mencarelli, B. Procacci, Photosensitized oxidation of alkyl phenyl sulfoxides. C-S bond cleavage in alkyl phenyl sulfoxide radical cations, J. Org. Chem., 73 (2008) 5675-5682.

[181] E.L. Clennan, C. Liao, Role of sulfide radical cations in electron transfer promoted molecular oxygenations at sulfur, J. Am. Chem. Soc., 130 (2008) 4057-4068.

[182] P.F. Donovan, D.A. Conley, Some organic tetrafluoroborates, J. Chem. Eng. Data, 11 (1966) 614-&.

[183] Y.K. Che, M.H. Ma, H.W. Ji, J.C. Zhao, L. Zang, Visible photooxidation of dibenzothiophenes sensitized by 2-(4-methoxyphenyl)-4, 6-diphenylpyrylium: An electron transfer mechanism without involvement of superoxide, J. Phys. Chem. B, 110 (2006) 2942-2948.

[184] A.E. Greyshock, P.J. Vikesland, Triclosan Reactivity in Chloraminated Waters, Environ. Sci. Technol., 40 (2006) 2615-2622.

[185] L. Xing, J. Sun, H. Liu, H. Yu, Combined toxicity of three chlorophenols 2,4-dichlorophenol, 2,4,6-trichlorophenol and pentachlorophenol to Daphnia magna, J. Environ. Monit., 14 (2012) 1677-1683.

[186] Y. Peng, Y. Luo, X.-P. Nie, W. Liao, Y.-F. Yang, G.-G. Ying, Toxic effects of Triclosan on the detoxification system and breeding of Daphnia magna, Ecotoxicology, 22 (2013) 1384-1394.

[187] C. Tournaire, S. Croux, M.-T. Maurette, I. Beck, M. Hocquaux, A.M. Braun, E. Oliveros, Antioxidant activity of flavonoids: Efficiency of singlet oxygen (1Δg) quenching, J. Photochem. Photobiol. B, 19 (1993) 205-215.

[188] ISO, Water quality-determination of the inhibition of the mobility of Daphnia magna straus (Cladocera, Crustacea)-acute toxicity test, 1996, pp. pp. 6341.

[189] G.J. Kavarnos, N.J. Turro, Photosensitization by reversible electron transfer: theories, experimental evidence, and examples, Chem. Rev., 86 (1986) 401-449.

[190] J. Xuan, W.-J. Xiao, Visible-Light Photoredox Catalysis, Angew. Chem. Int. Ed., 51 (2012) 6828-6838.

[191] D. Ravelli, S. Protti, M. Fagnoni, A. Albini, Visible light photocatalysis. A green choice?, Curr. Org. Chem., 17 (2013) 2366-2373.

[192] S. Fukuzumi, K. Ohkubo, Selective photocatalytic reactions with organic photocatalysts, Chem. Sci., 4 (2013) 561-574.

[193] D. Staveness, I. Bosque, C.R.J. Stephenson, Free Radical Chemistry Enabled by Visible Light-Induced Electron Transfer, Acc. Chem. Res., 49 (2016) 2295-2306.

[194] K.L. Skubi, T.R. Blum, T.P. Yoon, Dual Catalysis Strategies in Photochemical Synthesis, Chem. Rev., 116 (2016) 10035-10074.

[195] M.H. Shaw, J. Twilton, D.W.C. MacMillan, Photoredox Catalysis in Organic Chemistry, J. Org. Chem., 81 (2016) 6898-6926.

[196] P.F. Heelis, The Photophysical and Photochemical Properties of Flavins (Isoalloxazines), Chem. Soc. Rev., 11 (1982) 15-39.

[197] C. Lu, W. Lin, W. Wang, Z. Han, S. Yao, N. Lin, Riboflavin (VB2) photosensitized oxidation of 2[prime or minute]-deoxyguanosine-5[prime or minute]-monophosphate (dGMP) in aqueous solution: a transient intermediates study, Phys. Chem. Chem. Phys., 2 (2000) 329-334.

[198] G. Porcal, S.G. Bertolotti, C.M. Previtali, M.V. Encinas, Electron transfer quenching of singlet and triplet excited states of flavins and lumichrome by aromatic and aliphatic electron donors, Phys. Chem. Chem. Phys., 5 (2003) 4123-4128.

[199] A. Masek, E. Chrzescijanska, M. Zaborski, M. Maciejewska, Characterisation of the antioxidant acitivity of riboflavin in an elastomeric composite, C. R. Chimie, 15 (2012) 524-529.

[200] S.L.J. Tan, R.D. Webster, Electrochemically Induced Chemically Reversible Proton-Coupled Electron Transfer Reactions of Riboflavin (Vitamin B2), J. Am. Chem. Soc., 134 (2012) 5954-5964.

[201] W. Chen, J.-J. Chen, R. Lu, C. Qian, W.-W. Li, H.-Q. Yu, Redox reaction characteristics of riboflavin: A fluorescence spectroelectrochemical analysis and density functional theory calculation, Bioelectrochemistry, 98 (2014) 103-108.

[202] A. Pajares, J. Gianotti, G. Stettler, S. Bertolotti, S. Criado, A. Posadaz, F. Amat-Guerri, N.A. Garcia, Modelling the natural photodegradation of water contaminants - A kinetic study on the light-induced aerobic interactions between riboflavin and 4-hydroxypyridine 2, J. Photochem. Photobiol., A, 139 (2001) 199-204.

[203] W. Massad, S. Criado, S. Bertolotti, A. Pajares, J. Gianotti, J.P. Escalada, F. Amat-Guerri, N.A. Garcia, Photodegradation of the herbicide Norflurazon sensitised by Riboflavin. A kinetic and mechanistic study, Chemosphere, 57 (2004) 455-461.

[204] E. Haggi, S. Bertolotti, N.A. Garcia, Modelling the environmental degradation of water contaminants. Kinetics and mechanism of the riboflavin-sensitised-photo oxidation of phenolic compounds, Chemosphere, 55 (2004) 1501-1507.

[205] Y. Barbieri, W.A. Massad, D.J. Diaz, J. Sanz, F. Amat-Guerri, N.A. Garcia, Photodegradation of bisphenol A and related compounds under natural-like conditions in the presence of riboflavin: Kinetics, mechanism and photoproducts, Chemosphere, 73 (2008) 564-571.

[206] M. Diaz, M. Luiz, P. Alegretti, J. Furlong, F. Amat-Guerri, W. Massad, S. Criado, N.A. Garcia, Visible-light-mediated photodegradation of 17 beta-estradiol: Kinetics, mechanism and photoproducts, J. Photochem. Photobiol., A, 202 (2009) 221-227.

[207] A. Pajares, M. Bregliani, M.P. Montana, S. Criado, W. Massad, J. Gianotti, I. Gutierrez, N.A. Garcia, Visible-light promoted photoprocesses on aqueous gallic acid in the presence of riboflavin. Kinetics and mechanism, J. Photochem. Photobiol., A, 209 (2010) 89-94.

[208] T. Hering, B. Muhldorf, R. Wolf, B. Konig, Halogenase-Inspired Oxidative Chlorination Using Flavin Photocatalysis, Angew. Chem., Int. Ed., 55 (2016) 5342-5345.

[209] R. Lechner, B. Konig, Oxidation and Deprotection of Primary Benzylamines by Visible Light Flavin Photocatalysis, Synthesis-Stuttgart, (2010) 1712-1718.

[210] T. Nevesely, E. Svobodova, J. Chudoba, M. Sikorski, R. Cibulka, Efficient Metal-Free Aerobic Photooxidation of Sulfides to Sulfoxides Mediated by a Vitamin B-2 Derivative and Visible Light, Adv. Synth. Catal., 358 (2016) 1654-1663.

[211] J.M.R. Narayanam, J.W. Tucker, C.R.J. Stephenson, Electron-Transfer Photoredox Catalysis: Development of a Tin-Free Reductive Dehalogenation Reaction, J. Am. Chem. Soc., 131 (2009) 8756-8757.

[212] L. Furst, B.S. Matsuura, J.M.R. Narayanam, J.W. Tucker, C.R.J. Stephenson, Visible Light-Mediated Intermolecular C–H Functionalization of Electron-Rich Heterocycles with Malonates, Org. Lett., 12 (2010) 3104-3107.

[213] J.J. Devery, J.D. Nguyen, C. Dai, C.R.J. Stephenson, Light-Mediated Reductive Debromination of Unactivated Alkyl and Aryl Bromides, ACS Catal., 6 (2016) 5962-5967.

[214] I. Ghosh, T. Ghosh, J.I. Bardagi, B. König, Reduction of aryl halides by consecutive visible light-induced electron transfer processes, Science, 346 (2014) 725.

[215] I. Ghosh, L. Marzo, A. Das, R. Shaikh, B. König, Visible Light Mediated Photoredox Catalytic Arylation Reactions, Acc. Chem. Res., 49 (2016) 1566-1577.

[216] J.D. Nguyen, E.M. D'Amato, J.M.R. Narayanam, C.R.J. Stephenson, Engaging unactivated alkyl, alkenyl and aryl iodides in visible-light-mediated free radical reactions, Nat. Chem., 4 (2012) 854-859.

[217] E.H. Discekici, N.J. Treat, S.O. Poelma, K.M. Mattson, Z.M. Hudson, Y. Luo, C.J. Hawker, J.R. de Alaniz, A highly reducing metal-free photoredox catalyst: design and application in radical dehalogenations, Chem. Commun., 51 (2015) 11705-11708.

[218] I. Ghosh, B. König, Chromoselective Photocatalysis: Controlled Bond Activation through Light-Color Regulation of Redox Potentials, Angew. Chem. Int. Ed., 55 (2016) 7676-7679.

[219] L. Zeng, T. Liu, C. He, D. Shi, F. Zhang, C. Duan, Organized Aggregation Makes Insoluble Perylene Diimide Efficient for the Reduction of Aryl Halides via Consecutive Visible Light-Induced Electron-Transfer Processes, J. Am. Chem. Soc., 138 (2016) 3958-3961.

[220] M. Haring, R. Perez-Ruiz, A. Jacobi von Wangelin, D.D. Diaz, Intragel photoreduction of aryl halides by green-to-blue upconversion under aerobic conditions, Chem. Commun., 51 (2015) 16848-16851.

[221] M. Majek, U. Faltermeier, B. Dick, R. Pérez-Ruiz, A. Jacobi von Wangelin, Application of Visible-to-UV Photon Upconversion to Photoredox Catalysis: The Activation of Aryl Bromides, Chem. Eur. J., 21 (2015) 15496-15501.

[222] M. Marin, M.A. Miranda, M.L. Marin, A comprehensive mechanistic study on the visible-light photocatalytic reductive dehalogenation of haloaromatics mediated by Ru (bpy) 3 Cl 2, Catal. Sci. Technol., 7 (2017) 4852-4858.

[223] S.E. Braslavsky, Glossary of terms used in photochemistry, 3rd edition (IUPAC Recommendations 2006), Pure Appl. Chem., 79 (2007) 293-465.

[224] J.W. Sease, F.G. Burton, S.L. Nickol, Mechanism of electrolytic reduction of carbon-halogen bond. II. A rho sigma study, J. Am. Chem. Soc., 90 (1968) 2595-2598.

[225] M. Neumann, S. Füldner, B. König, K. Zeitler, Metal-Free, Cooperative Asymmetric Organophotoredox Catalysis with Visible Light, Angew. Chem. Int. Ed., 50 (2011) 951-954.

[226] G.R. Buettner, The Pecking Order of Free Radicals and Antioxidants: Lipid Peroxidation, α-Tocopherol, and Ascorbate, Arch. Biochem. Biophys., 300 (1993) 535-543.

[227] S.G. Bertolotti, C.M. Previtali, A.M. Rufs, M.V. Encinas, Riboflavin/Triethanolamine as Photoinitiator System of Vinyl Polymerization. A Mechanistic Study by Laser Flash Photolysis, Macromolecules, 32 (1999) 2920-2924.

[228] R. Wizinger, P. Ulrich, Zur Kenntnis der Thiopyryliumsalze, Helv. Chim. Acta, 39 (1956) 207-216.

[229] J.R. Lakowicz, Principles of Fluorescence Spectroscopy, Plenum Press1983.

[230] F.M. Hamer, 215. Preparation of 4[prime or minute]-cyanines, J. Chem. Soc., (1939) 1008-1013.

[231] I. Vayá, V. Lhiaubet-Vallet, M.C. Jiménez, M.A. Miranda, Photoactive assemblies of organic compounds and biomolecules: drug–protein supramolecular systems, Chem. Soc. Rev., 43 (2014) 4102-4122.

# 12.Summary/ Resumen/ Resum

## 12.1. Summary

In the last decades, photoinduced-redox processes mediated through visible light have obtained great attention due to the generally mild operating conditions that they offer. As a result, they constitute a real alternative within the so-called Advanced Oxidation processes. Besides, they are becoming an outstanding methodology in organic synthesis, which has opened the door to new synthetic and chemical routes. However, despite the growth of the field, little attention has been paid to the mechanistic pathways behind these processes.

The main objective of this thesis was to gain deeper understanding of different photoredox processes carried out using organic photocatalysts. More specifically, the viability of several organic photocatalysts was studied, and besides, a careful mechanistic study based on time resolved techniques supported the postulated mechanisms. With this information, a methodology determining the key points to consider in a photoredox system were established.

Firstly, in Part I, two photocatalysts, pyrylium and thiapyrylium salts, which operate through an oxidative electron transfer, have been used with different objectives. In Chapter 3, the viability of the photodegradation of two common pollutants from cork industry and the operating mechanism has been evaluated. In Chapter 4, the direct detection of all the $TPP^+$ derived short-lived intermediates in the photocatalyzed oxidation of a mixture of pollutants using $TPP^+$ is proposed as a methodology to assess the photodegradation extent. In the last chapter of Part I, Chapter 5, $TPTP^+$ is used to establish the characteristics of an ideal photocatalyst. Besides, the study claimed the influence of the concentration of the target substances in the efficiency of the excited states or, in general, of the key short-lived intermediates.

Secondly, in Part II, Chapter 6, rose bengal, a typical photocatalyst used in wastewater remediation, known for working *via* Type II mechanism, was evaluated for the removal of two common drugs. In addition, a second one, perinaphtenone, which

gives rise to even a higher singlet oxygen quantum yield than rose Bengal, was tested. In Chapter 7, $NMQ^+$, a non-typical photocatalyst able of generate singlet oxygen from its singlet excited state, was used in the photooxidation of three different pollutants. In every case analyzed in Chapters 6 and 7, the major contribution of Type I *vs* Type II mechanism was demonstrated.

Finally, in Part III, Chapter 8 was devoted to the photocatalytic reduction of organic bromides. In this case, riboflavin, a naturally occuring organic dye, was used as a photocatalyst. Analogously, careful attention was paid to the behavior of the intermediates, as well as to the thermodynamics of the steps involved in the photocatalytic cycle.

## 12.2. Resumen

En las últimas décadas, los procesos redox fotoinducidos mediados por luz visible han recibido gran atención debido a las suaves condiciones de operación en que se llevan a cabo. Como resultado, se han logrado posicionar como una alternativa más dentro de los Procesos de Oxidación Avanzada. Además, se han convertido en una metodología excepcional en síntesis orgánica, que ha abierto la puerta a nuevas rutas químicas con aplicaciones sintéticas. Sin embargo, a pesar del crecimiento del campo, se ha prestado poca atención a los mecanismos por los que operan estos procesos.

El principal objetivo de esta tesis es avanzar en la comprensión de distintos procesos fotoredox llevados a cabo empleando fotocatalizadores orgánicos. Más específicamente, se ha estudiado la viabilidad de distintos fotocatalizadores orgánicos, y además, se ha realizado un estudio mecanístico detallado basado en técnicas resueltas en el tiempo. A partir de estos resultados, se ha establecido una metodología para determinar los puntos clave a considerar en un sistema fotoredox.

En primer lugar, en la Parte I, se eligieron dos fotocatalizadores, sales de pirilio y tiapirilio, que operan mediante transferencia electrónica oxidativa, con distintos objetivos. En el Capítulo 3, se evaluó su aplicabilidad en la fotodegradación de dos contaminantes de la industria del corcho y se estudió el mecanismo por el que se produce dicha fotodegradación. En el Capítulo 4, se demostró la utilidad de la detección directa de todos los intermedios de vida corta derivados del $TPP^+$ implicados en la oxidación fotocatalizada como herramienta para evaluar el nivel de fotodegradación. En el Capítulo 5, se empleó $TPTP^+$ para establecer las características de un fotocatalizador ideal y la influencia de la concentración de las sustancias a oxidar en la eficiencia de los estados excitados, o en general, de los intermedios clave de vida corta.

En segundo lugar, en la Parte II, Capítulo 6, se evaluó el potencial del rosa bengala en la eliminación de dos fármacos. Éste es un fotocatalizador típico en la remediación de aguas residuales conocido por actuar *via* mecanismo Tipo II. Se incluyó además un segundo fotocatalizador, perinaftenona, cuyo rendimiento cuántico de oxígeno singlete es incluso mayor a rosa bengala. En el Capítulo 7, se llevó a cabo la fotooxidación de tres contaminantes, usando $NMQ^+$, un fotocatalizador inusual, capaz de generar oxígeno

singlete desde su estado excitado singlete. En todos los casos analizados en los Capítulos 6 y 7, se pudo demostrar la mayor contribución del mecanismo Tipo I sobre el mecanismo Tipo II en la fotodegradación de los diferentes contaminantes.

Finalmente, en la Parte II, el Capítulo 8 se dedicó a la reducción fotocatalítica de bromuros orgánicos, empleando riboflavina, un colorante orgánico natural, como fotocatalizador. De nuevo, se prestó especial atención a la detección y comportamiento de las especies intermedias, lo que resultó de acuerdo a los datos termodinámicos.

## 12.3. Resum

En les últimes dècades, els processos redox fotoinduïts mitjan per llum visible han rebut gran atenció degut a les suaus condicions d'operació en que es donen. Com a resultat, s'han aconseguit col·locar com una alternativa mes dins dels Processos d'Oxidació Avançada. A més, han estat convertint-se en una metodologia excepcional en síntesi orgànica, que ha obert la porta a noves rutes químiques amb aplicacions sintètiques. No obstant això, a pesar del creixement del camp, s'ha prestat poca atenció als mecanismes pels que operen aquests processos.

El principal objectiu d'esta tesi va es avançar en la comprensió de diferents processos fotoredox duts a terme emprant fotocatalitzadors orgànics. Més específicament, es va estudiar la viabilitat de distints fotocatalitzadors orgànics, i a més, es va realitzar un estudi mecanístic al detall basat en tècniques resoltes en el temps. Amb aquests resultats, es va establir una metodologia per a determinar els punts clau a considerar en un sistema fotoredox.

En primer lloc, en la Part I, es van elegir dos fotocatalitzadors, sals de pirili i tiapirili, els quals operen per mitjà de transferència electrònica oxidativa, amb distints objectius. En el Capítol 3, es va avaluar la seua aplicabilitat en la fotodegradació de dos contaminants de la indústria del suro i es va estudiar el mecanisme pel qual es produeix dita fotodegradació. En el Capítol 4, es va demostrar la utilitat de la detecció directa de tots els intermedis de curt temps de vida derivats del TPP+ implicats en l'oxidació fotocatalitzada com a ferramenta per avaluar el nivell de fotodegradació. En el Capítol 5, es va emprar $TPTP^+$ per a establir les característiques d'un fotocatalitzador ideal i l'influencia de la concentració de les substàncies a oxidar en la eficiència dels estats oxidats, o en general, del intermedis claus de vida curta.

En segon lloc, en la Part II, Capítol 6, es va avaluar el potencial del rosa bengala en l'eliminació de dos fàrmacs. Aquest es un fotocatalitzador típic en la remediació d'aigües residuals conegut per actuar *via* mecanisme Tipus II. Es va incloure a més un segon fotocatalitzador, perinaftenona, el del qual rendiment quàntic d'oxigen singlet és inclús major a rosa bengala. En el Capítol 7, es va dur a terme la fotooxidació de tres contaminants, usant $NMQ^+$, un fotocatalitzador inusual, capaç de generar oxigen singlet

des del seu estat excitat singlet. En tots els casos analitzats als Capítols 6 i 7, es va poder demostrar la major contribució del mecanisme Tipus I sobre el mecanisme Tipo II en la fotodegradació dels diferents contaminants.

Finalment, en la Part II, el Capítol 8 es va dedicar a la reducció fotocatalítica de bromurs orgànics, emprant riboflavina, un colorant orgànic natural, com fotocatalitzador. De nou, es va prestar especial atenció a la detecció i comportament de les espècies intermèdies, el que va resultar d'acord amb les dades termodinàmiques.

.

# 13. Dissemination of the results

## 13.1. Papers

- R. Martinez-Haya, M.A. Miranda, M.L. Marin "Type I *vs* Type II photodegradation of pollutants" *Catalysis Today*, 2018, *313*, 161 – 166.
- R. Martinez-Haya, C. Sabater, M. A. Castillo, M.A. Miranda, M.L. Marin, "A Mechanistic Study on the Potential of Quinolinium Salts as Photocatalysts for the Abatement of Chlorinated Pollutants" *Journal of Hazardous Material,* 2018, *351*, 277-284.
- R. Martinez-Haya, J. Gomis, A. Arques, A.M. Amat, M.A. Miranda, M.L. Marin, "Direct Detection of the Triphenylpyrylium-derived Short-lived Intermediates in the Photocatalyzed Degradation of Acetaminophen, Acetamiprid, Caffeine and Carbamazepine", *Journal of Hazardous Material,* 2018, *356,* 91 – 97.
- R. Martinez-Haya, M.A. Miranda and M. L. Marin, "Metal-Free Photocatalytic Reductive Dehalogenation Using Visible-Light: A Time-Resolved Mechanistic Study", *Eur. J. Org. Chem.* 2017, 2164–2169.
- R. Martinez-Haya, J. Gomis, A. Arques, M. L. Marin, A. M. Amat, and M.A. Miranda, "Time-resolved kinetic assessment of the role of singlet and triplet excited states in the photocatalytic treatment of pollutants at different concentrations", *Appl. Catal. B* 2017, *203*, 381-388.
- R. Martinez-Haya, M.H. Barecka, P. Miro, M.L. Marin, M.A. Miranda, "Photocatalytic Treatment of Cork Wastewater Pollutants. Degradation of Gallic Acid and Trichloroanisole using Triphenyl(thia)pyrylium salts", *Appl. Catal. B* 2015, *103*, 433-438.

## 13.2. Congresses

- Poster: "Time resolved mechanistic study of visible light mediated metal-free photocatalytic reductive dehalogenation" at III Young Researches from the Catalysis Spanish Society Meeting (Valencia, June 2018).
- Flash oral communication + poster: "Type I vs Type II Photodegradation of Pollutants" at Environmental Applications of Advanced Oxidation Processes Congress (Prague, June 2017). Awarded as one of the 12 best contributions in the category "Student Paper Comunication".

- Oral communication:“Removal of chlorinated aromatic pollutants photocatalyzed by N-methylquinolinium tetrafluoroborate” at V Spanish-Portuguese Conference on Photochemistry Congress (Toledo, September 2016).
- Oral communication: “Photocatalytic Oxidation of Cork Wastewater Pollutants Using Triphenyl(thia)pyrylium Salts.” at XXXV Bienal Meeting of the Spanish Royal Society of Chemistry (La Coruña, July 2015).